Chairman:	Prof. Dr Jan Colpaert, Hasselt University
Promoter:	Prof. Dr Tanja Junkers, Hasselt University
Members of the jury:	Prof. Dr Wouter Maes, Hasselt University
	Prof. Dr Sébastien Perrier, Warwick University
	Prof. Dr Ian Baxendale, Durham University
	Prof. Dr Hans Börner, Humboldt-Universität zu Berlin
	Prof. Dr Dagmar D'hooge, Ghent University

"Everything is theoretically impossible, until it is done."

Robert A. Heinlein

"Science never solves a problem without creating ten more."

George Bernard Shaw

TABLE OF CONTENTS

CHAPTER 1

Introduction

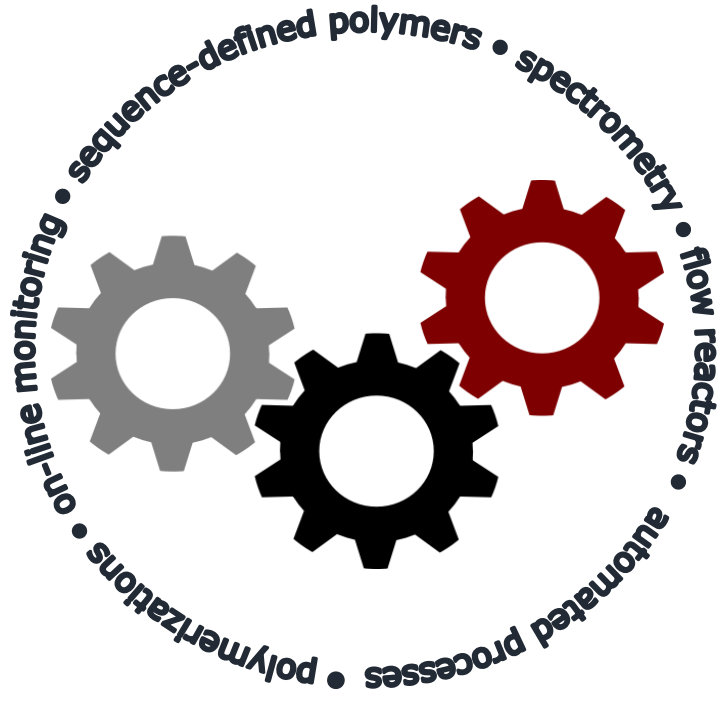

1.1 Polymers

Polymers, imagine today's life without them. No Television, no clothes, no glue, no toys, no computers, no paint, no cars, *etc*. They are everywhere around us and have become an essential part of our daily lives. Think about the origin of life without natural polymers, Earth would be just another dead rock flying through space. DNA (life's database), proteins (responsible for the functioning and regulation of our organs and tissues), wood, cotton, silk, rubber, *etc.* are all composed of natural polymers. Polymers, often also referred to as macromolecules, are defined by the International Union of Pure and Applied Chemistry (IUPAC) as "molecules of high relative molecular mass, the structure of which essentially comprises the multiple repetition of units derived, actually or conceptually, from molecules of low relative molecular mass".[1] In other words, a polymer is a very large molecule that is composed out of many repeating units, derived from the Greek words "*poly*" and "*meros*" which literally translates as "*many parts*". Figure 1.1a shows a simplified model of a polymer consisting of multiple building blocks, Figure 1.1b represents poly(styrene) with styrene repeating units.

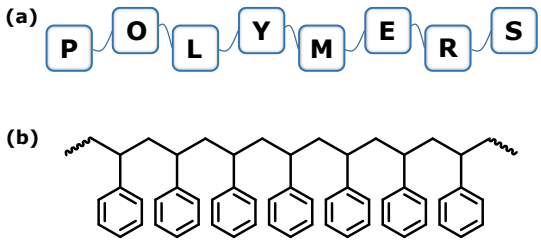

Figure 1.1. (a) Representative scheme spelling "polymers", a simplified model of a polymer consisting of multiple building blocks and (b) Synthetic polymer consisting of styrene repeating units linked together to form poly(styrene).

The first synthetic polymer molecule was invented by Leo H. A. Baekeland, in 1907, and first commercialized in 1910 under the trade name Bakelite®. A phenolic resin provided the foundation of the modern plastics industry.[2] Bakelite was used in e.g. electronic devices and aeronautics due to its good electrically and thermally insulating properties. However, in that time the molecular nature of polymers was not yet understood. In the 1920's, Hermann Staudinger introduced the concept of macromolecules; large molecules of high molecular weight composed of individual repeating units (smaller molecules) joined together by covalent bonds by a process called polymerization.[3] Nowadays, the terms "*polymer molecule*", referred to as "*polymer*", and "*macromolecule*" are acknowledged as synonyms by the scientific community and IUPAC.[4] Therefore both forms are used throughout this thesis.

So, even though there was no clear understanding of their characteristics in the beginning, the fascinating properties of polymers have resulted in their incorporation into our daily lives. Nowadays, the ever-growing field of polymer research contains the refinement and fine-tuning of synthetic polymers with highly defined properties and structures. Together with further developments in polymer technology, high-tech materials are within reach with properties far beyond traditional materials like wood, metals, *etc.* used in the early days of mankind.

1.2 Polymer Design & Synthesis

Over the years, different techniques have been developed for the design and synthesis of polymer materials. Overall, two main reaction pathways can be distinguished, i.e. step- and chain-growth polymerization, both leading to well-defined polymer architectures.

The two most important step-growth polymerizations are condensation (loss of a small molecule upon monomer reaction) and addition (electron rearrangement upon monomer reaction) polymerization. In step-growth, (multi)functional monomers undergo coupling reactions to initially form dimers, which, in turn, can either react with another (multi)functional monomer to form trimers or react with another initially formed dimer to form a tetramer, *etc*. This process continues and polymer chains are grown stepwise in time as schematically shown in Figure 1.2.[5]

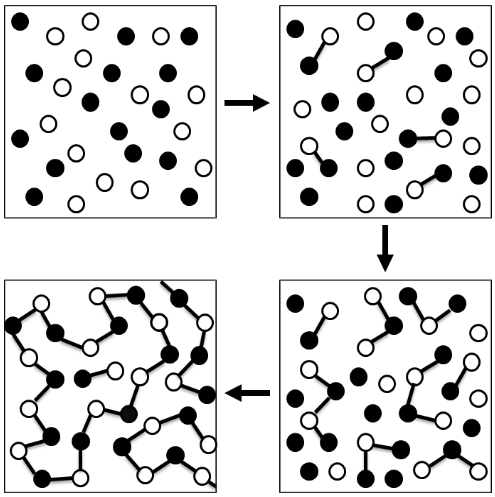

Figure 1.2. Schematic representation of a step-growth polymerization process. Single (multi)functional monomers react to form dimers, trimers, tetramers, *etc*.

The average chain length increases only moderately with monomer conversion and high molecular weight polymers are only observed at near to full monomer conversion, dependent on reaction stoichiometry, as depicted in Figure 1.3.

Radical chain-growth polymerizations on the other hand are processes where (unsaturated) monomers are added one at a time to the active site of a growing polymer chain. Upon addition of a monomer, the chain is elongated and the active site is regenerated to react with another monomer species. Prominent examples of polymers synthesized via chain-growth processes are poly(ethylene), poly(propylene) and poly(vinyl chloride). In contrast to step-growth, high molecular weight polymers can already be observed at initial monomer conversions during a free radical chain-growth polymerization.

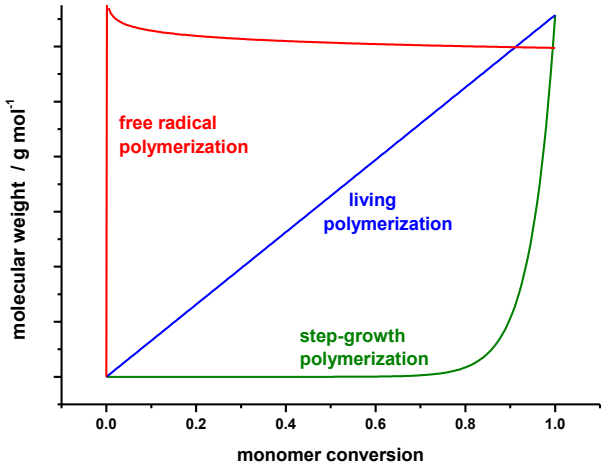

Figure 1.3. Molecular weight *vs.* conversion plot for step-growth, chain-growth and living polymerization mechanisms. Figure reproduced from G. Odian 1981.[6]

The focus of this thesis will be on radical chain-growth polymerization processes. However, other methods such as anionic, cationic and ring opening metathesis chain-growth polymerizations are also frequently used for the synthesis of polymeric materials. Many different strategies to perform free radical polymerizations (FRP) were developed such as solution polymerizations, bulk

polymerizations, emulsion polymerizations and suspension polymerizations to mention a few.

A radical chain-growth polymerization process, under normal reaction conditions, consists of three stages (a) initiation, (b) propagation and (c) termination, as schematically represented in Scheme 1.1. In a first step, initiator radicals react with an unsaturated monomer unit (initiation) after dissociation caused by an external source (light, heat, *etc*.). Secondly, this active initiator-monomer species reacts with a second monomer species (propagation). Propagation of the polymer chains continues until all monomer is depleted. Finally, radicals can also undergo irreversible termination reactions such as disproportionation or combination of the active growing chains which causes "dead" polymer chains.

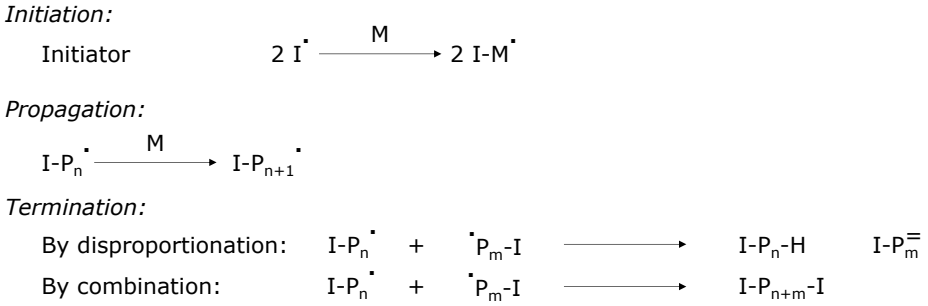

Scheme 1.1. Scheme of a radical chain-growth polymerization process. Scheme taken from M. H. Conradi 2014.[7]

In the absence of termination processes, growing polymer chains never "die" and can keep growing until all monomer is depleted. Such polymerization reactions were classified as "living polymerizations" by Szwarc and coworkers in 1956.[8] Due to their living character, a good control over polymer molecular weight and

dispersity can be provided. In an ideal living polymerization process (fast initiation and no termination or irreversible chain transfer), a linear relationship between the number average molecular weight (M_n) and monomer conversion is expected, as shown in Figure 1.3. However, in practice, radical polymerizations cannot truly become "living" due to the presence of unavoidable radical-radical coupling reactions (disproportionation and combination).

Controlled radical polymerization (CRP) reactions demonstrate a high level of chain endgroup and molecular weight control. In CRP reactions, irreversible termination events are mostly suppressed (with the exception of RAFT polymerization) by a reversible radical termination process which translates into a lower concentration of active radicals that can cause irreversible termination to occur. Most prominent controlled radical polymerization techniques, also called reversible deactivation radical polymerizations (RDRP)[9], are reversible addition-fragmentation chain transfer (RAFT)[10] polymerization, atom transfer radical polymerization (ATRP)[11] and nitroxide-mediated polymerization (NMP).[12]

A general reaction scheme of the RAFT polymerization steps and mechanisms, mainly used throughout this thesis, is shown in Scheme 1.2. It is important to mention that the kinetics of propagation (k_p) and termination (k_t) of a RAFT polymerization process can be assumed to be similar to free radical polymerizations since the radical concentration is not reduced by the RAFT agent. This is different from other controlled radical polymerization techniques where the concentration of radicals is kept low due to the deactivation of active species. Termination processes are less likely to occur due to the rapid exchange of the RAFT control agent and not by reducing the radical concentration. The RAFT

mechanism mainly follows FRP kinetics in terms of initiation, propagation and termination processes. However, after initiation (**1**), an active radical species can now react with the RAFT agent to enter the pre-equilibrium stage (radical addition, **3**). Once an intermediate species is formed, fragmentation can occur to form either the initial growing radical species or a reinitiating radical species R· (**4**). The stabilizing Z-group and R-leaving group can be tuned to provide optimal control over the polymerization. When the RAFT agent is consumed the process enters the main equilibrium. At this point, the addition-fragmentation process now continues.

The RAFT process is compatible with a broad range of monomers due to the possibility to design and finetune the RAFT control agent according to the monomers utilized. Typically dithioester and trithiocarbonate RAFT agents are utilized for the polymerization of more activated monomers (MAM)s such as (meth)acrylates, (meth)acrylamides and styrenics.[13] The less active RAFT agents, e.g. dithiocarbamates or xanthates, offer good control over the polymerization of less activated monomers (LAM)s such as vinylics. The more active RAFT agents, dithioesters and trithiocarbonates, inhibit polymerization of a LAM. A switchable RAFT agent, that can be used to control polymerization of both MAMs and LAMs, has also been reported.[14-15] Requirements for specific end-functionalities or polymer architectures may also influence the choice of RAFT agents utilized.[16]

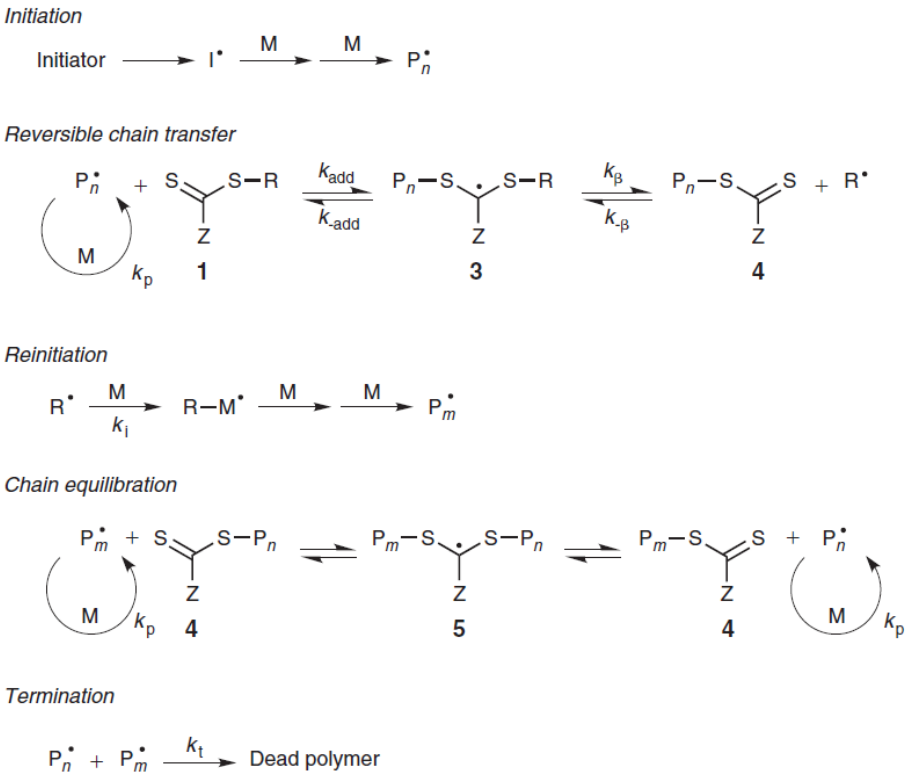

Scheme 1.2. Schematic representation of the RAFT polymerization process. Scheme reproduced from S. H. Thang and coworkers 2005.[17]

1.3 Polymer Architectures

Polymerizations can be designed to target specific polymer architectures, from linear to more complex hyperbranched structures with highly determined functionalities and composition. The most common, but definitely not limited to, are highlighted in Figure 1.4. Physical (e.g. solubility, melting point, glass transition temperature, *etc.*) and mechanical (stress-strain relationship) properties of polymer materials are highly influenced and determined by the polymer's architecture.

In Figure 1.4, three main classes can be observed, being *polymer topology* (related to the shape of the polymer structure), *polymer functionality* (chemical functionalities present in the chains) and *polymer composition* (order of monomer units along the polymer backbone).

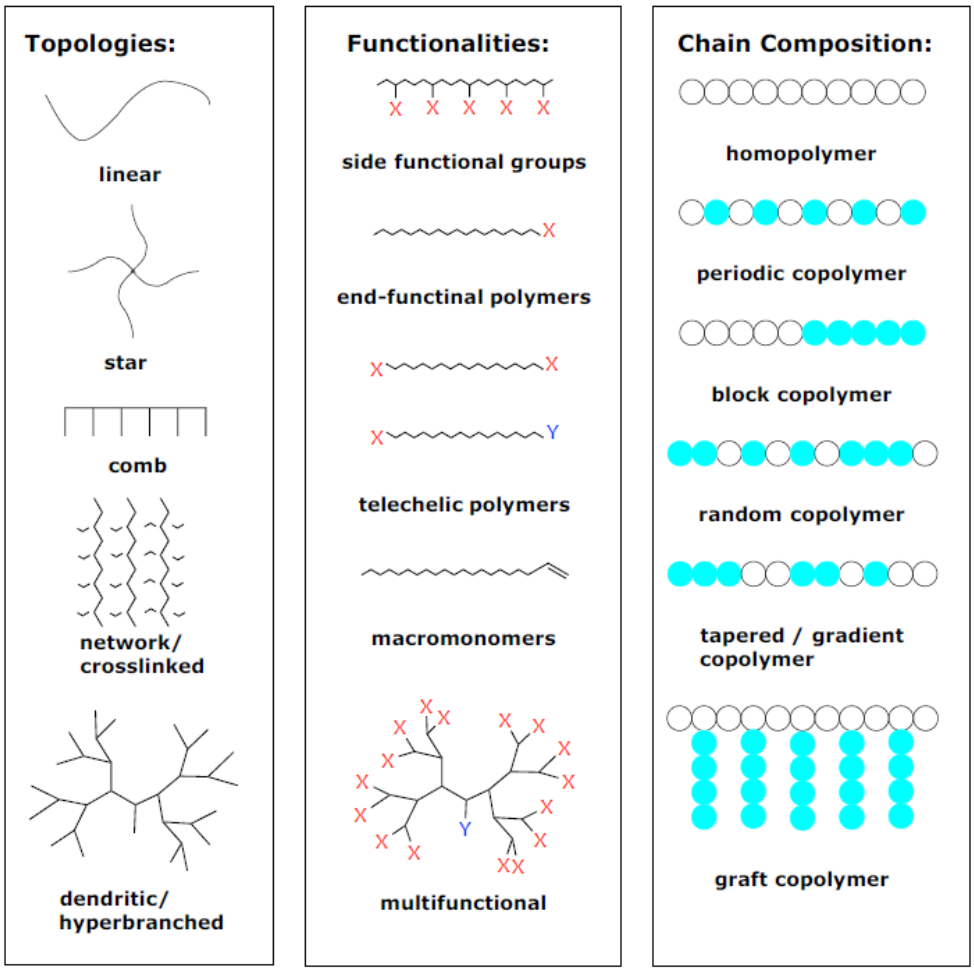

Figure 1.4. General overview of the most common polymer architectures divided in the three main aspects: topologies, functionalities, and chain compositions.

As an example to illustrate the role of the architecture, high- and low-density poly(ethylene) mainly differ in their degree of branching. High-density poly(ethylene) has a low degree of branching, as such containing elevated intermolecular forces, and is therefore used in applications such as bullet-proof vests due to it stiffness. Low-density poly(ethylene), on the other hand, is highly branched and therefore much more flexible and used in applications such as plastic bags.

1.4 Precision Polymers

1.4.1 Sequence-Controlled/Defined Polymers

Biopolymers, such as proteins and DNA, have highly selective and complex functions, fundamentally based on their primary structure, i.e. the specific order of repeating units and functionalities along their backbone. Inspired by this natural phenomenon, the production of synthetic materials is experiencing a shift towards new exciting classes of precision polymers that can be considered as information-containing macromolecules. In synthetic polymer chemistry, the versatility of monomer building blocks is endless compared to nature where DNA only uses 4 nucleotides and proteins/peptides only have a library of 20 amino acids to encode. Today, synthetic polymer materials are designed with almost unlimited variations in chain length, dispersity, topology, composition and functionality. However, the ability to control the exact order and sequence of monomers in a polymer chain is still one of the last major challenges. With such materials, polymers could be synthesized that feature a precise – and more importantly freely selectable – order of monomers in a monodisperse chain. In other words, such materials mimic peptides with the only difference being that instead of a peptide bond, other

moieties are used to connect the single building blocks. It is expected that these synthetic analogs will also be able to rearrange in precisely controlled primary, secondary, tertiary and quaternary structures and can be used to perform advanced tasks such as signal transduction, selective transport or catalysis. These promising materials can thus potentially be used for emerging applications in the field of biomimetics, artificial peptides, molecular recognition or data storage.

In recent years, one of the last frontiers in polymer chemistry has started to attract significant attention, namely the so called monomer sequence-controlled materials. Regulation of the monomer sequence in polymerizations – the so called sequence-controlled multiblock copolymers having a polydisperse nature – is of high interest to mimic biological materials in their functionality. Radical chain-growth mechanisms, RAFT polymerizations in particular, are explored in here towards sequence-controlled materials. Via controlled radical polymerization techniques, numerous multiblock copolymers have to date been achieved, mostly using acrylates or acrylamides, to encode information in the main chain. These polymers show an impressive number of blocks put in order, but are inherently of a polydisperse nature.[18-20] Although a large number of other non-radical routes are known,[21-29] the synthesis of polydisperse sequence-controlled multiblock copolymers, which significantly differ from sequence-defined (precision) materials in terms of molecular weight and physical properties, is beyond the scope of this work. Note that sequence-control generally refers to controlling the order in which certain functionalities appear along the backbone, irrespective of the number of inserted functionalities (polydisperse), while sequence-defined refers to monodisperse, and hence perfectly controlled sequences as shown in Figure 1.5. However, truly following the concept of nature, thus to synthesize monodisperse

materials, broadens the functionality of these materials further and opens new perspectives. Therefore the synthesis of monodisperse (precision) polymers with unprecedented control over the primary monomer sequence is herein investigated. A brief introduction of both radical and non-radical chemical strategies will be discussed in the following sections.

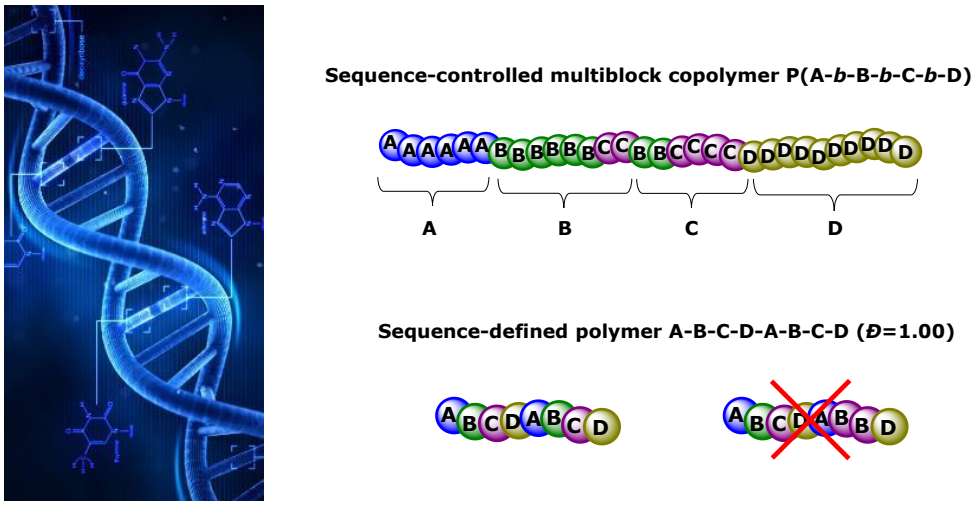

Figure 1.5. (left) DNA structure and (right) Schematic representation of sequence-controlled and sequence-defined polymer structures.

1.4.2 Precision Polymers via Non-Radical Routes

Many different synthesis strategies have been suggested, with most of them making use of click-like chemistry or reactions as known from step-growth polymerizations. The reason for this is simply that addition and condensation reactions allow the addition of one monomer unit at a time, thus minimizing dispersity of the reaction products. Although the main focus of this thesis is on precision polymers via the controlled radical RAFT polymerization technique, a brief overview of the most important classes of non-radical routes will be

discussed here. A more detailed review was published recently.[30] Two main non-radical synthesis routes are known: *i)* the homogeneous liquid-phase and *ii)* solid-phase synthesis.

1.4.2.1 Homogeneous Liquid-Phase Synthesis

Different synthetic non-radical strategies are known for the *homogeneous liquid-phase synthesis* of sequence-defined (precision) macromolecules. Most iterative approaches in the liquid-phase involve the (multistep) synthesis of functionalized starting materials performing simple organic chemistry reactions. Starting materials can be coupled stepwise, one by one, to form monodisperse macromolecules with control of the primary structure. However, disadvantages of iterative stepwise approaches are that the formation of larger macromolecules can be time-consuming and purification steps may be needed after each coupling.

An example of an unidirectional iterative growth strategy in solution is the implementation of multicomponent reactions to precisely control the primary backbone structure via the Passerini three and Ugi four-component reaction.[31] To limit the number of synthetic reaction steps, a bifunctional or macrocyclic core can be utilized for which two building blocks can be added in a single reaction step to grow an oligomer in two directions. The concept was nicely demonstrated by Barner-Kowollik and coworkers[32-33] investigating a photochemical protocol for the generation of sequence-defined macromolecules (Scheme 1.3).

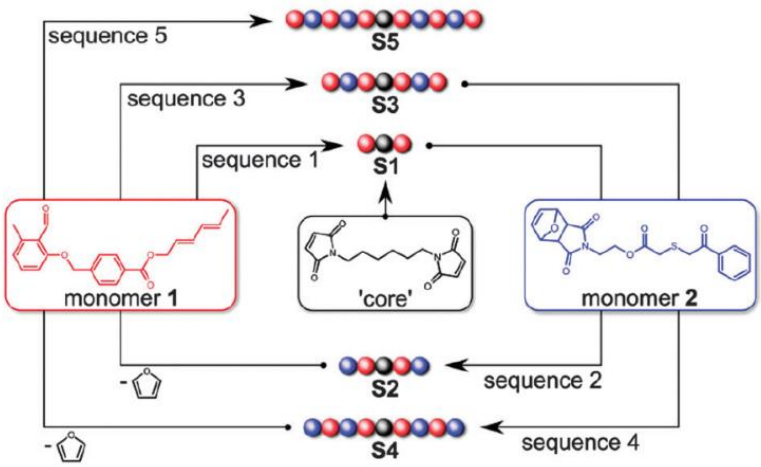

Scheme 1.3. The iterative synthesis of the sequence-defined macromolecule **S5** based on orthogonal molecular synthons: monomer **1** reacts with the core in the first sequence to provide **S1**, then successively reacts with synthon **2** in the second sequence to provide **S2**. Subsequent to the deprotection steps, the cycle is repeated up to the fifth sequence **S5**. Scheme reproduced from C. Barner-Kowollik and coworkers 2015.[32]

Another approach to limit the iterative reaction steps and rapidly reach monodisperse higher molecular weight sequences is by exponential growth strategies. However, exponential growth strategies are limited to palindromic or repetitive sequences and introducing versatility and side chains in the repeating units is difficult. Hawker and coworkers synthesized a monodisperse oligo(ε-caprolactone) 64-mer via an exponential growth strategy to give just one example.[34] Another important class of materials to mention is the templated chemistry approach to control monomer sequences, for which a detailed review was recently published by ten Brummelhuis.[35] This research field covers any polymerization process where bio- or synthetic polymer templates are utilized to

control the material properties of the final product. Alibi and coworkers reported the synthesis of well-defined bioactive macrocyclic oligo(thioetheramide)s via a one-pot acid catalyzed cascade reaction (> 20-mers).[36-37]

1.4.2.2 Solid-Phase Synthesis

Synthesis of sequence-defined non-natural macromolecules on a solid insoluble support, so-called *solid-phase synthesis*, has been heavily investigated in recent years. The technique was introduced by Robert Bruce Merrifield in 1963 by growing a short peptide sequence on a covalently bound solid resin particle.[38] A great advantage of this method is the simplicity of its workup by filtration and washing steps. However, after cleavage of the synthesized sequence from the solid support, additional purification steps are often necessary due to incomplete or side reactions. Also, the scalability of this technique is generally limited.

Recently, Madder and coworkers reported on thiolactone based chemistry on a solid support.[39] This thiolactone protecting group free chemistry allows for chain elongation via a two-step orthogonal iterative method. Due to the orthogonality of the reactions, no protection/deprotection chemistry is involved. The thiolactone containing building blocks were pre-synthesized allowing the side chains and the backbone to be varied, as demonstrated by the synthesis of a plethora of different sequence-specific 10-mers. The reaction protocol was optimized and transferred to an automated synthesizer which significantly reduced the process time from 3-5 days to 33 hours. A similar chemoselective "AB+CD" iterative approach was reported by Lutz and coworkers, as shown in Scheme 1.4.[40] A library of eight sequence-defined oligomers, whose sequence is based on a (0,1) binary code, was prepared through chemoselective repeating cycles of amidification and

copper-assisted alkyne-azide cycloaddition reactions from a resin. The same group have also reported on sequences of DP > 100 utilizing protection/deprotection group chemistry on a solid support.[41]

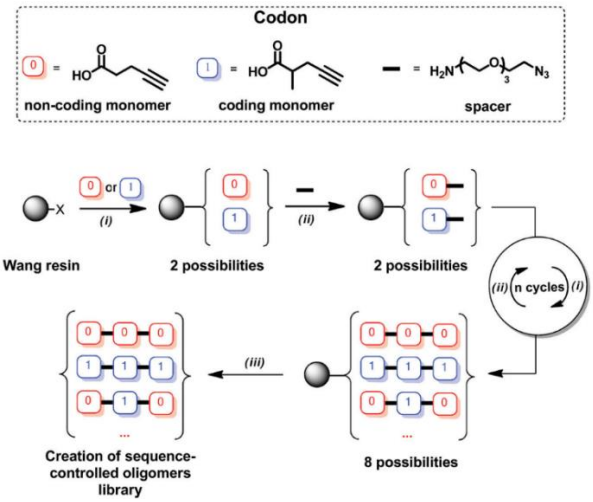

Scheme 1.4. "AB + CD" iterative approach for the synthesis of sequence-defined macromolecules. Scheme reproduced from J.-F. Lutz and coworkers 2014.[40]

Peptoid chemistry has been studied and reviewed in great detail by Zuckermann and coworkers.[42-44] Oligo(peptoid)s are bioinspired polymeric materials that have several advantages and a similar backbone structure compared to peptides. Synthesis of oligo(peptoid)s can be performed in peptide synthesizer resulting in near monodisperse oligomers up to 50 monomer units.[42]

Furthermore, other iterative synthesis strategies (on solid supports) are known but not explained in detail here.[45-48] Read-out strategies, so-called sequencing[49], to decipher and analyze encoded sequences are also discussed in the literature.[50]

1.4.3 Precision Polymers via Radical Routes

Since the advent of controlled polymerizations, the development of highly complex macromolecular materials has significantly improved and today the synthesis of virtually any polymer architecture is in one way or the other accessible with imagination being the only limiting factor. Advances have also been made towards achieving monodisperse oligomers via controlled radical polymerization methodologies. Such approaches require nothing less than removing – or more realistically – circumventing the statistical nature of radical chain growth as can be observed in Figure 1.6. The general concept of a radical chain growth process, one (or multiple) monomer unit(s) at a time, is highlighted. Sawamoto and coworkers used the exceptional bulkiness of certain monomers to reduce the propagation rate which allowed for only one monomer insertion at a time.[51] Recently, a modular strategy to produce discrete oligomers via a visible-light-mediated radical chain process was introduced by utilizing the high selectivity of the photoinduced electron/energy transfer (PET) RAFT process.[52-53]

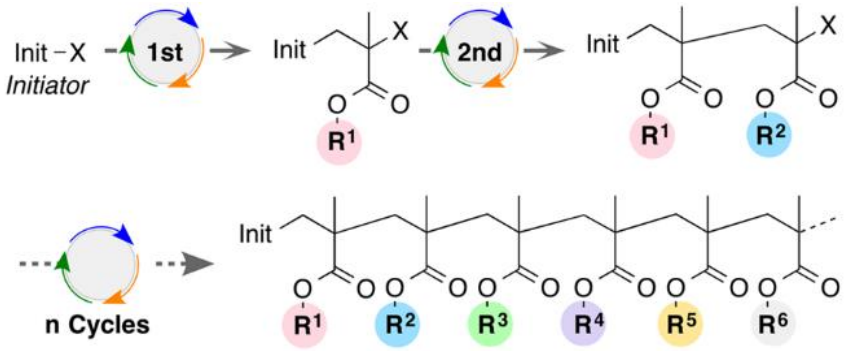

Figure 1.6. General concept of a chain growth process where one (or in some cases multiple) monomer units are added in each cycle. Figure reproduced from Sawamoto and coworkers 2016.[51]

Moad and coworkers first showed how RAFT polymerization can be used to create single unit monomer insertion (SUMI) products by utilizing the distinct reactivity differences between various radical adducts in the RAFT pre- and main-equilibria.[54] In this way, up to two monomer units could be efficiently inserted into the C-S bond of a RAFT agent. Advantages of this approach are that monodisperse products could be directly obtained, but since growing polymer chains become inevitably and successively closer in reactivity, the concept is difficult to be extended beyond the creation of dimers. In a similar approach, our group demonstrated that one can perform SUMIs while using only acrylates (and thus monomers of very similar reactivity) by accepting the statistical nature of the reactions, but performing advanced product separation, in which the desired SUMI products are isolated from their by-products (species in which either no monomer or several monomers were built in). The family of acrylate monomers is of high interest due to their commercial availability and tunability through post-polymerization modification, e.g. transesterification. Specifically for SUMI reactions, they are known for their high propagation rate. As such, insertions are fast, typically on the timescale of tens of minutes or faster. Our group reported on the synthesis of monodisperse 4-mer oligoacrylates via RAFT and photo copper mediated polymerization.[55-56] Purification of polydisperse oligomer mixtures was performed using automated recycling size-exclusion chromatography (rec-SEC).[57] In rec-SEC, the SUMI product mixture is repeatedly recycled over columns with size exclusion limits from 1000 to 5000 Da. With each additional cycle, the products with different hydrodynamic volumes are separated further and further. Separation of SUMI products becomes more tedious upon increasing the number of monomer units in the oligomer chain since the hydrodynamic volume of the SUMI species does not increase linearly with increasing chain

length. As such, more cycles are required for separation of higher chain lengths. However, rec-SEC is an excellent technique to purify the oligomer mixtures up to an oligomer chain length of 4 or 5 units. Recently, flash column chromatography (FCC) was introduced for this purpose. Isolation of oligomers with up to 11 monomer units and thus (including the RAFT-typical groups) 13 functionalities in precise order is demonstrated and discussed in detail in Chapter 6.[58]

1.5 Microreactor Technology

Optimizing and tuning the reaction conditions in batch processes is usually very time and energy consuming and easily puts restrictions on the upscaling from milligram to kilogram scale or higher. Microreactor application has, over the last decade, started a silent revolution in chemical synthesis. Via implementation of flow reactions, accelerated synthesis of compounds under stable and very reproducible reaction conditions has became available and a growing number of reactions are currently adapted to microreactor technology (MRT) protocols. Microreactors feature significant advantages such as ideal heat dissipation, high operational stability and – as a consequence from the strictly isothermal conditions provided – allow for a relatively easy upscaling. Microflow polymerizations are challenging due to the inherent viscosity increases during reactions, which makes handling of continuous flows in the microfluidic channels problematic. Nevertheless, by dilution of reactants, stable flows can be reached and polymerization protocols have been adapted with high success to MRT. Generally, fast and economic procedures could be identified, yielding polymer materials with very high definition and reproducibility. Figure 1.7 shows a commercial microreactor setup (Labtrix® Start, Chemtrix BV) and picture of a commonly used microreactor chip with an internal volume of 19.5 μL, as used throughout this

thesis. The setup consists of 2 pump units, a reactor and a heating unit. More details are given in Chapter 2.

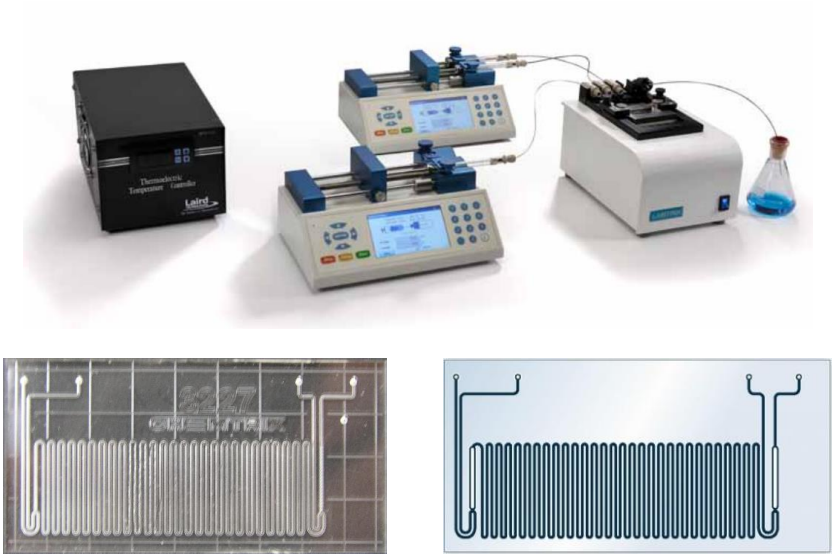

Figure 1.7. (top) Commercially available Labtrix® Start set-up and (bottom) Microreactor chip (19.5 μL) utilized throughout this thesis.

A lot of progress has been made during the last decade. However, most MRT polymerizations were carried out as a proof of concept or for laboratory reaction screening rather than targeting the continuous synthesis of larger amounts of functional materials. Realizing flow reaction settings on a microfluidic lab-on-a-chip-type reactor features several advantages. Despite the small reactor volumes, significant amounts of reaction product can be obtained due to the continuous production and the possibility to operate the device at over-pressures allowing for operational temperatures significantly above the ambient pressure boiling point of the solvent. At the same time, disadvantages of classical tubular reactors are avoided due to the high operational stability and ideal heat transfer, providing

isothermal conditions even for highly exothermic reactions. Upscaling of reactions in microreactors is simple and can be achieved via massive parallelization, resolving the need for tedious optimization protocols during classical scale-up.

In conclusion, the polymer field can benefit tremendously from MRT. Polymerizations have been found to proceed faster, with better control and with higher reproducibility compared to the batch alternative. This is a significant advantage in the realm of precision polymer design which will be discussed more into detail in Chapters 2 and 5. The high potential of MRT was only briefly discussed, a detailed overview can be found in some excellent reviews.[59-61] However, the full capacity of this technique will only unfold when suitable on-line characterization is made available, as discussed in the next section.

1.6. On-Line Monitoring of Polymerizations

Precise engineering of macromolecular materials requires close monitoring of the reaction conditions and polymerization progress, be it in the field of industrial-scale free-radical polymerization or small- or intermediate-scale controlled polymerization for the synthesis of precisely engineered block copolymers. On-line automated monitoring can hereby be an invaluable tool to steer reactions, especially when processes are carried out in multistep fashion. Polymerizations are generally highly exothermic, fast, and sensitive to small impurities (i.e. trace amounts of water in anionic chain growth polymerization). On-line monitoring of polymerizations can be defined as using characterization techniques that allow for a constant surveillance of the reactions without interruption. Ideally, the chosen characterization methods are non-invasive, although this will not always be the case and should not be a limiting factor. In this respect, many known

characterization techniques are not suitable for such reaction interrogation tasks. Characterizations must be fast and proceed without much delay in order to be able to react to changing environments and to influence the progress of a reaction directly. Operation of such a reactor setup can be used for the optimization of polymer reactions that require in-depth product monitoring in order to push the limits towards new products that would otherwise be inaccessible or not economically viable to synthesize by any other off-line sampling methods. Our group recently published a detailed review on the current status of on-line monitoring of polymerizations that covers all currently existing spectroscopy and spectrometry techniques in batch and flow processes.[62]

On-line monitoring tools available for MRT are today still mostly limited to spectroscopic analysis such as infrared, UV-Vis detection and recently real time on-line NMR spectroscopy.[63-66] Thus, even though on-line reaction monitoring tools exist for classical organic microreactor synthesis, no sufficient analytical tools are yet available for polymer reactions (since the chemical nature of polymers often either does not change during reactions, or is known regardless). Therefore, product analysis must be carried out off-line, slowing down optimization procedures and thus not fully exploiting the high-throughput potential of MRT. Important when performing polymerization reactions is information on average molecular weights, product distributions as well as endgroup patterns. Thus, on-line characterization via size-exclusion chromatography and soft ionization mass spectrometry would be extremely valuable towards future generation material development (Figure 1.8).

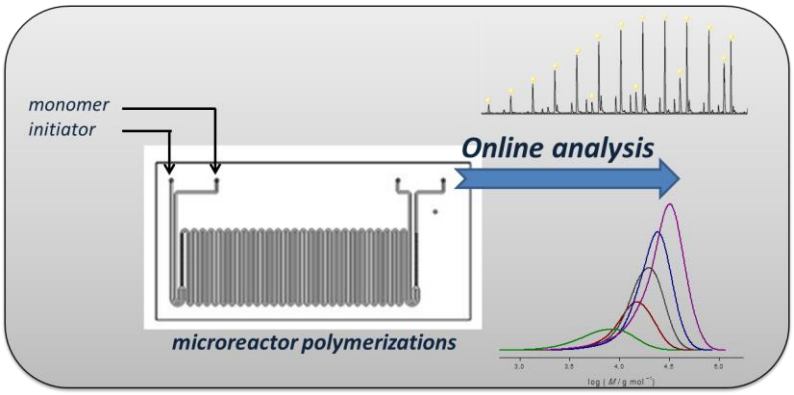

Figure 1.8. Schematic representation of the on-line monitoring of polymerization processes in a continuous flow reactor via electrospray ionization mass spectrometry (ESI-MS) and size-exclusion chromatography (SEC).

SEC is the standard technique used to carry out reliable determinations on molecular weight. Hadziioannou and coworkers reported the development of a new method for on-line characterization of polymers termed "continuous online rapid size-exclusion chromatography monitoring of polymerizations" (CORSEMP), which consists of automated sampling, dilutions, and injections (every 12 minutes) of polymers synthesized in a continuous flow setup.[67] Haddleton and coworkers introduced on-line rapid gel permeation chromatography (GPC) to monitor batch polymerization reactions.[68] On-line monitoring of polymerizations via coupling with ESI-MS is discussed in detail in Chapter 2. It is one of the aims of this thesis to fill this significant gap in MRT analytics and to use this new ability for the accelerated optimization of complex polymer reactions.

1.7 Aim and Outline of the Thesis

The aim of the research presented in this thesis is to develop novel on-line characterization tools dedicated to the monitoring of polymerization reactions in microfluidic reactors and to use this monitoring ability subsequently for the advanced synthesis of highly-defined materials. Furthermore, after successful implementation of mass spectrometry to the microreactor technology flow systems, various synthetic targets are approached. In addition, the development and processing of so-called sequence-controlled polymers is studied and first steps towards real applications are taken.

Chapter 2 focuses on the development of a technique for the continuous on-line monitoring of polymerization (chemical) processes by electrospray ionization mass spectrometry (ESI-MS) via coupling with a commercial microreactor system. A real time polymer growth was monitored. Furthermore, a single unit monomer insertion (SUMI) reaction of an acrylate monomer into a macroRAFT agent is screened and optimized.

The kinetics of *n*-butyl acrylate radical polymerization are revealed in a single experiment in **Chapter 3**. A reversible addition-fragmentation chain transfer (RAFT) polymerization of *n*-butyl acrylate was monitored by real time on-line mass spectrometry in a temperature interval from 100 to 190 °C for reaction times between 1 and 10 minutes.

In **Chapter 4**, the Passerini three-component reaction was studied using an on-line ESI-MS/microreactor setup. After screening, a reaction protocol was

proposed for the delivery of high yields within short minute range time frames under equimolar reactant concentrations. The established reaction protocol was then transferred to a conventional batch process for the synthesis of different diblock copolymer conjugates.

Chapter 5 focuses on the efficiency of SUMI reactions via the RAFT polymerization technique. Kinetic simulations of the radical insertion process very well fitted the experimentally obtained batch and microflow synthesis results. Furthermore, the optimized SUMI conditions were applied to upscale the SUMI synthesis reaction in a mesoflow reactor.

Sequence-defined linear monodisperse 18- and 20-mer oligoacrylates were synthesized in **Chapter 6** in a two-step approach. First, oligoacrylate sequences were synthesized via RAFT polymerization followed by disulfide coupling utilizing RAFT endgroup chemistry.

Chapter 7 continues in the field of sequence-defined materials by the synthesis of artificial peptides. Monodisperse 5-mers, consisting of acrylamide monomer units, are coupled with poly(ethylene glycol) (PEG) polymer chains. The pentamer-PEG conjugates were tested on their drug loading and release capabilities and compared to their peptide-PEG analogues.

Chapter 8 describes the used materials and all characterization methods related to the work described in **Chapter 2-7**. A summary (English and Dutch) and outlook are postulated in **Chapter 9**. Next, an overview of **publications, posters** and **conference contributions** is given. Finally, **acknowledgements** (het

dankwoord) are addressed to all people that contributed to this work, in one way or the other, throughout my PhD.

1.8 References

1. Jenkins, A. D.; Kratochvil, P.; Stepto, R. F. T.; Suter, U. W. *Pure and Applied Chemistry* **1996**, *68*, 2287.

2. Kaufmann, C. B. *ACS Symposium Series* **2011**, *1080*, 1.

3. Staudinger, H. *Chemische Berichte* **1924**, *57*, 1203.

4. Miloslav, N.; Jiri, J.; Bedrich, K., https://goldbook.iupac.org/html/M/M03667.html (Accessed August 2017).

5. polymerdatabase, http://www.polymerdatabase.com/polymer%20chemistry/Stepgrowth%20Polymerization.html (Accessed August 2017).

6. Odian, G. *Principles of polymerization*, 2nd ed.; John Wiley & Sons; New York **1981**, 280.

7. Conradi, M. H. *Development of Photoinitiated Polymer Conjugation Reactions based on [2+2] Cycloadditions of Functionalized Polymers,* Ph.D. Thesis **2014**.

8. Szwarc, M. *Nature* **1956**, *178*, 1168.

9. Jenkins, A. D.; Jones, R. G.; Moad, G. *Pure and Applied Chemistry* **2010**, *82*, 483.

10. Chiefari, J.; Chong, Y. K.; Ercole, F.; Krstina, J.; Jeffery, J.; Le, T. P. T.; Mayadunne, R. T. A.; Meijs, G. F.; Moad, C. L.; Moad, G.; Rizzardo, E.; Thang, S. H. *Macromolecules* **1998**, *31*, 5559.

11. Wang, J.-S.; Matyjaszewski, K. *Journal of American Chemical Society* **1995**, *117*, 5614.

12. Solomon, D. H. *Journal of Polymer Science Part A: Polymer Chemistry* **2005**, *43*, 5748.

13. Moad, G.; Rizzardo, E.; Thang, S. H. *Polymer* **2008**, *49*, 1079.

14. Keddie, D. J.; Guerrero-Sanchez, C.; Moad, G.; Rizzardo, E.; Thang, S. H. *Macromolecules* **2011**, *44*, 6738.

15. Benaglia, M.; Chiefari, J.; Chong, Y. K.; Moad, G.; Rizzardo, E.; Thang, S. H. *Journal of American Chemical Society* **2009**, *131*, 6914.

16. Moad, G.; Chong, Y. K.; Rizzardo, E.; Postma, A.; Thang, S. H. *Polymer* **2005**, *46*, 8458.

17. Moad, G.; Rizzardo, E.; Thang, S. H. *Australian Journal of Chemistry* **2005**, *58*, 379.

18. Engelis, N. G.; Anastasaki, A.; Nurumbetov, G.; Truong, N. P.; Nikolaou, V.; Shegiwal, A.; Whittaker, M. R.; Davis, T. P.; Haddleton, D. M. *Nature Chemistry* **2017**, *9*, 171.

19. Gody, G.; Maschmeyer, T.; Zetterlund, P. B.; Perrier, S. *Nature Communications* **2013**, *4*, 2505.

20. Gody, G.; Barbey, R.; Danial, M.; Perrier, S. *Polymer Chemistry* **2015**, *6*, 1502.

21. Rieger, E.; Alkan, A.; Manhart, A.; Wagner, M.; Wurm, F. R. *Macromolecular Rapid Communications* **2016**, *37*, 833.

22. Li, J.; He, J. *ACS Macro Letters* **2015**, *4*, 372.

23. Kawamura, M.; Kanazawa, A.; Kanaoka, S.; Aoshima, S. *Polymer Chemistry* **2015**, *6*, 4102.

24. Zhang, L.; Kucera, L. R.; Ummadisetty, S.; Nykaza, J. R.; Elabd, Y. A.; Storey, R. F.; Cavicchi, K. A.; Weiss, R. A. *Macromolecules* **2014**, *47*, 4387.

25. Li, Z.-L.; Zeng, F.-R.; Ma, J.-M.; Sun, L.-H.; Zeng, Z.; Jiang, H. *Macromolecular Rapid Communications* **2017**, DOI: 10.1002/marc.201700050.

26. Weiss, R. M.; Li, J.; Liu, H. H.; Washington, M. A.; Giesen, J. A.; Grayson, S. M.; Meyer, T. Y. *Macromolecules* **2017**, *50*, 550.

27. Gutekunst, W. R.; Hawker, C. J. *Journal of the American Chemical Society* **2015**, *137*, 8038.

28. Wei, B.; Li, W.; Zhao, Z.; Qin, A.; Hu, R.; Tang, B. Z. *Journal of the American Chemical Society* **2017**, DOI: 10.1021/jacs.6b12767.

29. Zhang, Z.; You, Y.-Z.; Wu, D.-C.; Hong, C.-Y. *Macromolecules* **2015**, *48*, 3414.

30. Solleder, S. C.; Schneider, R. V.; Wetzel, K. S.; Boukis, A. C.; Meier, M. A. R. *Macromolecular Rapid Communications* **2017**, *38*, DOI: 10.1002/marc.201600711.

31. Solleder, S. C.; Zengel, D.; Wetzel, K. S.; Meier, M. A. R. *Angewandte Chemie International Edition* **2016**, *55*, 1204.

32. Zydziak, N.; Feist, F.; Huber, B.; Mueller, J. O.; Barner-Kowollik, C. *Chemical Communications* **2015**, *51*, 1799.

33. Zydziak, N.; Konrad, W.; Feist, F.; Afonin, S.; Weidner, S.; Barner-Kowollik, C. *Nature Communications* **2016**, *7*, DOI: 10.1038/ncomms13672.

34. Takizawa, K.; Tang, C.; Hawker, C. J. *Journal of the American Chemical Society* **2008**, *130*, 1718.

35. ten Brummelhuis, N. *Polymer Chemistry* **2015**, *6*, 654.

36. Porel, M.; Thornlow, D. N.; Artim, C. M.; Alabi, C. A. *ACS Chemical Biology* **2017**, *12*, 715.

37. Porel, M.; Thornlow, D. N.; Phan, N. N.; Alabi, C. A. *Nature Chemistry* **2016**, *8*, 590.

38. Merrifield, R. B. *Journal of the American Chemical Society* **1963**, *85*, 2149.

39. Martens, S.; Van den Begin, J.; Madder, A.; Du Prez, F. E.; Espeel, P. *Journal of the American Chemical Society* **2016**, *138*, 14182.

40. Trinh, T. T.; Oswald, L.; Chan-Seng, D.; Lutz, J.-F. *Macromolecular Rapid Communications* **2014**, *35*, 141.

41. Al Ouahabi, A.; Kotera, M.; Charles, L.; Lutz, J.-F. *ACS Macro Letters* **2015**, *4*, 1077.

42. Knight, A. S.; Zhou, E. Y.; Francis, M. B.; Zuckermann, R. N. *Advanced Materials* **2015**, *27*, 5665.

43. Sun, J.; Zuckermann, R. N. *ACS Nano* **2013**, *7*, 4715.

44. Zuckermann, R. N. *Peptide Science* **2011**, *96*, 545.

45. Edwardson, T. G. W.; Carneiro, K. M. M.; Serpell, C. J.; Sleiman, H. F. *Angewandte Chemie International Edition* **2014**, *53*, 4567.

46. Grate, J. W.; Mo, K.-F.; Daily, M. D. *Angewandte Chemie International Edition* **2016**, *55*, 3925.

47. Wan, Z.; Li, Y.; Bo, S.; Gao, M.; Wang, X.; Zeng, K.; Tao, X.; Li, X.; Yang, Z.; Jiang, Z.-X. *Organic & Biomolecular Chemistry* **2016**, *14*, 7912.

48. Hartmann, L. *Macromolecular Chemistry and Physics* **2011**, *212*, 8.

49. Amalian, J.-A.; Trinh, T. T.; Lutz, J.-F.; Charles, L. *Analytical Chemistry* **2016**, *88*, 3715.

50. Mutlu, H.; Lutz, J.-F. *Angewandte Chemie International Edition* **2014**, *53*, 13010.

51. Oh, D.; Ouchi, M.; Nakanishi, T.; Ono, H.; Sawamoto, M. *ACS Macro Letters* **2016**, *5*, 745.

52. Xu, J.; Fu, C.; Shanmugam, S.; Hawker, C. J.; Moad, G.; Boyer, C. *Angewandte Chemie International Edition* **2016**, *129*, 8496.

53. Fu, C.; Huang, Z.; Hawker, C. J.; Moad, G.; Xu, J.; Boyer, C. *Polymer Chemistry* **2017**, *8*, 4637.

54. Houshyar, S.; Keddie, D. J.; Moad, G.; Mulder, R. J.; Saubern, S.; Tsanaktsidis, J. *Polymer Chemistry* **2012**, *3*, 1879.

55. Vandenbergh, J.; Reekmans, G.; Adriaensens, P.; Junkers, T. *Chemical Communications* **2013**, *49*, 10358.

56. Vandenbergh, J.; Reekmans, G.; Adriaensens, P.; Junkers, T. *Chemical Science* **2015**, *6*, 5753.

57. Zeng, L.; Burton, L.; Yung, K.; Shushan, B.; Kassel, D. B. *Journal of Chromatography A* **1998**, *794*, 3.

58. Haven, J. J.; De Neve, J. A.; Junkers, T. *ACS Macro Letters* **2017**, *6*, 743.

59. Wilms, D.; Klos, J.; Frey, H. *Macromolecular Chemistry and Physics* **2008**, *209*, 343.

60. Tonhauser, C.; Natalello, A.; Löwe, H.; Frey, H. *Macromolecules* **2012**, *45*, 9551.

61. Junkers, T. *Macromolecular Chemistry and Physics* **2017**, *218*, 1600421.

62. Haven, J. J.; Junkers, T. *European Journal of Organic Chemistry* **2017**, DOI:10.1002/ejoc.201700851.

63. Griffiths-Jones, C. M.; Hopkin, M. D.; Jönsson, D.; Ley, S. V.; Tapolczay, D. J.; Vickerstaffe, E.; Ladlow, M. *Journal of Combinatorial Chemistry* **2007**, *9*, 422.

64. Carter, C. F.; Lange, H.; Ley, S. V.; Baxendale, I. R.; Wittkamp, B.; Goode, J. G.; Gaunt, N. L. *Organic Process Research & Development* **2010**, *14*, 393.

65. Clegg, I. M.; Pearce, J.; Content, S. *Applied Spectroscopy* **2012**, *66*, 151.

66. Sans, V.; Porwol, L.; Dragone, V.; Cronin, L. *Chemical Science* **2015**, *6*, 1258.

67. Rosenfeld, C.; Serra, C.; O'Donohue, S.; Hadziioannou, G. *Macromolecular Reaction Engineering* **2007**, *1*, 547.

68. Levere, M. E.; Willoughby, I.; O'Donohue, S.; Cuendias, A. d.; Grice, A. J.; Fidge, C.; Becera, C. R.; Haddleton, D. M. *Polymer Chemistry* **2010**, *1*, 1086.

CHAPTER 2

Watching Polymers Grow: Real Time Monitoring of Polymerizations via an On-line ESI-MS/microreactor Coupling

Microreactors and **ESI Mass Spectrometry**

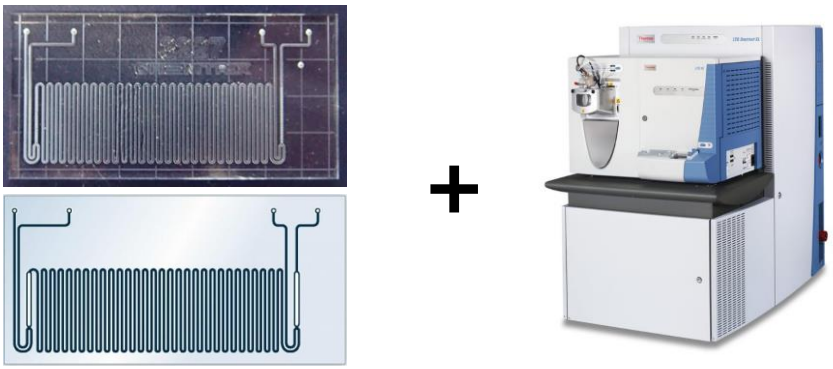

A perfect **on-line** monitoring couple

Haven, J. J.; Vandenbergh, J.; Junkers, T. *Chemical Communications* **2015**, *51*, 4611.

2.1 Abstract

A technique for the continuous on-line monitoring of polymerization processes by electrospray ionization mass spectrometry (ESI-MS) is presented for coupling with a commercial microreactor system. Its potential is demonstrated by monitoring polymerizations in real time during synthesis. Further, a single acrylate monomer insertion into a macro-RAFT agent, as used in the synthesis of monodisperse sequence-defined materials, was optimized by on-line screening of reaction conditions.

2.2 Introduction

On-line analysis of chemical processes provides real time data and thus allows for rapid kinetic screening and consequently efficient optimization of chemical reactions. Microreactor chip based systems feature significant advantages compared to batch reactors such as ideal heat dissipation, high operational stability and – as a consequence from the strictly isothermal conditions provided – relatively easy scale up of reaction conditions from milligram to kilogram scale or higher. A combination of both – continuous flow processing and on-line monitoring – constitutes an ideal tool in any chemical synthesis. Yet, on-line monitoring tools available for MRT are today still mostly limited to spectroscopic analysis such as infrared, UV-Vis detection and recently real time on-line NMR spectroscopy.[1-4] For batch processing, also several other tools exist to study the reaction mechanisms[5-7] which are, however, not directly applicable to flow reactions. Other product analysis techniques such as chromatographic or mass-spectrometric detection must usually be carried out off-line for MRT, slowing down optimization procedures and thus preventing the full exploitation of the high-throughput potential. Especially for polymerizations, the classical analysis tools are not sufficient for a meaningful on-line analysis of the reactions. Monitoring via spectroscopic methods often provides only limited information for polymerization reactions other than monomer conversions. Techniques such as electrospray ionization mass spectrometry (ESI-MS) to determine specific product patterns are much more valuable for modern precision polymer design and must hence be made available.[8-10]

Simple, but not continuous, on-line couplings of microreactor devices to mass spectrometers have been described in the literature.[5,11-12] Several approaches using either a six-port switching valve with a sample loop, a mass rate attenuator or other automated sampling methods have been utilized for sample transfer and injection into the MS.[13-16] Sam and coworkers[17] first implemented a low dead volume mixing tee, instead of a true microreactor, directly to the ionization probe. Other examples involve the investigation of reactive intermediates, reaction mechanisms and kinetics of chemical reactions in solution where a polyether ether ketone (PEEK) mixing tee was connected to the ionization probe by a fused silica transfer capillary allowing reactions times from 0.7 to 28 s in continuous flow mode. Reaction times could be varied by varying the length of the transfer capillary.[18-25] Continuous on-line monitoring of polymerization reactions was made available for the first time by Santos and Metzger.[26-27] They investigated the mechanism of the homogeneously catalyzed Ziegler-Natta polymerization of ethene and the Brookhart polymerization of alkenes, in early stages of the polymerization, by utilizing the same setup as mentioned above. While their approach allowed for important insights into the mechanisms, the setup was severely limited to certain reaction conditions (requiring extremely low reactant concentrations and limiting the choice of solvents available for the reaction) since only a micromixer element was employed rather than a microreactor chip (Figure 1.7, Chapter 1).

In this Chapter, the development of an on-line ESI-MS/microreactor coupling for fast and efficient screening and high-throughput optimization of chemical reactions – most prominently polymerizations but not limited to those – is described. This on-line setup allows for the continuous 'nonstop' analysis of the

reaction mixture at any given set of reaction conditions and microreactor residence times. Practically any instance in time of a reaction can be directly imaged by sweeping over a range of microreactor residence times, giving access to continuous data sampling with respect to product structure and composition under synthesis conditions. In another application, such a setup could also be used for continuous quality control of flow reactions, e.g. in commercial production settings. Sampling transfer from the flow microreactor to the probe is directly achieved under constant flow conditions without requirement of a sampling method. In such microreactors virtually any chemical reaction can be performed in a wide range of conditions and reactant concentrations, allowing for significantly higher flexibility with regards to reaction conditions and residence times.

In what follows, the procedure to achieve continuous ESI-MS coupling with a commercially available microreactor system (Labtrix Start, Chemtrix BV) is described (which has proven its use in organic synthesis[28] and in particular for precision polymer synthesis[29-30]), followed by two distinct examples that were chosen to demonstrate the high potential of such a technique for rapid kinetic screening and optimization of polymerization protocols. In particular the synthesis of high precision, added value polymers as further discussed will benefit from such an outcome since these materials require intense optimization and the isothermal conditions/high operational stability provided by microreactor technology to be economically feasible.

2.3 Experimental Section

2.3.1 Microreactor Setup

Microreactions were performed in a Labtrix Start R2.2 system (Chemtrix BV, NL), fitted with a glass microreactor chip (3227, reactor volume = 19.5 µL, a range of microreactor chips (different volume, design, *etc.*) are available) containing an SOR-2 static micromixer. Figure 2.1 shows a picture of the microreactor setup. Reactant solutions were introduced into the reactor through two 1 mL gas-tight syringes (SGE) capable of delivering two solutions at flow rates between 0.1 and 40 $\mu L \cdot min^{-1}$. The system was maintained at 20 bar of back-pressure by means of a pre-set ultralow dead volume (6 µL) back-pressure regulator (Upchurch Scientific, USA), in order to prevent boiling of the reactants and solvent system when temperatures above the atmospheric boiling point were employed. The flow rates were controlled via syringe pumps (Chemyx Inc., USA) and the reactor temperature was controlled via a thermoelectric cooler temperature controller MTTC1410 (Melcor Thermal Solutions). The 3227 microreactor chip (reactor volume = 19.5 µL) has two main reagent inlets, one quench inlet at the end and one main reaction outlet.

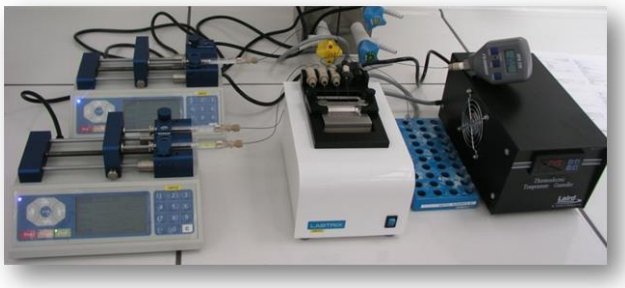

Figure 2.1. Commercially available microreactor setup.

2.3.2 ESI-MS/microreactor Coupling

Details of the microreactor setup are described in the Experimental Section 2.3.1. A flow chart and picture of the on-line ESI-MS/microreactor setup is shown in Figure 2.2. Reagent solutions are injected via syringe pumps (**A**) directly into the microreactor chip (**D**). The reaction temperature is regulated by a temperature controller (**C**) and microreactor heating unit (**B**). An in-line back-pressure regulator (**E**) (20 bar) increases the flow stability, allows for operation above ambient pressure boiling points of reactants and creates overpressure which contains the microreactor oxygen free if necessary. Reaction mixtures that exit the microreactor and pass through the back-pressure regulator are diluted with ESI-MS solvent mixtures by implementation of a T-splitter (Valco VICI stainless steel Tee) (**F**). Suitable ESI-MS solvent mixtures are introduced by a HPLC pump (Knauer, Germany) (**G**) and provided from the solvent reservoir (**H**). One dilution factor can be chosen for a certain concentration in the microreactor since the dimensions of the microreactor are very small. The quench inlet present in a 3227 microreactor chip can be utilized as a pre-dilution channel and can speed up the flow that exits the microreactor to have less dead time before injection into the ESI-MS. The diluted reaction mixture is split by a second T-splitter (Valco VICI stainless steel Tee) (**I**) to meet the flow requirements of the probe. Theoretically, a 360:1 fixed split is obtained by 45 cm polyether ether ketone (PEEK) tubing (1/32'' O.D. and 90 µm I.D.) and 340 cm perfluoroalkoxy alkane (PFA) tubing (1/16'' O.D. and 1/32'' I.D.) and calculated as follows:

$$\frac{F_{PEEK}}{F_{PFA}}\left(split\ ratio\right) = \frac{(l_{PFA} * r_{PEEK}^4)}{(l_{PEEK} * r_{PFA}^4)} = 0.002775\ (1:360)$$

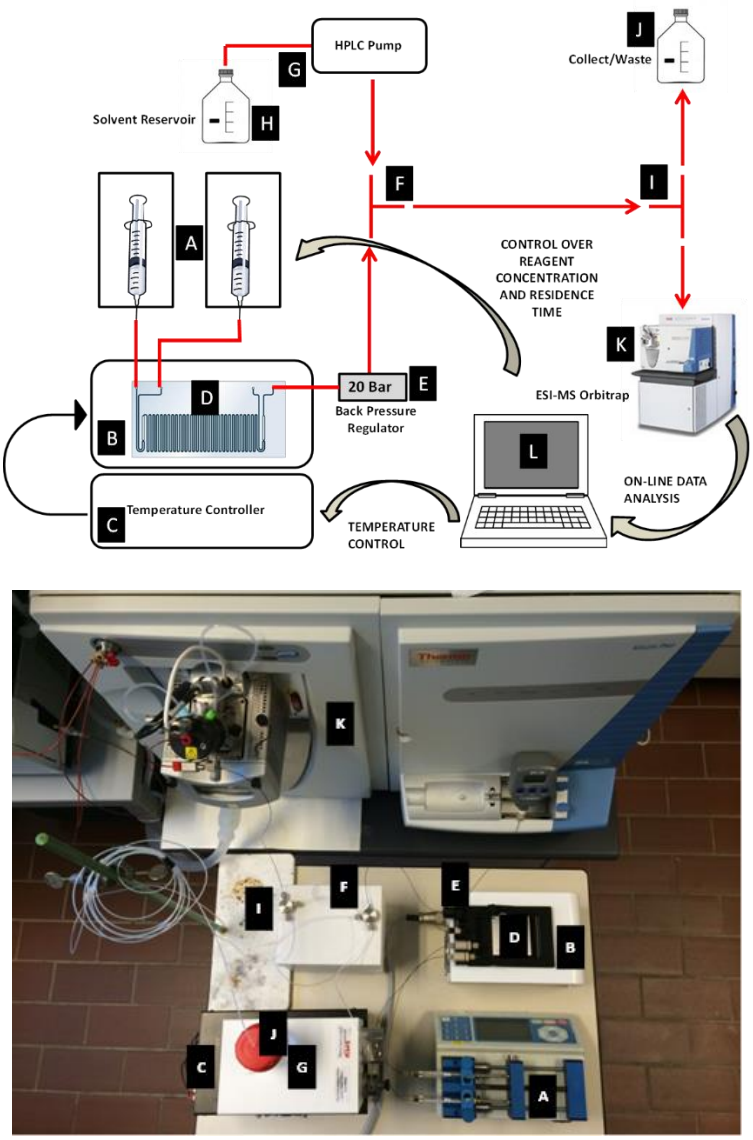

Figure 2.2. (top) Schematic flow chart of the on-line ESI-MS/microreactor setup with **A** Syringe Pumps (Chemyx) - **B** Heating Block - **C** Temperature Controller - **D** Glass Microreactor Chip - **E** Back-Pressure Regulator - **F** T-Splitter for Dilution - **G** HPLC Pump - **H** Solvent Reservoir - **I** T-Splitter for Flow Rate Control - **J** Waste Reservoir - **K** ESI-MS - **L** Computer Control and (bottom) Picture of the on-line setup.

The split ratio was experimentally validated by collecting solvent from the PEEK tubing for 13 minutes at a flow rate of 2000 µL/min (HPLC pump, before stainless steel Tee split). The volume was then measured by a microliter syringe (Hamilton, 100 µL), 70 µL was collected. Experimentally, the exact split ratio is 370:1 which is very close to the theoretically calculated value (360:1). The PFA split flow is drained or collected (**J**) while the PEEK split flow is directly injected into the ESI-MS (LTQ Orbitrap Velos Pro, ThermoFischer Scientific) (**K**). A fixed split can be applied that serves a large range of dilution factors due to the relatively broad ESI-MS window. Data are continuously collected by a central computer (**L**) and analyzed by Thermo Scientific Xcalibur software.

The dead volume in between the microreactor exit and the ESI chamber (nozzle) is 305 µL, calculated by considering the tubing lengths, tubing internal diameters and swept volumes of T-splitters and back-pressure regulator. The corresponding dead time that correlates with the dead volume depends on the flow rate of the reaction mixture in the microreactor (residence time), the dilution factor and the fixed split flow to the ESI-MS. In this work, as an example, a 2 mL/min dilution flow and 3.9 µL/min microreactor flow (5 minutes residence time) were applied which results in 3.13 min dead time. The dead time between the microreactor and the ESI-MS is mainly due to the unavoidable dead swept volume (6 µL) of the in-line back-pressure regulator (BPR). The dead time can be reduced by decreasing the PEEK tubing length between the microreactor and the first T-split (dilution), although a minimal PEEK tubing length is required for practical reasons. After the first T-split it is only a matter of seconds before injection into the MS since the flow rate is increased by dilution with proper MS solvent mixtures.

2.3.3 Synthetic Procedures

Materials and characterization methods are described in Chapter 8.

2.3.3.1 Synthesis of RAFT Agents

Reversible addition-fragmentation chain transfer (RAFT) agents 2-(dodecylthiocarbonothioylthio)propionic acid (**DoPAT**) and 2-cyano-2-propyl dodecyl trithiocarbonate (**CPD-TTC**) were synthesized according to literature procedures.[31-32]

2.3.3.2 Microreactor Synthesis of Poly(*n*-butyl acrylate)

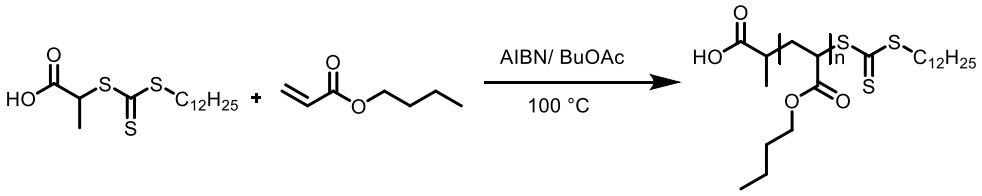

In a typical procedure, 17.58 mmol (2.25 g, 30 equiv.) of the monomer *n*BA, 0.06 mmol (0.01 g, 0.1 equiv.) of 2,2'-azobisisobutyronitrile (AIBN), 0.59 mmol (0.21 g, 1 equiv.) of 2-(dodecylthiocarbonothioylthio)propionic acid (DoPAT) and 1.5 mL of butyl acetate were added into a glass vial and sealed by a rubber septum. The solution was degassed for 15 min by N_2 purging, and subsequently inserted into the glovebox. The glass vial was opened and the solution was transferred to two gas-tight 1 mL syringes (SGE, Australia). The syringes were attached to the on-line ESI-MS/microreactor setup and a time-sweep experiment from 1 to 5 minutes microreactor residence time was performed as discussed further in section 2.4.1. Number average molecular weights and polydispersities of the polymer were measured manually by size exclusion chromatography (SEC) at 1 min (1100 $g.mol^{-1}$, 1.16) and 5 min (2700 $g.mol^{-1}$, 1.11) residence time in the microreactor (a sample was taken manually at the two fixed residence times). ESI-MS:

$[478.225 + n128.084]^{Na+}$. ESI-MS and SEC spectra (plots) are provided in the supporting information of the corresponding manuscript.[33]

2.3.3.3 Insertion of *n*-butyl acrylate into CPD-TTC RAFT Agent (A)

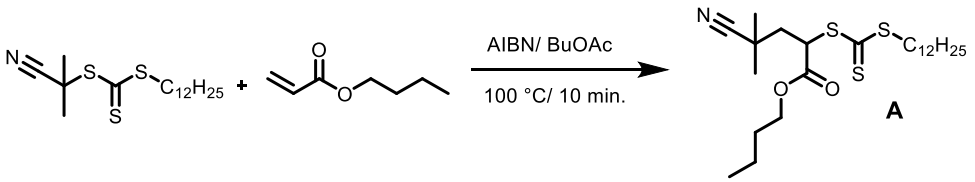

In a typical procedure, 15.60 mmol (2.00 g, 10 equiv.) of the monomer *n*BA, 0.08 mmol (13.00 mg, 0.05 equiv.) of AIBN, 1.56 mmol (0.54 g, 1 equiv.) of 2-cyano-2-propyl dodecyl trithiocarbonate (CPD-TTC) RAFT agent and 2 mL of butyl acetate were added into a sealed Schlenk tube. The schlenk tube was subjected to 3 freeze-pump-thaw cycles, and subsequently inserted into the glovebox. The schlenk tube was opened and the mixture was transferred into a glass vial with a stirring bar inside. The glass vial was placed in a copper heat-block at 100 °C. The mixture was reacted for 10 min at 100 °C and subsequently quenched by cooling the vial in liquid nitrogen and subjecting it to ambient atmosphere. Subsequently the mixture was transferred into an aluminium pan to evaporate the excess solvent and monomer, yielding 0.690 g of the crude product mixture. The mixture was purified via preparative HPLC (recycling SEC) to yield 0.347 g (48%) of pure *n*BA macro-RAFT agent (**A**). ^{1}H-NMR (300 MHz, $CDCl_3$, δ): 4.99 (dd, *J* = 9.7 and 4.5 Hz, 1H, CHCOO, backbone), 4.17 (t, *J* = 6.6 Hz, 2H, $CH_2OC{=}O$, side chain), 3.36 (t, *J* = 7.5 Hz, 2H, $CH_2SC{=}S$, chain end), 2.45 (dd, *J* = 14.4 and 9.7 Hz, 1H, $C\underline{H}_2CH$, backbone), 2.02 (dd, *J* = 14.4 and 4.5 Hz, 1H, $C\underline{H}_2CH$, backbone), 1.79−1.57 (m, 2H, CH_2, side chain + 2H, CH_2, chain end), 1.47 (s, 3H, CN-C-CH_3), 1.44−1.32 (br, 2H, CH_2, side chain + 2H, CH_2, chain end + 3H, CN-C-CH_3),

1.30−1.18 (br, 16H, CH_2, chain end), 0.97−0.90 (t, *J* = 7.4 Hz, 3H, CH_3, side chain), 0.90−0.83 (t, *J* = 6.8 Hz, 3H, CH_3, chain end). ^{13}C-NMR (75 MHz, $CDCl_3$, δ): 220.85, 169.91, 123.77, 66.31, 49.16, 42.25, 37.61, 32.04, 31.78, 30.42, 29.74, 29.67, 29.55, 29.47, 29.20, 29.02, 27.96, 27.56, 26.40, 23.39, 22.82, 19.20, 14.26, 13.81. ESI-MS (m/z): 496.24 ($M+Na^+$). NMR, Rec-SEC, SEC and ESI-MS spectra (plots) are provided in the supporting information of the corresponding manuscript.[33]

2.3.3.4 Insertion of 2-ethylhexyl acrylate into A

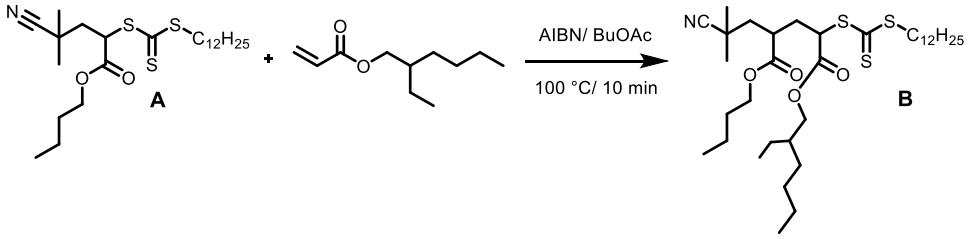

0.711 mmol (0.131 g, 5 equiv.) of the monomer 2-ethylhexylacrylate (EHA), 0.158 mmol (0.069 g, 1 equiv.) of macroRAFT agent **A** and 0.006 mmol (1.000 mg, 0.04 equiv.) of AIBN was prepared with butyl acetate as reaction solvent (V_{tot} = 2 mL). Chemicals were weighted in a glass vial with stirring bar and inserted into the glovebox and butyl acetate (V_{tot} = 2 mL) was added. The solution was stirred for 15 min to remove the residual oxygen. The solution was transferred to two gas-tight 1 mL syringes (SGE) and subsequently employed on the microreactor setup. The conditions applied to the microreactor were 100 °C and 5 min residence time. The reaction mixture was collected 7.4 h and transferred into an aluminum pan to evaporate the excess solvent and monomer. The crude product mixture was purified via preparative HPLC (recycling SEC) to obtain macroRAFT agent **B** as a yellowish oil in 43% yield (35 mg). ^{1}H-NMR (300 MHz,

$CDCl_3$, δ): 4.98−4.82 (m, 1H, CHCOO, backbone, EHA unit), 4.20−3.94 (br, 4H, $CH_2OC=O$, side chains), 3.35 (t, *J* = 7.5 Hz, 2H, $CH_2SC=S$, chain end), 2.82−2.66 (br, 1H, CHCOO, backbone, *n*BuA unit), 2.50−1.82 (br, 4H, $C\underline{H_2}CHC\underline{H_2}CH$, backbone), 1.75−1.50 (m, 2H, CH_2, *n*BuA side chain + 1H, CH, EHA side chain + 2H, CH_2, chain end), 1.46−1.15 (br, 10H, CH_2, side chains + 18H, CH_2, chain end + 6H, CN-C-$(CH_3)_2$), 0.94 (t, *J* = 7.4 Hz, 3H, CH_3, *n*BuA side chain), 0.91−0.80 (br, 3H, CH_3, chain end + 6H, CH_3, EHA side chain). ^{13}C-NMR (75 MHz, $CDCl_3$, δ): 221.27, 221.02, 174.30, 170.30, 170.17, 124.18, 68.37, 65.43, 50.55, 49.79, 42.66, 40.63, 40.29, 38.77, 37.62, 35.22, 34.71, 32.02, 31.74, 31.67, 30.59, 30.53, 30.40, 30.37, 29.74, 29.67, 29.55, 29.46, 29.21, 29.01, 27.98, 27.00, 26.96, 26.87, 26.75, 24.97, 23.83, 23.78, 23.09, 22.81, 19.31, 14.25, 14.19, 13.88, 11.10. ESI-MS (m/z): 680.38 ($M+Na^+$). NMR, Rec-SEC, SEC and ESI-MS spectra (plots) are provided in the supporting information of the corresponding manuscript.[33]

2.4 Results & Discussion

2.4.1. Watching Polymers Grow

The setup employed herein is shown in Figure 2.2 and described in detail in the experimental section 2.3.2. In short, reactions take place in a conventional microreactor chip (**D**). The reaction mixture is diluted prior to the back-pressure regulator with ESI-MS typical solvent mixtures (**G**,**F**) and part of that solution is then directly injected into the ESI-MS nozzle (**K**). One of the many advantages of such a setup is the high flexibility in terms of concentrations and reaction conditions that can be investigated. The herein used microreactor is highly flexible and allows reactions to be carried out between -10 and +195 °C. By choice of the reactor chip and mostly via flow rates, residence times below 1 s and up to 40 min can be achieved. All reactions are carried out under slightly elevated pressure to increase flow stability and to allow for operation above ambient pressure boiling points of reactants. Typical final polymer concentrations are in the range of 10-20 wt%. An issue to overcome with such on-line ESI-MS/microreactor coupling is the sample transfer from the microreactor to the ESI probe. When the microreactor is operated under true synthesis conditions, a reaction mixture is obtained at the reactor outlet that is unsuitable for MS analysis due to a mismatch in sample concentration, solvent, absence of doping agents and flow rate. These obstacles can, however, be conveniently overcome by a strong dilution of the reactor flow mixture after the back-pressure regulator (**E**) with suitable doped ESI solvent mixtures followed by splitting the flow in a T-splitter to meet the flow requirements of the probe. Dilution also serves thereby as an effective solvent change to decrease the sample concentration down to the micromolar range. A wide concentration window in the microreactor can be accessed; higher flow rates of

increased sample concentrations can be dynamically compensated for by adjusting the dilution factor.

As a first demonstration of how the on-line monitoring may be employed, a controlled radical polymerization was monitored, namely a reversible addition-fragmentation chain transfer (RAFT) polymerization (Scheme 2.1) of *n*-butyl acrylate (*n*BA) with the RAFT agent 2-(dodecylthiocarbonothioylthio)propionic acid (DoPAT) and 2,2'-azobisisobutyronitrile (AIBN) as thermal initiator.

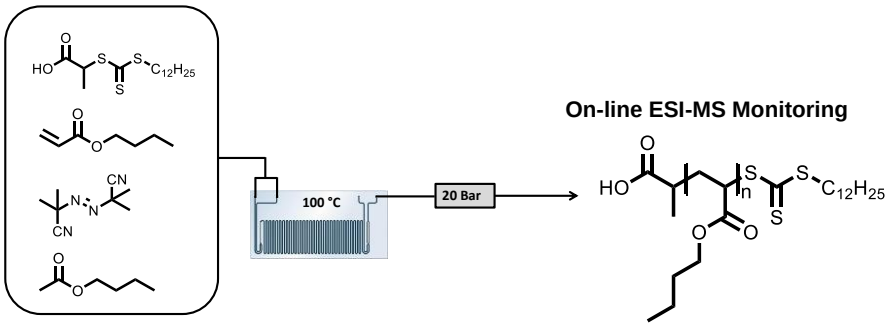

Scheme 2.1. On-line monitoring of a RAFT polymerization process by changing the microreactor residence time from 1 to 5 minutes at 100 °C.

RAFT polymerizations are characterized by a linear growth of the polymer chains with monomer conversion while retaining a high endgroup fidelity, which is a prerequisite for construction of precision materials. Typically, a RAFT polymerization is characterized by taking samples during the course of the polymerization whereby endgroup patterns are checked off-line via soft-ionization MS methods.[11] Here, the polymerization was continuously monitored by the on-line setup by sweeping over a given residence time range. Initial conditions applied to the microreactor were set to 1 minute residence time and 100 °C

reaction temperature. A polymer growth from 1100 to 2700 g·mol^{-1} (M_n) was recorded by increasing the residence time in the microreactor from 1 to 5 minutes. Figure 2.3 shows the ESI-MS spectrum at t_{res} = 1 minute, initial mass spectrum of poly(*n*-butyl acrylate) before sweeping over the residence time, and t_{res} = 5 minutes after the time-sweep experiment (final spectrum). A video of the time-sweep experiment is provided in the electronic supporting information of the corresponding article.[33] Within the time span of 5 minutes, an almost continuous set of kinetic data was obtained based on the specific product patterns recorded for each individual residence time.

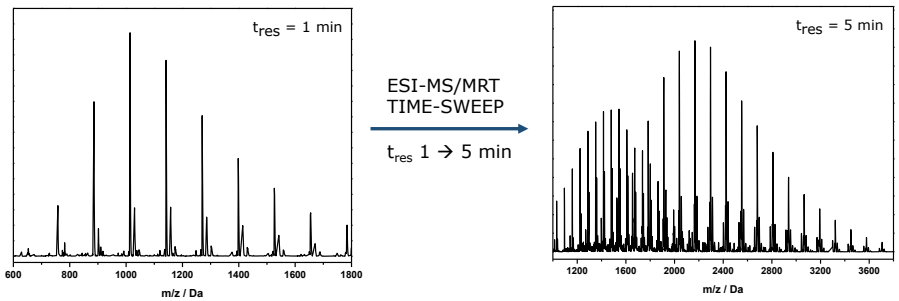

Figure 2.3. ESI-MS spectra of poly(*n*-butyl acrylate) RAFT polymerization after 1 minute and 5 minutes microreactor residence time. A polymer growth from 1100 to 2700 g·mol^{-1} (M_n) was recorded via an on-line ESI-MS/microreactor time-sweep.

2.4.1.2 Tracing AIBN Derived Endgroups in a RAFT Polymerization

To show the power of the newly developed ESI-MS/microreactor coupling a well-known "side" reaction in thermally intitiated polymerization via the RAFT technique was monitored. One of the polymer species detected in ESI-MS are polymer chains that carry a living trithiocarbonate (TTC) chain end but not the

RAFT reinitiating 'R' group as the non-living chain end ([R-[M]$_n$-TTC]). Instead, they carry an AIBN derived cyanoisopropyl (CIP) initiator endgroup ([CIP-[M]$_n$-TTC], Figure 2.4). The number of AIBN derived polymer chains typically depends on the residence time (t_{Res}) of the polymer mixture in the microreactor since AIBN initiator molecules constantly decompose throughout the polymerization. To determine the amount of CIP-initiated radicals obtained, the polymerization reaction was screened (microreactor time-sweep) from 1 to 5 minutes microreactor residence time as explained previously.

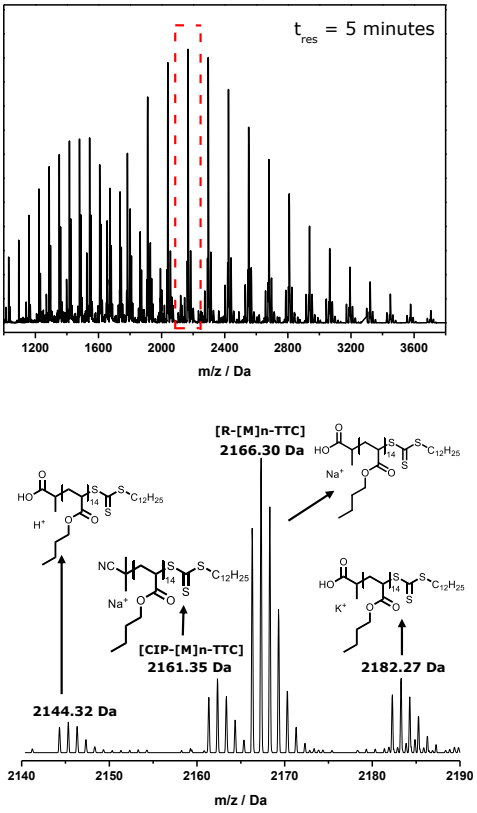

Figure 2.4. (top) ESI-MS spectrum of poly(*n*-butyl acrylate) RAFT polymerization after 5 minutes microreactor residence time and (bottom) zoomed ESI-MS spectrum with the CIP-initiated polymer species [CIP-[M]n-TTC] assigned.

Figure 2.5 shows the percentage of CIP-initiated polymer against the recorded time. The conditions applied to the microreactor were changed from 1 min to 5 min residence time, from that point on the ESI-MS spectra were recorded (time zero). The dead volume of the on-line setup, in between the microreactor exit and injection into the ESI probe, was calculated to be 305 µL which corresponds to 190 s (taking into account tubing lengths, tubing internal diameters, swept volumes and flow rates (see Experimental Section 2.3.2)). After increasing the residence time, an increase in the CIP-initiated polymer chains was observed after approximately 190 s recorded time, which correlates with the dead volume/time of the on-line setup and the conditions applied. Figure 2.5 was constructed by analysing the corresponding CIP-initiated polymer peak of the most intense polymer peak for each ESI-MS spectrum during the polymer growth. Spectra were analyzed every 3 seconds during the 600 seconds recorded time and in total 200 data points were analyzed. This method of analysis of the recorded ESI-MS spectra was a very time-consuming process since all spectra were analyzed manually. Therefore, at a later stage, this process was automated via a custom-made software script as described in Chapter 3. Using this script allows analysis of the full ESI-MS spectra taking into account every repeating unit of all polymer distributions present in each spectrum during the time-sweep experiment (> 55000 data points could be acquired in one single experiment as discussed in Chapter 3).

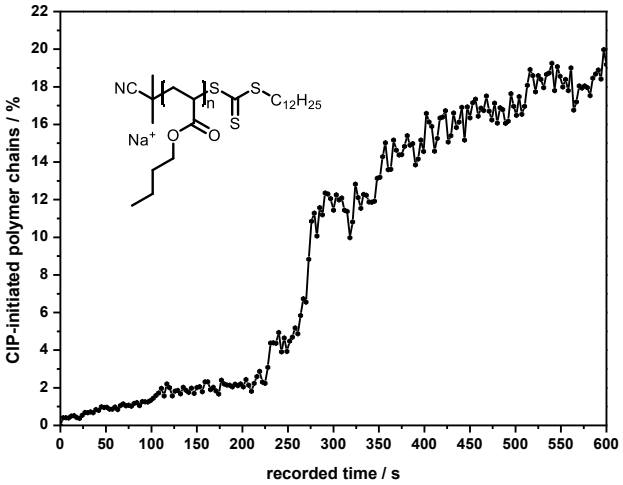

Figure 2.5. CIP-initiated polymer chains against recorded time in ESI-MS. The corresponding CIP-initiated polymer peak of the most intense polymer peak in the ESI-MS spectrum was analyzed every 3 seconds. In total 200 data points were analyzed.

Figure 2.6 represents the residence time of the reaction mixture in the microreactor, not to be confused with the recorded time in Figure 2.5. The conversion of the time axis, from recorded time to microreactor residence time, is carried out as follows:

From the time given in Figure 2.5, the dead volume time of 190 seconds is subtracted, then referred to as t_m. It is important to define at which time a certain volume increment had already been in the reactor at the time that the flow rate was changed (start of measurement). This specific residence time t_1 is given by:

$$t_1 = (1 - x_v) \cdot \frac{V_{reactor}}{f_1}$$

Whereby x_v represents the volume fraction that the volume increment has passed at t_1, $V_{reactor}$ the total volume of the reactor and f_1 the flow rate before the start of the measurement. The remaining residence time t_2 until exit from the reactor after switching flow rates is then consequently defined as:

$$t_2 = x_v \cdot \frac{V_{reactor}}{f_2} \quad \text{and} \quad x_v = t_2 \cdot \frac{f_2}{V_{reactor}}$$

With f_2 being the flow rate after the start of the measurement. The total residence time of any volume increment in the reactor is thus:

$$t_{res} = t_1 + t_2 = (1 - x_v) \cdot \frac{V_{reactor}}{f_1} + x_v \cdot \frac{V_{reactor}}{f_2}$$

Since $t_2 = t_m$, x_v can be inserted and the above equation can be rearranged to correlate t_m with the microreactor residence time t_{res}:

$$t_{res} = t_1 + t_m = \left(1 - t_m \cdot \frac{f_2}{V_{reactor}}\right) \cdot \frac{V_{reactor}}{f_1} + t_m$$

$$<=> t_{res} = \frac{V_{reactor}}{f_1} - t_m \cdot \frac{f_2}{f_1} + t_m$$

$$<=> t_{res} = \frac{V_{reactor}}{f_1} + t_m \left(1 - \frac{f_2}{f_1}\right)$$

Figure 2.6 (black trace) shows the fraction of AIBN derived polymer chains present in the polymer mixture as a function of residence time (polynomial fit applied, red trace). The ESI-MS peak intensity of [CIP-$[M]_n$-TTC] relative to [R-$[M]_n$-TTC] was analyzed every 3 seconds for the polymer repeating group that displayed the highest overall intensity, allowing to obtain 80 datapoints within few minutes (note

that higher scan rates are possible, but inevitably result in a lower S/N ratio). A continuous increase of CIP-initiated polymer chains from 2-17% was observed. 17% is, compared to the initial RAFT:AIBN (10:1) ratio, slightly higher than expected, which can be explained by the fact that with increasing chain length part of the distribution moves out of the ESI-MS observation window thus leading to a slight overestimation of the CIP-containing chains.[34] That the increase in CIP-terminated chain is not more steady can be explained by chemical bias effects. The onset period is in agreement with the time required to pass the characteristic pre-equilibrium stage of the RAFT process. It must therefore be noted that the example given in Figure 2.6 only serves the purpose of demonstrating that quasi-continuous data are accessible and was chosen accordingly. Much more detailed data evaluations (such as focus on each specific monomer repeat unit) are easily possible and can be subject of further investigations (see Chapter 3 for detailed kinetic investigation of poly(*n*-butyl acrylate)).

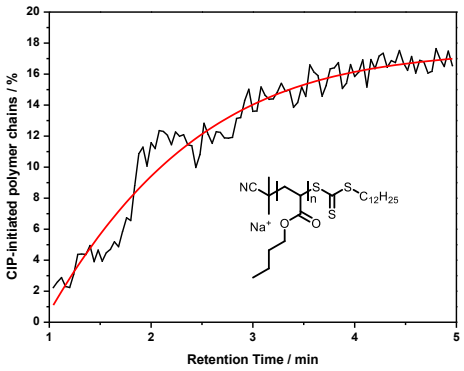

Figure 2.6. Fraction of CIP-initiated polymer chains as a function of residence time (1 to 5 minutes) in the RAFT polymerization of *n*BA at 100 °C in the microreactor (black trace). A polynomial fit was applied (red trace).

2.4.2 Single Unit Monomer Insertion (SUMI)

2.4.2.1 On-Line Monitoring of SUMI Reactions

To demonstrate the ESI-MS monitoring capacity for a more challenging case, the technique was applied for the accelerated optimization of a sequence-defined reaction. In sequence-defined polymerizations, the aim is to prepare monodisperse chains that carry encoded information and thus mimic biological precision.[35-39] A way to achieve such structures is to carry out controlled radical polymerizations (CRPs) in which only a few monomer units (ideally one) are added per polymerization, followed by isolation of the desired monodisperse product.[33,40-45] In Chapter 6, successfully consecutive single unit monomer insertion (SUMI) and multiple unit monomer insertion (MUMI) is demonstrated for the batch synthesis of 20-mers with a series of 4 different monomers using the RAFT polymerization technique.[43] Tedious optimization of the reaction conditions is required for SUMI reactions in order to increase the product yield and to minimize product isolation efforts (as these pose the biggest hurdle in the synthesis process) while SUMI reactions require optimization on very small scale due to the high value of even small amounts of starting material. In the microreactor, the SUMI of 2-ethylhexyl acrylate (EHA) was performed into the monodisperse macroRAFT agent α-[*n*BA]$_1$-ω (**A**), yielding the monodisperse product α-[*n*BA]$_1$-[EHA]$_1$-ω (**B**) as well as the side products **C** and **D** (α-[*n*BA]$_1$-[EHA]$_{2\text{-}3}$-ω, Scheme 2.2).The α and ω functional endgroups are derived from the RAFT agent inherent to the RAFT polymerization process. Details of the reaction are described in the experimental section 2.3.3. Although the SUMI reaction was optimized for **B**, the higher insertion products **C** and **D** are unavoidable due to the statistical nature of the radical addition. MacroRAFT agent **A** was synthesized in

batch and isolated via preparative HPLC (Recycling SEC) to obtain **A** in 49% isolated yield (experimental section 2.3.3.3). Secondly, the on-line ESI-MS/microreactor setup was then applied for the SUMI of EHA in **A**. The reaction was screened (see Table 2.1) for different reaction temperatures, residence times and reagent ratios in one single continuous experiment, thus again with minimal time and usage of only trace amounts of material. From the obtained data, optimum conditions were determined. These conditions were applied in an upscaled microreactor flow synthesis of **B**.

Within one single experiment, a large range of residence times and reagent ratios (by mixing EHA and **A** solutions from syringes with individual flow rates and by adjusting the reactor temperature) were screened. Results for the various conditions are given in Tables 2.1, 2.2 and 2.3. Table 2.1 and 2.2 represent the ESI-MS peak abundances and show the screening conditions and results for the synthesis of insertion product **B** (Scheme 2.2). Table 2.1 represents the peak abundances measured in ESI-MS for the insertion products **A**, **B**, **C** and **D**, which can be misleading due to the to mass and ionization biases where higher insertion products are expected to ionize more easily (e.g. due to their increased number of ester groups present in the side chains). Table 2.2 represents the relative peak abundances for **A** and **B** while **C** and **D** are removed from consideration (further explained in section 2.4.2.2). In Table 2.3 values are given for **A** and **B** that represent the true [**A**]:[**B**] molar ratios in the reaction mixture that exits the microreactor, which are determined based on ESI-MS calibration experiments discussed in section 2.4.2.2.

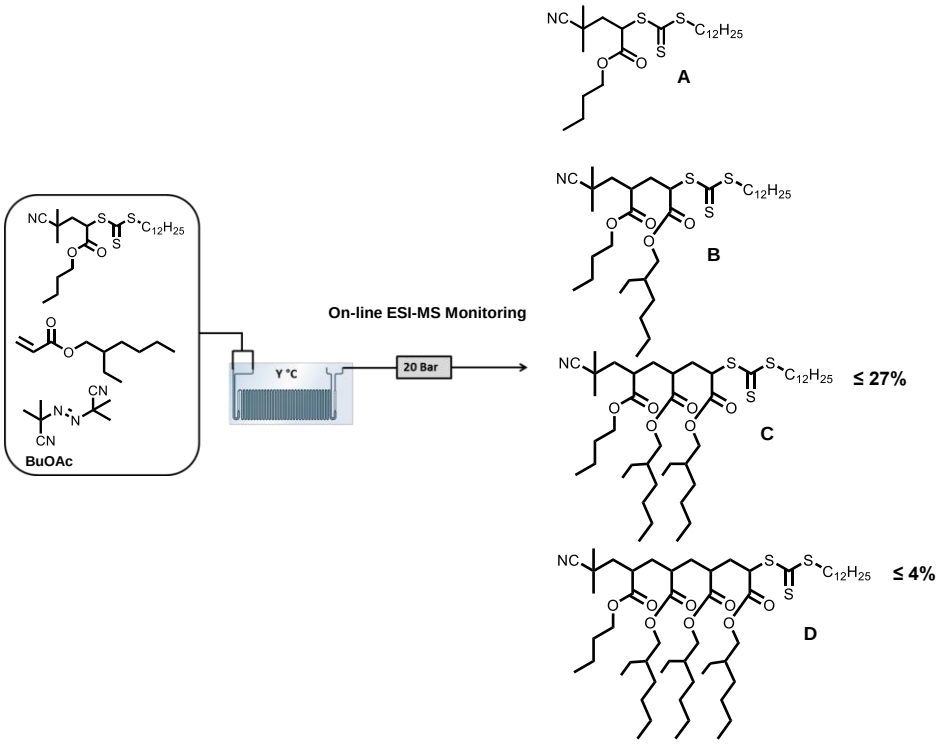

Scheme 2.2. Synthesis of the monodisperse macroRAFT agent **B** (microreactor synthesis). To isolate the desired product **B**, side products **A**, **C** and **D** need to be removed from the crude reaction product by preparative HPLC (recycling size exclusion chromatography).

Table 2.1 Screening conditions and ESI-MS results for the synthesis of insertion product **B**. The optimal reaction conditions are highlighted in bold (condition **11**).

Condition	Temperature (°C)	[EHA] : [1]	Residence Time (min)	A (%)	B (%)	C (%)	D (%)
1	95	5:1	10	50	38	10	2
2	95	10:1	5	41	50	9	0
3	95	10:1	7,5	11	58	27	4
4	100	1:1	5	70	30	0	0
5	100	2:1	5	47	49	4	0
6	100	2:1	10	22	62	16	0
7	100	3:1	8	9	61	27	3
8	100	4:1	6	12	60	25	3
9	100	5:1	2,5	40	54	6	0
10	100	5:1	4	16	62	20	2
11	**100**	**5:1**	**5**	**9**	**60**	**26**	**4**
12	110	3:1	2,5	19	65	16	0
13	110	3:1	4	9	68	19	4
14	110	2:1	4	28	61	11	0
15	110	2:1	5	20	64	16	0

Table 2.2. Screening conditions and ESI-MS results for the synthesis of insertion product **B**. Product **C** and **D** are left out of consideration. The optimal reaction conditions are highlighted in bold (condition **11**).

Condition	Temperature (°C)	[EHA] : [A]	Residence Time (min)	A : B
1	95	5:1	10	57 : 43
2	95	10:1	5	45 : 55
3	95	10:1	7,5	16 : 84
4	100	1:1	5	70 : 30
5	100	2:1	5	49 : 51
6	100	2:1	10	26 : 74
7	100	3:1	8	13 : 87
8	100	4:1	6	15 : 85
9	100	5:1	2,5	43 : 57
10	100	5:1	4	21 : 79
11	**100**	**5:1**	**5**	**13 : 87**
12	110	3:1	2,5	23 : 77
13	110	3:1	4	12 : 88
14	110	2:1	4	32 : 68
15	110	2:1	5	24 : 76

Table 2.3. On-line ESI-MS screening results and conditions for the synthesis of macroRAFT agent **B**. Values for **A** and **B** represent the mole fractions in the reaction mixture. The optimal reaction conditions are highlighted in bold (condition **11**).

Condition	Temperature (°C)	[EHA]:[A]	Residence Time (min)	[A]:[B]
1	95	5:1	10	65:35
2	95	10:1	5	53:47
3	95	10:1	7,5	18:81
4	100	1:1	5	78:22
5	100	2:1	5	58:42
6	100	2:1	10	32:68
7	100	3:1	8	15:85
8	100	4:1	6	18:82
9	100	5:1	2,5	51:49
10	100	5:1	4	26:74
11	**100**	**5:1**	**5**	**16:84**
12	110	3:1	2,5	29:71
13	110	3:1	4	14:86
14	110	2:1	4	39:61
15	110	2:1	5	29:71

2.4.2.2 ESI-MS Calibration

Figure 2.7 and 2.8 show the ESI-MS calibration curves for the reaction products **A**, **B** and **C**. Product **D** is only observed in small amounts (< 4%, Table 2.1) and was therefore left out of consideration to facilitate ESI-MS calibration. Calibration curves were established to correlate measured ESI-MS peak abundances (Table 2.1) with obtained product yields (mole fraction in reaction mixture, Table 2.3) since the peak abundances measured in ESI-MS are not quantitative due to mass-bias effects. Calibration curves of reaction products **A**, **B** and **C** confirm that product **C** ionizes more readily than **A** and **B** due to the increasing number of ester groups. Figure 2.7 represents the mole fraction of **A** and **B** against the peak abundance measured in ESI-MS. As expected, **A** is highly underestimated relative to **B**. To establish the calibration curves, a polynomial fit was applied and utilized to correlate the measured peak abundances and the obtained yields after applying the optimal conditions to the microreactor. Figure 2.8 represents the mole fractions of **A**, **B** and **C** against ESI-MS peak abundances where one out of the three products was varied while the other two were equimolar. Product **C** was overestimated relative to **A** and **B** but the ionization effect was less relative to the observations in Figure 2.7. Figure 2.9 represents the **A**:**B** peak abundance in ESI-MS for a constant [**A**]:[**B**] ratio (50:50) in the calibration mixture while **C** was varied. The **A**:**B** ESI-MS peak abundance remains relatively constant for different values of **C** in the calibration mixture.

Conditions can be chosen based on the **A** and **B** calibration curves since the **A**:**B** ratio remains relatively constant for different values of **C** according to Table 2.2. The [**A**]:[**B**] peak ratio remains mostly unaffected by the presence of **C** (Figure 2.9), hence giving access to comparatively simple calibration. The optimal reaction

condition for the synthesis of **B** is the one featuring the lowest [**A**]:[**B**] molar ratio where products **C** and **D** are only detected in close to negligible amounts. Condition **11** (100 °C / 5 min / 5:1) was identified and then applied to the continuous flow synthesis procedure (crude reaction mixture was collected for 7.4 h). The crude product mixture was dried and subjected to Rec-SEC for product separation, which gave rise to isolated yields of 14% for **A** and 43% for **B**. The isolated yields thus correspond relatively well to the molar ratio in Table 2.3 (note that the on-line experiment represents yields before isolation and that product was collected over a period of 7.4 hours prior to workup; significant amounts of product are also lost during purification, especially at small scale).

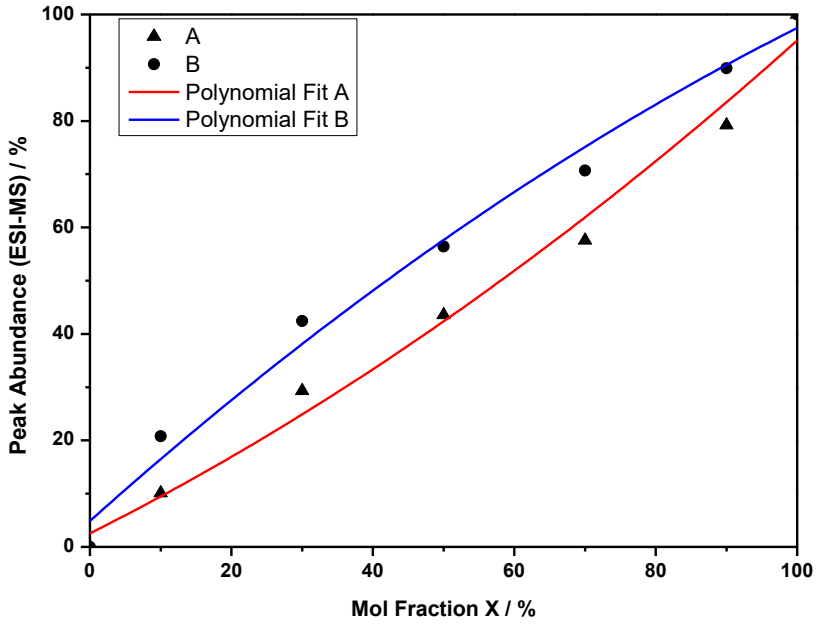

Figure 2.7. ESI-MS calibration curves for reaction products **A** and **B**.

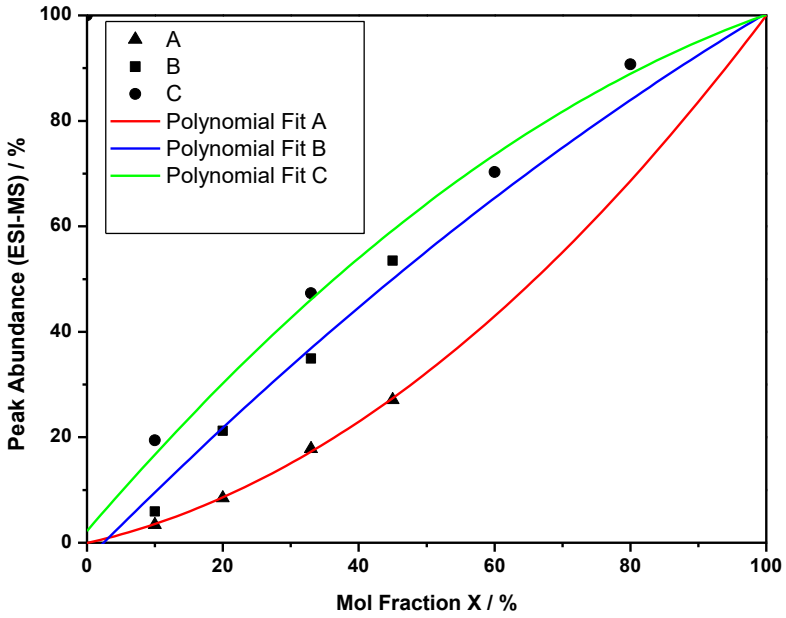

Figure 2.8. ESI-MS calibration curves for reaction products **A**, **B** and **C**.

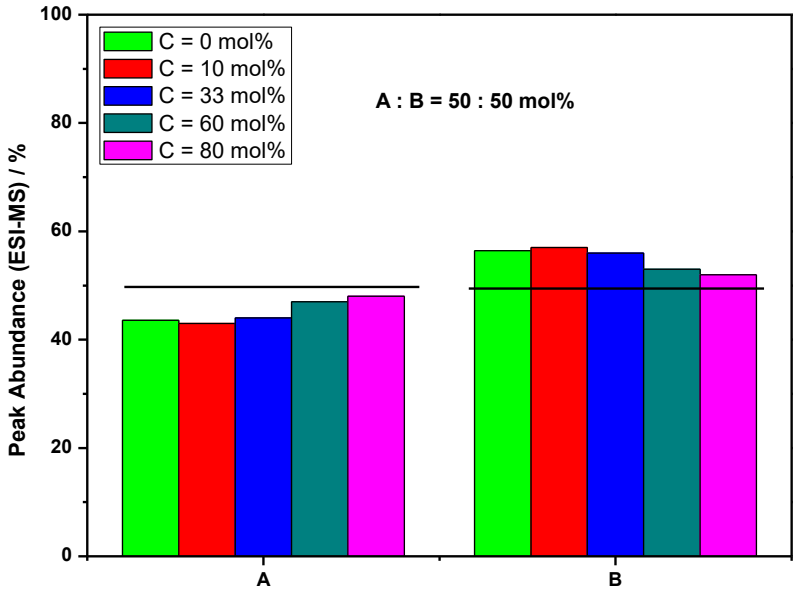

Figure 2.9. ESI-MS peak abundance of **A** and **B** for a constant **A**:**B** molar ratio in the calibration mixture while **C** is varied.

2.5 Conclusions

The on-line ESI-MS/microreactor monitoring shows high potential for the follow-up and optimization of chemical reactions. Polymerizations are easily and almost continuously monitored with respect to endgroup product patterns. At the same time, growth of species can be observed in real time, making correlation of endgroup distribution with the growth process accessible. For the example of a SUMI reaction, also the optimization potential of the setup is shown, demonstrating how optimal conditions for (flow) reactions can be found in minimal time and transferred to continuous synthesis for operation over extended periods of time. While in the present case, emphasis was put on polymerizations, application of the technique to conventional organic synthesis as regularly carried out in the employed microreactor system will pose no significant problem.

2.6 References

1. Griffiths-Jones, C. M.; Hopkin, M. D.; Jönsson, D.; Ley, S. V.; Tapolczay, D. J.; Vickerstaffe, E.; Ladlow, M. *Journal of Combinatorial Chemistry* **2007**, *9*, 422.

2. Carter, C. F.; Lange, H.; Ley, S. V.; Baxendale, I. R.; Wittkamp, B.; Goode, J. G.; Gaunt, N. L. *Organic Process Research & Development* **2010**, *14*, 393.

3. Clegg, I. M.; Pearce, J.; Content, S. *Applied Spectroscopy* **2012**, *66*, 151.

4. Sans, V.; Porwol, L.; Dragone, V.; Cronin, L. *Chemical Science* **2015**, *6*, 1258.

5. Santos, L. S. *European Journal of Organic Chemistry* **2008**, 235.

6. *Monitoring Polymerization Reactions: From Fundamentals to Applications,* ed. Reed, W. M.; Alb, A. M. *Wiley Louisiana,* **2014***,* Ch. 11, pp. 231-246.

7. Hungenberg, K.-D.; Reed, W. F. *Macromolecular Reaction Engineering* **2017**, DOI: 10.1002/mren.201700030.

8. Gruendling, T.; Weidner, S.; Falkenhagen, J.; Barner-Kowollik, C. *Polymer Chemistry* **2010**, *1*, 599.

9. Haven, J. J.; Baeten, E.; Claes, J.; Vandenbergh, J.; Junkers, T. *Polymer Chemistry* **2017**, *8*, 2972.

10. Haven, J. J.; Zaquen, N.; Rubens, M.; Junkers, T. *Macromolecular Reaction Engineering* **2017**, DOI: 10.1002/mren.201700016.

11. Fabris, D. *Mass Spectrometry Reviews* **2005**, *24*, 30.

12. Santos, L. S.; Knaack, L.; Metzger, J. O. *International Journal of Mass Spectrometry* **2005**, *246*, 84.

13. Browne, D. L.; Wright, S.; Deadman, B. J.; Dunnage, S.; Baxendale, I. R.; Turner, R. M.; Ley, S. V. *Rapid Communications in Mass Spectrometry* **2012**, *26*, 1999.

14. Bristow, T. W.; Ray, A. D.; O'Kearney-McMullan, A.; Lim, L.; McCullough, B.; Zammataro, A. *Journal of the American Society for Mass Spectrometry* **2014**, *25*, 1794.

15. M.Brivio; Liesener, A.; Oosterbroek, R. E.; Verboom, W.; Karst, U.; Berg, A. v. d.; Reinhoudt, D. N. *Analytical Chemistry* **2005**, *77*, 6852.

16. Fritzsche, S.; Ohla, S.; Glaser, P.; Giera, D. S.; Sickert, M.; Schneider, C.; Belder, D. *Angewandte Chemie International Edition* **2011**, *50*, 9467.

17. Sam, J. W.; Tang, X. J.; Magliozzo, R. S.; Peisach, J. *Journal of the American Chemical Society* **1995**, *117*, 1012.

18. Griep-Raming, J.; Meyer, S.; Bruhn, T.; Metzger, J. O. *Angewandte Chemie International Edition* **2002**, *41*, 2738.

19. Meyer, S.; Metzger, J. O. *Analytical and Bioanalytical Chemistry* **2003**, *377*, 1108.

20. Meyer, S.; Koch, R.; Metzger, J. O. *Angewandte Chemie International Edition* **2003**, *42*, 4700.

21. Santos, L. S.; Pavam, C. H.; Almeida, W. P.; Coelho, F.; Eberlin, M. N. *Angewandte Chemie International Edition* **2004**, *43*, 4330.

22. Santos, L. S.; Rosso, G. B.; Pilli, R. A.; Eberlin, M. N. *Journal of Organic Chemistry* **2007**, *72*, 5809.

23. Marquez, C. A.; Wang, H.; Fabbretti, F.; Metzger, J. O. *Journal of the American Chemical Society* **2008**, *130*, 17208.

24. Silva, B. V.; Violante, F. A.; Pinto, A. C.; Santos, L. S. *Rapid Communications in Mass Spectrometry* **2011**, *25*, 423.

25. Wang, H.; Yim, W.; Guo, Y.; Metzger, J. O. *Organometallics* **2012**, *31*, 1627.

26. Santos, L. S.; Metzger, J. O. *Angewandte Chemie International Edition* **2006**, *45*, 977.

27. Santos, L. S.; Metzger, J. O. *Rapid Communications in Mass Spectrometry* **2008**, *22*, 898.

28. *Micro Reaction Technology in Organic Synthesis, ed. C. Wiles and P. Watts, CRC Press, London, 2011*.

29. Vandenbergh, J.; Thales, M. O.; Junkers, T. *Journal of Polymer Science Part A: Polymer Chemistry* **2013**, *51*, 2366.

30. Vandenbergh, J.; Tiago, T.; Baeten, E.; Junkers, T. *Journal of Polymer Science Part A: Polymer Chemistry* **2014**, *52*, 1263.

31. Ferguson, C. J.; Hughes, R. J.; Nguyen, D.; Pham, B. T. T.; Gilbert, R. G.; Serelis, A. K.; Such, C. H.; Hawkett, B. S. *Macromolecules* **2005**, *38*, 2191.

32. Chen, M.; Moad, G.; Rizzardo, E. *Polymer Chemistry* **2009**, *47*, 6704.

33. Haven, J. J.; Vandenbergh, J.; Junkers, T. *Chemical Communications* **2015**, *51*, 4611.

34. Vandenbergh, J.; Junkers, T. *Macromolecules* **2014**, *15*, 5051.

35. Zamfir, M.; Lutz, J.-F. *Nature Communications* **2012**, *3*, 1138.

36. Pfeifer, S.; Lutz, J.-F. *Journal of the American Chemical Society* **2007**, *129*, 9542.

37. Gody, G.; Maschmeyer, T.; Zetterlund, P. B.; Perrier, S. *Nature Communications* **2013**, *4*, 2505.

38. Zydziak, N.; Feist, F.; Huber, B.; Mueller, J. O.; Barner-Kowollik, C. *Chemical Communications* **2015**, *51*, 1799.

39. Zydziak, N.; Konrad, W.; Feist, F.; Afonin, S.; Weidner, S.; Barner-Kowollik, C. *Nature Communications* **2016**, *7*, 13672.

40. Houshyar, S.; Keddie, D. J.; Moad, G.; Mulder, R. J.; Saubern, S.; Tsanaktsidis, J. *Polymer Chemistry* **2012**, *3*, 1879.

41. Moad, G.; Guerrero-Sanchez, C.; Haven, J. J.; Keddie, D. J.; Postma, A.; Rizzardo, E.; Thang, S. H. *in Sequence-Controlled Polymers: Synthesis, Self-assembly and Properties,* Ed. Lutz, J.-F.; Meyer, T. Y.; Ouchi, M.; Sawamoto, M. *ACS Symposium Series; American Chemical Society, Washington, DC,* **2014***, Vol. 1170,* Ch. 9, pp. 133-147.

42. Vandenbergh, J.; Reekmans, G.; Adriaensens, P.; Junkers, T. *Chemical Science* **2015**, *6*, 5753.

43. Haven, J. J.; De Neve, J. A.; Junkers, T. *ACS Macro Letters* **2017**, *6*, 743.

44. Haven, J. J.; Vandenbergh, J.; Kurita, R.; Gruber, J.; Junkers, T. *Polymer Chemistry* **2015**, *6*, 5752.

45. Gody, G.; Zetterlund, P. B.; Perrier, S.; Harrisson, S. *Nature Communications* **2016**, *7*, 10514.

CHAPTER 3

The Kinetics of *n*-Butyl Acrylate Radical Polymerization Revealed in a Single Experiment by Real Time On-line Mass Spectrometry Monitoring

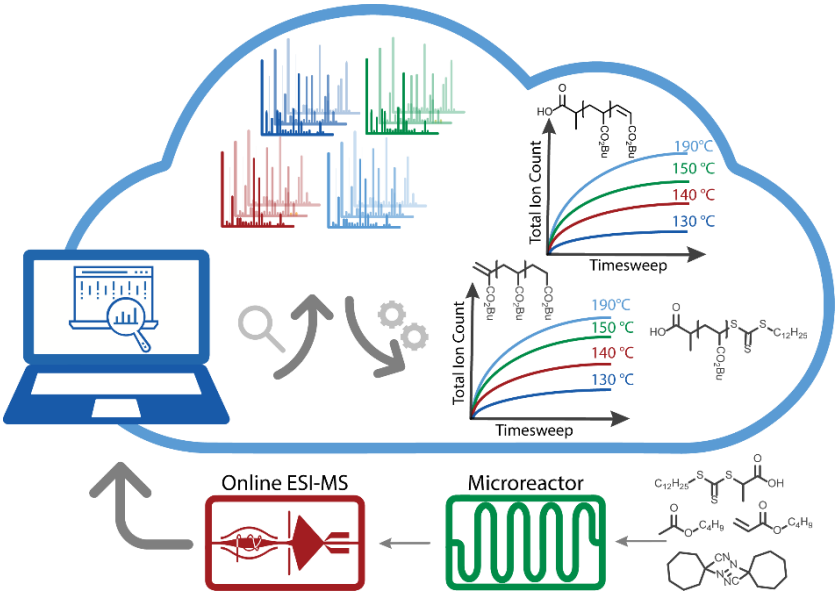

Haven, J. J.; Zaquen, N.; Rubens, M.; Junkers, T. *Macromolecular Reaction Engineering* **2017**, DOI: 10.1002/mren.201700016.

3.1 Abstract

The high-temperature trithiocarbonate-mediated RAFT (reversible addition-fragmentation chain transfer) polymerization of *n*-butyl acrylate is studied using a high-resolution mass spectrometric on-line monitoring method. Therefore, an Orbitrap mass spectrometer, ideally suited for polymer analysis, is coupled to a continuous flow microreactor. Via adjustment of flow rates in the reactor, time-sweep experiments can be carried out to allow monitoring of the entire polymerization process in a single experiment. The *n*-butyl acrylate polymerization is monitored in a temperature interval from 100 to 190 °C for reaction times between 1 and 10 minutes. In all cases full monomer conversions are reached and even at the highest temperatures relatively good molecular weight control and reasonably low dispersities are obtained. Endgroup analysis from mass spectrometry reveals, however, that the desired RAFT product is already less abundant than some side products at the lower temperatures. The herein described on-line monitoring technique gives access to quasi-continuous data acquisition, and is found to be very robust, and low in scattering when compared to classical batch sampling techniques.

3.2 Introduction

Acrylates – as one of the most commonly used monomers and in particular *n*-butyl acrylate[1-20] – have been investigated in great detail. Acrylate polymerizations differ significantly from the ideal free radical polymerization reaction scheme, especially at elevated temperatures. These differences originate from the formation of midchain radicals (MCR). More recently, it was reported that MCRs are not stationary but are able to move along the polymer backbone.[21] A MCR migration mechanism allows them to 'travel' along the polymer backbone through size-selective reaction pathways. Once a stable tertiary MCR is formed it can (*i*) react with monomer in a cross propagation step leading to chain branching. Alternatively, (*ii*) they can also terminate at a significantly reduced rate compared to SPRs or (*iii*) undergo β-scission reactions to yield macromonomer (MM) and SPRs. Kinetic parameters for propagation of SPRs and bimolecular termination events are well known in literature.[22] While the mechanistic reaction steps of MCRs are widely accepted, various attempts to determine individual rate coefficients of the MCR reaction pathways have been reported.[23-27] However, parameters are only partially known (mostly with relatively high uncertainty) for reaction steps arising from MCRs. Crucial information in the assessment of MCR follow-up reactions is the study of endgroup patterns in the polymer. While size-exclusion chromatography (SEC) does not give significant information on polymer endgroups, NMR spectroscopy can yield limited information about the endgroup composition. However, it rapidly loses its sensitivity with increasing degree of polymerization (DP_n). Soft ionization mass spectrometry techniques such as electrospray ionization (ESI) enable in contrast unambiguous determination of polymer endgroups within the chain length distribution. Although the obtained

spectra via ESI are not quantitative – due to ionization biases – and are restricted to lower molecular weight materials (typically 200-4000 m/z), they can map the product spectrum (e.g. exact composition of polymer chains) in very high detail and accuracy. Studies on acrylate polymerizations via soft ionization techniques have been reported.[28-30]

So far, the bottle neck in ESI-MS analysis – as with many other spectroscopic and spectrometric methods – lies in the fact that reactions are often only studied post-mortem, hence after polymerization has been stopped. This limits the amount of information available and moreover limits the number of data points available for each individual reaction. It may be hypothesized that if polymerizations could be monitored in much greater detail, more insights could be accessible with regards to determination of rate coefficients. An increased amount of data points would make fitting of data statistically more reliable, which of course is also correlated to data scattering and reproducibility of the results (which often is also a limiting factor in kinetic studies).

In Chapter 2, an on-line electrospray ionization mass spectrometry (ESI-MS)/microreactor monitoring setup was introduced that enables quasi-continuous acquisition of data throughout a single polymerization experiment. For the reversible addition-fragmentation chain transfer (RAFT)[31-35] *n*-butyl acrylate polymerization, time-sweeps from 1 to 10 minutes residence time were performed across a wide temperature range (100, 110, 120, 130, 140, 150 and 190 °C). Polymerization conditions were selected to evaluate the limits of the *n*-butyl acrylate RAFT polymerization with > 99% endgroup fidelity (100 °C and 10 minutes microreactor residence time) to an almost complete loss of polymer

endgroups (190 °C and 10 minutes microreactor residence time). The main RAFT polymer distribution (polymers with α, ω RAFT polymer endgroups), termination products as well as β-scission polymer products were identified and monitored continuously. To supplement the endgroup pattern data obtained from ESI-MS, time dependent information on monomer conversion (^{1}H-NMR) and average molecular weight distributions (SEC) were additionally acquired via off-line reaction screening under identical conditions employing microreactor technology. With these data on hand, a comprehensive understanding of the RAFT high temperature acrylate polymerization becomes possible, for which we provide here a first qualitative analysis. It should, however, be noted that the aim of this study was not the determination of kinetic information, but rather to demonstrate which level of information can be obtained from on-line MS monitoring of microreactor polymerizations, and how powerful this technique can be for future investigations.

3.3 Experimental Section

Materials and characterization methods are described in Chapter 8.

3.3.1 Microreactor Setup

Details of the microreactor setup are discussed in Chapter 2, section 2.3.1.

3.3.2 ESI-MS/microreactor Coupling

The ES-MS/ Microreactor coupling as described in literature is used for the detailed investigation towards the RAFT polymerization of *n*BA.[36-38] Details of the setup are discussed in Chapter 2 (section 2.3.2).

3.3.3 Synthetic Procedures

3.3.3.1 Synthesis of DoPAT RAFT Agent

2-(dodecylthiocarbonothioylthio)propionic acid (**DoPAT**) was synthesized according to a literature procedure.[39]

3.3.3.2 Off-Line Poly(*n*-butyl acrylate) RAFT Polymerization

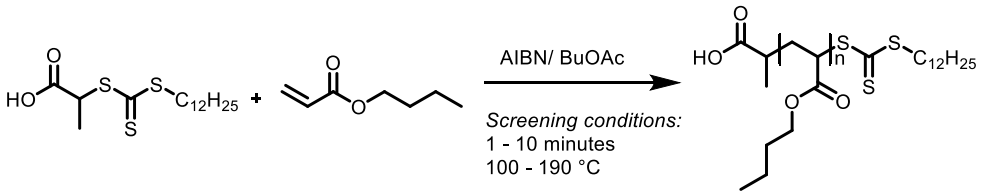

In a typical procedure, 35.93 mmol (4.60 g, 30 equiv.) of the monomer *n*BA, 0.12 mmol (29.27 mg, 0.1 equiv.) of 1,1'-azobiscyclohexanecarbonitrile (VAZO-88), 1.19 mmol (0.42 g, 1 equiv.) of 2-(dodecylthiocarbonothioylthio)propionic acid (DoPAT) and 3 mL of butyl acetate were added to a Schlenk tube and subjected to three freeze-pump-thaw cycles and subsequently inserted into the glovebox. The Schlenk tube was opened and the solution was transferred to two gastight 1

mL syringes (SGE), after which the syringes were connected to the Labtrix® system and used to pump the solutions into the microreactor (3227, microreactor volume 19.5 µL). Several reaction times (1 to 10 minutes residence time) as well as reaction temperatures (100 to 190 °C) were screened by collecting samples into small vials which were quenched by cooling the vial in liquid nitrogen and subjecting the contents to ambient atmosphere. Polymerization mixtures were analyzed by SEC and NMR to determine the molecular weights and monomer conversions of the collected samples.

3.3.3.3 On-Line Poly(*n*-butyl acrylate) RAFT Polymerizations

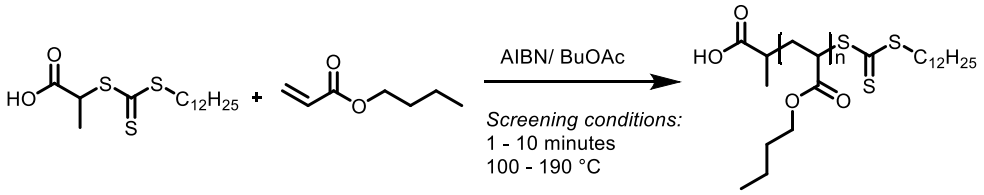

Sample preparation (gas tight syringes) for the on-line RAFT polymerizations followed a similar procedure as described above, concentrations chosen were identically. The gas tight syringes were filled in the glovebox and directly employed with the ESI-MS/microreactor setup. The reaction (residence) times were screened (time-sweeps) from 1 to 10 minutes and temperatures were chosen in a range between 100 and 190 °C.

3.3.5 Python Software Script

A Python software script was developed by a colleague, Maarten Rubens (Ph.D. Student), for extraction of the relevant data from the ESI-MS data set. The data generated by the Python script consist of m/z intensities pairs for all scans recorded during the on-line ESI-MS measurement. These data were subsequently saved as an excel file for further processing. The Python script acts as an interface

to enable the use of Thermo MSFileReader C++ dynamic-link library, provided by ThermoFisher for the processing of MS data.[40] The complete software script is provided in the supporting information of the corresponding manuscript.[41]

3.4 Results & Discussion

3.4.1 Midchain Radical Pathways

Besides propagation (k_p) of the secondary propagating radical (SPR^X), the radical functionality of the growing chain end can be transferred to the polymer backbone to form a more stable tertiary radical (MCR^X), as shown in Scheme 3.1. Intermolecular transfer is a bimolecular process and requires dead (or dormant) polymer to be present. The intramolecular transfer pathway can also be seen as bimolecular between one of the monomeric units in the polymer backbone and the radical chain end functionality. Intramolecular transfer reactions to random positions on the backbone are assumed to occur with a general rate coefficient k_{intra}. More favored is the so-called intramolecular backbiting (k_{bb}, m = 1, Scheme 3.1) which is unimolecular and occurs via a [1,5] H-shift reaction electronically favored by a six-membered transition state structure. Other reactions that secondary propagating radicals (SPR^X) can undergo are propagation (k_p) as mentioned before, conventional bimolecular termination (k_t) events as combinations and disproportionation and transfer to the CTA (RAFT) agent ($k_{trans,CTA}$) inherent to the RAFT polymerization process. Theoretically a very small amount of the stable tertiairy $MCRs^X$ formed can react with the trithiocarbonate RAFT endgroup. These products are not shown in Scheme 3.1 since they are not identified in the recorded ESI-MS spectra as discussed in the literature previously.[42-43]

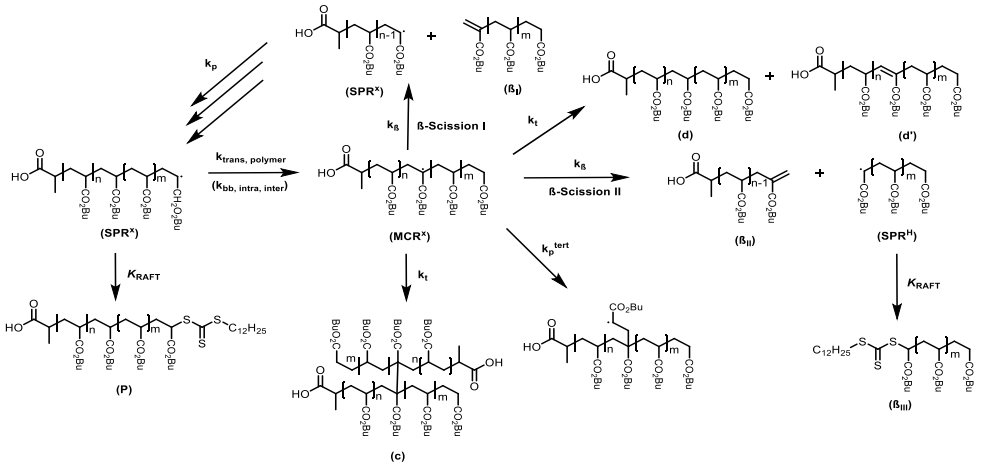

Scheme 3.1. Primary reaction pathways of a midchain radical (MCR^X).

Once a MCR is formed it can follow three different pathways (Scheme 3.1). Firstly, it can propagate further causing branched polymer structures, although at a significantly reduced rate (k_p^{tert}) compared to SPRs (k_p), by which the tertiary radical is transformed back into a SPR. Secondly two radicals can undergo termination (k_t) to form a 3- or 4-arm star structure referred to as combination [(c)] or disproportionation [(d)] yielding unbranched structures. MCR^X propagation (k_p^{tert}) and termination (k_t) products are not distinguishable from conventional SPR^X termination products via mass spectrometry. Thirdly, the formed MCR^X can undergo β-scission reactions to yield four different fragments. One is identical to the SPR^x, two other fragments are dead polymer chains carrying an unsaturated endgroup (so-called macromonomers β_I and β_{II}) and the fourth is also a secondary propagating radical (SPR^H) but without the reinitiating RAFT α-endgroup that can either propagate further (can form MCRs and undergo the same pathway as SPR^X) or enter the RAFT equilibrium and hence gain a trithiocarbonate endgroup (β_{III}).

A different type of reaction that has to be considered during RAFT polymerization at elevated temperatures is thermolysis of the living chain end via a concerted Chugaev elimination reaction (Scheme 3.2).[44-45] In this process the RAFT endgroup is removed to yield an unsaturated macromonomer (T_I, Scheme 3.2). Next to the Chugaev elimination route a second mechanism for thermolysis has been proposed namely consecutive homolysis of the C-S bond to end up with a secondary propagation radical (SPR^X, Scheme 3.1). Thus, at elevated temperature thermolysis needs to be considered as a potential MCR^X source although its contribution to the MCR follow-up reactions is expected to be relatively small.

Scheme 3.2. Thermolysis reaction of the RAFT living endgroups at elevated temperatures via a concerted Chugaev elimination process.

3.4.2 Time Dependent Off-Line Measurements

As a preparation for the envisaged ESI-MS on-line monitoring first supplementary data were collected. Since the aim is to provide a comprehensive dataset for modelling of the reactions, not only endgroup patterns, but also data on conversion, molecular weight and dispersity are required. Ideally, these would be likewise obtained via on-line monitoring. In the present case, they were obtained from classical off-line monitoring. It should be noted that modelling of the ESI-MS data alone is in principle sufficient.[46] Off-line molecular weight and conversion data can be used as a crosscheck rather than a direct fitting parameter. To obtain

a good reproducibility of the off-line sampling, the same microreactor system was used to prepare samples, giving access to very reliable data – as compared to off-line data collected from batch operations. Flow rates were set according to target residence times and after stabilization of the microreactor, resulting polymer mixtures were quenched and analyzed by NMR and SEC. Results are summarized in Table 3.1 and visualized in Figure 3.1 and Figure 3.2.

Table 3.1 lists the screening results for the off-line RAFT polymerization of *n*-butyl acrylate. RAFT polymerizations are generally characterized by a linear growth of the polymer chains with monomer conversion while retaining a high endgroup fidelity. Results clearly support this behavior, as expected, with an increase in residence time leads to an increase in conversion (as determined via ^{1}H-NMR) as well as number average molecular weight (M_n) value, while keeping the dispersity ($Đ$) values low (< 1.5). In addition, an increase in reaction temperature is accompanied with an increase in polymerization rate, as reactions performed > 120 °C reach maximum conversion in less than 10 minutes of reaction time. A maximum rate of polymerization seems to be reached at 150 °C, which can be explained by the rate of initiator consumption. At 150 °C, VAZO-88 is associated with a half-life time in the range of several seconds, hence from this temperature on reactions are not strictly driven anymore by classical initiation, but rather – at least to some extent – self-initiation of the polymerization. Yet, reactions were screened up to 190 °C to give a complete overview of the reaction (note that the microreactor is operated under pressures of 20 bar to prevent boiling of the solvent and monomer). A truly successful RAFT polymerization is not expected anymore under such conditions, but study of these reactions allows for further insights into kinetic trends.

Table 3.1. Off-line microreactor screening results for the RAFT polymerization of *n*-butyl acrylate at 100, 110, 120, 140, 150, 170 and 190 °C.

Entry	Reaction Temperature	Residence Time	Conversion[a]	*Đ*	M_n[b]
	°C	min			g·mol^{-1}
1	100	1	17	1.05	660
2	100	2.5	23	1.08	810
3	100	5	29	1.08	1100
4	100	10	75	1.08	1750
5	100	20	> 99	1.10	2700
6	110	1	21	1.13	920
7	110	2.5	27	1.13	1150
8	110	5	52	1.10	2250
9	110	7.5	65	1.09	2700
10	110	10	80	1.10	2780
11	120	1	64	1.13	1100
12	120	2.5	88	1.08	1830
13	120	5	84	1.10	2280
14	120	7.5	> 99	1.12	2410
15	120	10	> 99	1.21	2570
16	140	1	65	1.09	1820
17	140	2.5	90	1.14	2300
18	140	5	97	1.18	2400
19	140	7.5	> 99	1.23	2350
20	140	10	> 99	1.23	2400
21	150	1	70	1.15	2140
22	150	2.5	91	1.22	2390
23	150	5	94	1.27	2260
24	150	7.5	> 99	1.31	2250
25	150	10	> 99	1.34	2280
26	170	1	86	1.31	2480
27	170	2.5	93	1.31	2560
28	170	5	95	1.32	2550
29	170	7.5	96	1.32	2570
30	170	10	> 99	1.32	2600
31	190	1	79	1.24	1750
32	190	2.5	84	1.27	1810
33	190	5	87	1.27	1790
34	190	7.5	90	1.29	1780
35	190	10	93	2.90	1010

[a] Conversions are determined using ^{1}H-NMR in $CDCl_3$ of the crude reaction mixture.
[b] Molecular weights are determined via THF-SEC based on polystyrene standards and *n*BA MKHS parameters

In this context it is interesting to see that 190 °C still provides quite satisfying polymerization results at first glance. Polymerizations remain under good RAFT control up to very high temperatures and only from 170 °C on are decreasing product properties observed. This effect is also identified in Figure 3.1 where M_n as a function of monomer conversion is plotted for different reaction temperatures. Relatively high scatter is observed in the data, which can largely be attributed to the fact that polymerizations proceed so fast with increasing temperature that even after 1 minute reaction (residence) time very significant conversions are already reached. In addition to the side reactions, which are all associated with high activation energies and which thus become progressively prominent with increasing temperatures, deviations from ideal molecular weight must be expected as β-scission decreases the average molecular weight of the product. Yet, up to 170 °C increasing M_n with conversion is observed in all cases, whereas at 190 °C the molecular weight tends to remain more or less constant despite an increase in conversion.

The most ideal RAFT dataset was obtained at 110 °C, and hence these data were analyzed more closely in Figure 3.2. Molecular weights increase well within theoretical expectations and dispersity decreases over time, which is expected for a Poisson distribution. Overall, very good control over the reaction can be postulated for 110 °C, indicating that MCR reactions do not have a large negative effect on the polymerization at this temperature at least when only M_n and dispersity are used as a measure for success of the reaction.

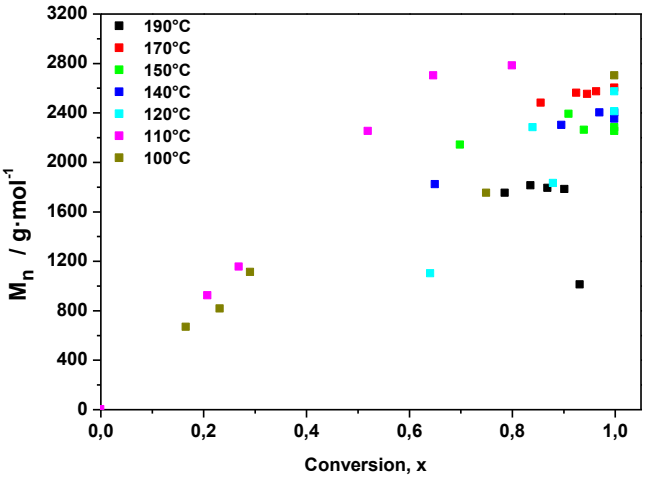

Figure 3.1. Number average molecular weight (M_n) as a function of the *n*-butyl acrylate monomer conversion during RAFT polymerization at different temperatures screened via off-line microreactor technology.

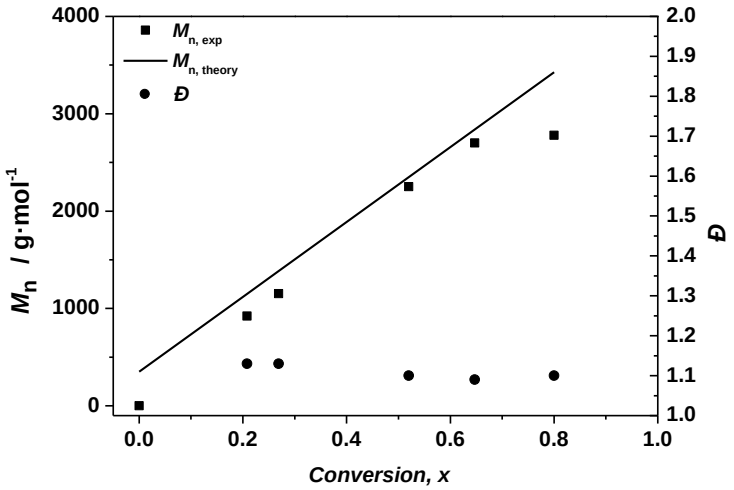

Figure 3.2. Number average molecular weight (M_n) as a function of the *n*-butyl acrylate monomer conversion during RAFT polymerization screened via off-line microreactor technology at 110 °C.

3.4.3 On-Line ESI-MS/microreactor Screening

In the following paragraph, on-line monitoring of the polymerization was carried out via ESI-MS coupling of the microreactor. Gastight syringes were filled with a degassed reaction mixture of *n*-butyl acrylate (*n*BA, 30 equiv.), RAFT agent 2-(dodecylthiocarbonothioylthio)propionic acid (DoPAT, 1 equiv.), 1,1'-azobiscyclohexanecarbonitrile (VAZO-88, 0.1 equiv.) as the thermal initiator and butyl acetate as the reaction solvent, identical to the off-line screening experiments. To carry out the time-sweep experiments, the microreactor flow rate was set at 19.5 μL/min corresponding to a residence time of 1 minute at a fixed microreactor temperature and concentration of the reaction mixture. Once a stable ESI-MS signal is obtained, the microreactor (19.5 µL) flow rate was adjusted from 19.5 to 1.95 µL/min (1 to 10 minutes residence time) and ESI-MS spectra were continuously acquired for 10 minutes. Note that the dead volume between the microreactor exit and ESI-MS nozzle needs to be accounted for when recalculating the time-sweep data (in practice data acquisition happens for 10 minutes + dead time). Via this technique all residence time points between 1 and 10 minutes are continuously recorded which allows access to any residence time point during polymerization. No quenching of the products is required as the temperature drops to room temperature almost instantly after the microreactor outlet.

Care has to be taken when performing these measurements, as the amount of data acquired in a short time interval (10 minutes) for each polymerization is very significant. As an example in this study, ESI-MS spectra are measured every 2.2 seconds. Hence, in total 275 ESI-MS spectra are acquired in a time-sweep from 1 to 10 minutes, giving access to all individual chains and products simultaneously.

To obtain information of a single polymer distribution present in the spectra, peak intensities for all polymer repeating units, in every single ESI-MS spectrum, need to be extracted.

In Figure 3.3 the different species observed during the polymerization of *n*-butyl acrylate at 100 to 150 °C (10 °C increments) and 190 °C are assigned at 10 minutes microreactor residence time, which correspond to their chemical structure shown in Scheme 3.3 and their exact isotopic mass displayed in Table 3.2. The ESI-MS spectra were analyzed and shown for a fixed time point (10 minutes microreactor residence time) in a time '*sweep*' from 1 to 10 minutes microreactor residence time. Spectra are only displayed for a zoomed region [1688-1785 m/z] covering a full monomer repeat unit, and hence all different species present. For different temperatures, identical polymer species were observed. However, peak intensities vary with the polymerization temperature. Under the assumption that all sub-distributions are subject to the same mass discrimination effects, a relative comparison is still possible and kinetic trends can be discerned. The main polymer distributions at 100 °C in Figure 3.3 are assigned to the sodium adduct of P*n*BA RAFT polymer species $[P]^{XNa+}$ [X = 1 (1782.0527 m/z for n = 11), 2 (1735.0675 m/z for n = 24) and 3 (1719.4023 m/z for n = 37)]. Bimolecular termination products ([c], [d] and [d']) as expected in a radical polymerization process are only observed in very low quantities, in line with the degenerative transfer active in RAFT. While the 100 °C spectrum shows few side products, hence demonstrating good control in line with the observations made during the off-line measurements described above, higher temperatures reveal a very significant and fast increase in side product formation. β-scission products [β_I (1688.0792 m/z for n = 13), β_{II} (1774.1163 m/z for n = 13) and β_{III} (1696.0150 m/z for n = 11)]

become significantly more prominent with temperature, as well as species stemming from RAFT endgroup elimination. While the Chugaev product is still not the most abundant species at 190 °C, β-scission products clearly exceed the main RAFT polymer peak at higher temperatures. This onset of RAFT endgroup elimination explains why control is lost at the highest temperature. The relatively high amount of scission products though do not directly contradict RAFT control. β-Scission products do not directly harm the RAFT equilibrium (in fact they undergo themselves addition-fragmentation equilibria with secondary propagating radicals) and merely result in a slight broadening of polymer distributions, a loss in RAFT endgroups is necessarily correlated with a loss of control. While this observation is completely in line with the kinetic picture known from the literature, the extent of macromonomer formation under conditions where the RAFT polymerization still shows fairly good control over molecular weight is astounding.

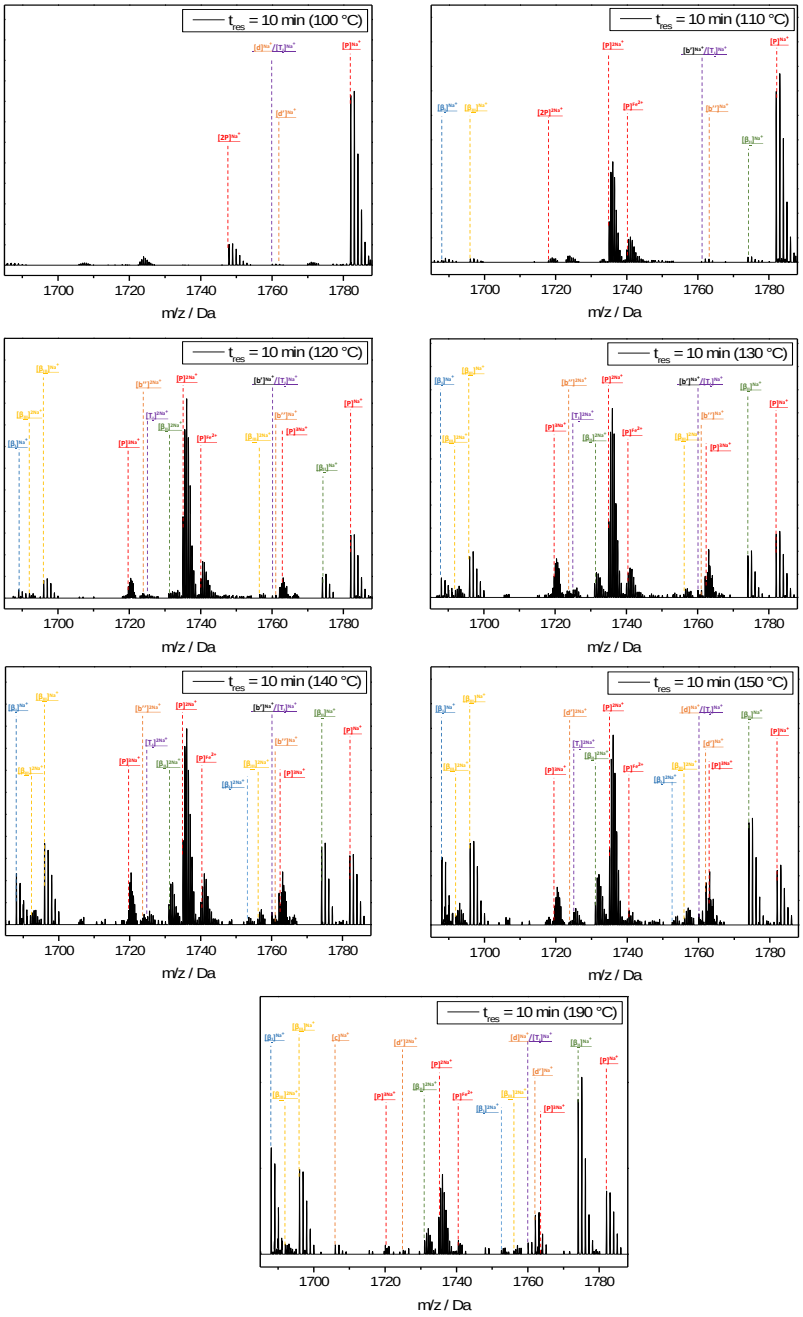

Figure 3.3. Zoomed [1688-1785 m/z] ESI-MS spectra from the different polymer species observed at 100, 110, 120, 130, 140, 150 and 190 °C at a fixed time point (10 minutes) in a time '*sweep*' from 1 to 10 min.

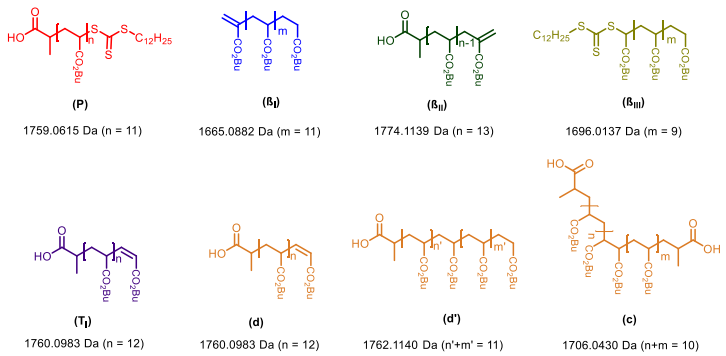

Scheme 3.3. Different polymer species (distributions) observed during on-line ESI-MS screening of the RAFT polymerization of *n*-butyl acrylate.

Closer inspection of the spectra also reveals that MCR scission leads to an excess of β_I macromonomers (Scheme 3.1). This effect has been described in detail before.[17-21]

Interestingly, and never reported before for a polymerizing system, a size selection additionally takes place, which results in a quite unusual product pattern in which the statistical distribution of endgroups is broken. Instead, a characteristic pattern is obtained with alternating peak abundancies with increasing chain length. Due to the migration of midchain radicals along the backbone, which always crosses two monomer units at a time, a preference for certain positions on the backbone results in a specific pattern in which odd and even lengths of the chains alternate in intensity. The size selection stems from the fact that with each migration, the radical moves exactly two monomer units on its chain (via a six-membered transition structure). Due to the preference to form proton-terminated macromonomers, this size selection becomes visible in the characteristic peak patterns.

Table 3.2. Theoretically and experimentally observed exact masses of the different polymer species observed during the RAFT polymerization of *n*-butyl acrylate.

Entry	Species	$m/z_{theoretical}$ (Da)	$m/z_{experimental}$ (Da)	Δm/z
1	$(P)^{Na^+}$	1782.0505	1782.0527	0.0022
2	$(P)^{2Na^+}$	1735.0638	1735.0675	0.0037
3	$(P)^{3Na^+}$	1719.4016	1719.4023	0.0007
4	$(P)^{Fe^{2+}}$	1740.0400	1740.0432	0.0032
5	$(2P)^{Na^+}$	1747.9390	1747.9427	0.0037
6	$(2P)^{2Na^+}$	1718.0068	1718.0088	0.0020
7	$(\beta_I)^{Na^+}$	1688.0772	1688.0792	0.0020
8	$(\beta_I)^{2Na^+}$	1752.1176	1752.1157	-0.0019
9	$(\beta_{II})^{Na^+}$	1774.1139	1774.1163	0,0024
10	$(\beta_{II})^{2Na^+}$	1731.0955	1731.0963	0.0008
11	$(\beta_{III})^{Na^+}$	1696.0137	1696.0150	0.0013
12	$(\beta_{III})^{2Na^+}$	1756.0873	1756.0898	0.0025
13	$(T_I)^{Na^+}$	1760.0983	1760.0992	0.0009
14	$(T_I)^{2Na^+}$	1724.0877	1724.0891	0.0014
15	$(d)^{Na^+}$	1760.0983	1760.0992	0.009
16	$(d')^{Na^+}$	1762.1140	1762.1161	0.0021
17	$(d')^{2Na^+}$	1725.0943	1725.0984	0.0041
18	$(c)^{Na^+}$	1706.043	1706.0476	0.0046

The migration effect is nicely observed at 150 °C as shown in Figure 3.4. As noted, this is the first time that this effect is observed for an actual polymerization. Before, it was only reported for post-polymerization high-temperature modifications of poly(acrylate) polymers and it was left to speculation if migration is in fact fast enough to be competitive with propagation. Hence, it may safely be concluded that, at least for solution polymerizations, at T > 140°C migration is a very significant effect and fully competitive with secondary radical propagation.

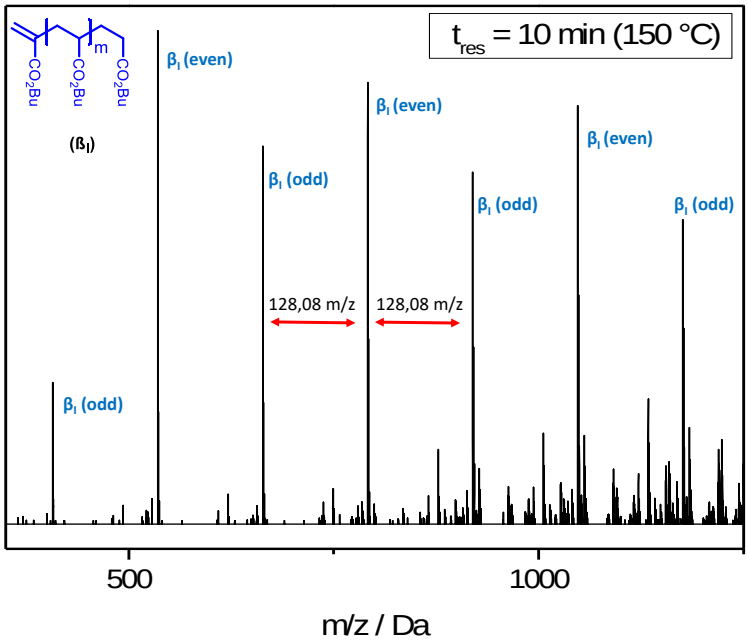

Figure 3.4. Zoomed [400-1200 m/z] ESI-MS spectrum of the RAFT polymerization of *n*-butyl acrylate at 150 °C and 10 minutes microreactor residence time measured via the on-line ESI-MS/microreactor setup.

After this qualitative analysis of the spectra (which in principle do not differ from off-line sampling of microreactor polymerizations, since they only represent a

state of the reaction at a fixed point in time), a more quantitative analysis of product evolutions over time can be made. Figure 3.5 shows microreactor time-sweeps where $(T_I)^{Na+}$ and $(\beta_I)^{Na+}$ product distributions were analyzed relative too the RAFT polymer species $[P]^{Na+}$ from 1 to 10 minutes microreactor residence times for 130, 140, 150 and 190 °C (ESI-MS intensities of side products were to low for 100, 110 and 120 °C). These two species were chosen for illustration as these are the side products with the highest impact on the polymerization; in principle, however, any species as listed in Table 3.2 can be analyzed by this method. Via a custom-made software script (See Experimental Section 3.3.5) a swift analysis of data becomes available.

As mentioned above, ESI-MS is in principle not quantitative. Yet, relative peak abundancies can be studied and it was shown before that for acrylate polymerizations reliable data can be obtained by this method. If all sub-distributions are identical throughout the whole spectrum, then comparison of peaks within one single monomer repeat unit is sufficient – as all repeat units will give the same result. However, during the present investigation the average chain length of the different species varies. To get a semi-quantitative result the addition of all repeating units of all sub-distributions is required (e.g. scission products are smaller in size than the main distribution). The used script does this job; it allows the analysis of large ESI-MS data sets. In the above time-sweeps over 55000 individual data points were considered and recalculated into the depicted graphs. All repeating units of the growing polymer distributions ($(P)^{Na+}$, $(\beta_I)^{Na+}$ and $(T_I)^{Na+}$) were evaluated for 130, 140, 150 and 190 °C. Lower temperatures (100, 110 and 120 °C) were screened but $(\beta_I)^{Na+}$ and $(T_I)^{Na+}$ ESI-MS intensities were too low and hence not further considered here.

The time-sweep experiments show that the reliability of the ESI-MS/microreactor coupling is very high. Compared to the off-line sampling data, potentially less scatter is observed in the on-line monitoring experiment and distinct datasets for the various temperatures with very clear trends are obtained. Not only is scatter low, but also data density is unmatched by any off-line sampling method. While the Chugaev elimination does not play a very significant role up to 120 °C, already 5 % of RAFT-eliminated product is found at the end of the polymerization at 130 °C. While at this temperature, an almost linear increase in the side product is observed, higher temperatures show that the product accumulates faster at shorter reaction times. At the highest temperature under investigation, 190 °C, already 25 % of all RAFT endroups are eliminated. As already qualitatively described above, even much higher levels of β-scission products (specifically β_I) are observed. Also here, the time-sweeps show a distinct increase in macromonomer product ratios with increasing time and a clear trend with temperature is also observable. At 190 °C, already after 1 minute reaction (residence) time, about 3 times more macromonomer, which rises up to an 8-fold excess, is observed. Interestingly, even if these results may seem disastrous for the 190 °C polymerization, still dispersities of around 1.3 are obtained up to relatively high conversions. This result underpins the overall robustness of RAFT polymerization – and the inadequacy of using dispersity and chain length control alone to assess the success of a controlled polymerization.

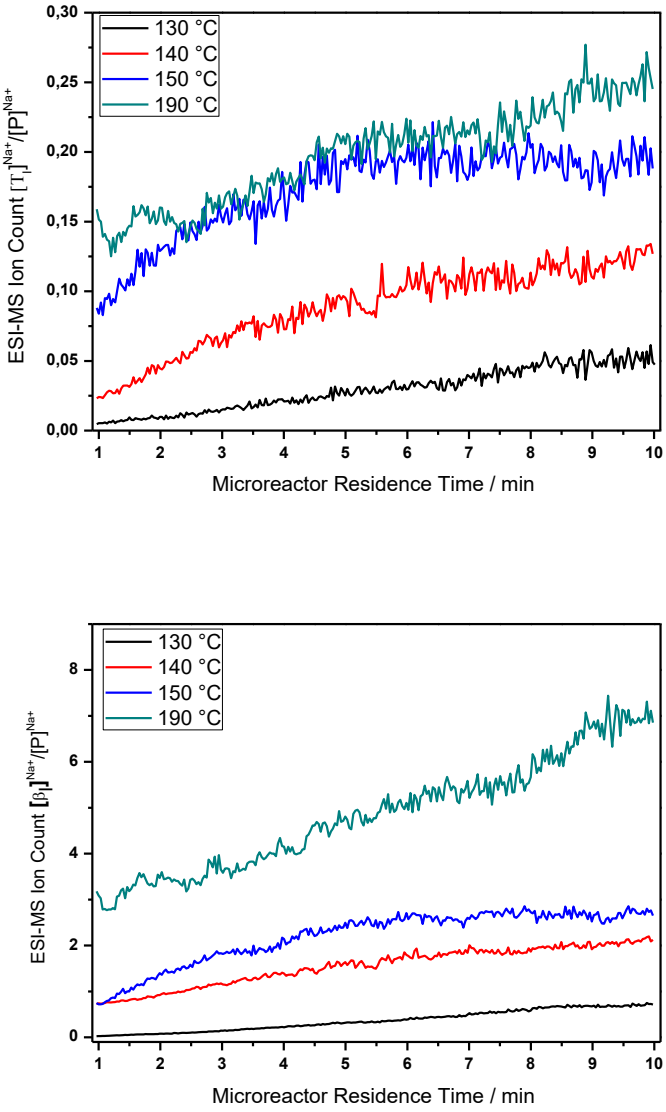

Figure 3.5. Time-sweep data for $(T_I)^{Na+}$ (top) and $(\beta_I)^{Na+}$ (bottom) products in relation to the main RAFT product species. To obtain quantitative data, the full product distributions were integrated in time rather than peaks from a single monomer repeat unit.

3.5 Conclusions

A comprehensive method for the detailed kinetic investigation of polymerization reactions has been introduced. By using high-resolution ESI-MS on-line monitoring of microreactor polymerizations a vast amount of data can be collected under highly reproducible and stable conditions. Data acquisition in such a setup is quasi-continuous, giving access to thousands of individual data points within a single experimental run. By adjusting reactor flow rates a complete reaction can be screened in time-sweep experiments. The RAFT polymerization initiated by VAZO-88 employing DOPAT as the control agent has been screened for high temperature polymerization between 100 and 190 °C and at reaction (residence) times between 1 and 10 minutes. On-line monitoring data was supplemented by off-line sampling of molecular weight and monomer conversion – information that is not available via mass spectrometry. From 150 °C on, all initiator has decayed within the observed polymerization time, and hence no significant acceleration is seen in the polymerization beyond this temperature. All reactions proceed to full monomer conversion. Even at these high temperatures, relatively good control over the polymerization was obtained when only average molecular weights and dispersities are considered. Side product formation – via β-scission reactions of MCRs stemming from intramolecular transfer to polymer reactions and via Chugaev elimination of the RAFT endgroups - is very significant at temperatures above 100 °C and specifically the β-scission products exceed the desired RAFT polymer structure at temperatures above 140 °C.

The on-line coupling method was found to deliver data with high time-resolution (second scale) and very low scatter. With such data at hand, future modelling

studies of these polymerizations should be able to give new insights into the exact mechanism of the polymerizations and allow for precise determination of rate coefficients. It should, however, be noted that modelling of these reactions is far from trivial. The data shown herein are only for demonstration purposes to show the capability of the method and the level of detail that can be gathered. Due to the high complexity of the reaction schemes and the very high level of detail of our data, we will provide full time-sweep datasets for any species in the mass spectrum to interested parties.

3.6 References

1. Junkers, T.; Theis, A.; Buback, M.; Davis, T. P.; Stenzel, M. H.; Vana, P.; Barner-Kowollik, C. *Macromolecules* **2005**, *38*, 9497.

2. Buback, M.; Junkers, T.; Müller, M. *Polymer* **2009**, *50*, 3111.

3. Dervaux, B.; Junkers, T.; Schneider-Baumann, M.; Prez, F. E. D.; Barner-Kowollik, C. *Journal of Polymer Science Part A: Polymer Chemistry* **2009**, *47*, 6641.

4. Junkers, T.; Schneider-Baumann, M.; Koo, S. P. S.; Castignolles, P.; Barner-Kowollik, C. *Macromolecules* **2010**, *43*, 10427.

5. Zorn, A. M.; Junkers, T.; Barner-Kowollik, C. *Macromolecules* **2011**, *44*, 6691.

6. Barner-Kowollik, C.; Junkers, T. *Journal of Polymer Science Part A: Polymer Chemistry* **2011**, *49*, 1293.

7. Barth, J.; Buback, M.; Barner-Kowollik, C.; Junkers, T.; Russell, G. T. *Journal of Polymer Science Part A: Polymer Chemistry* **2012**, *50*, 4740.

8. Bennet, F.; Rölle, T.; Fäcke, T.; Weiser, M.-S.; Bruder, F.-K.; Barner-Kowollik, C.; Junkers, T. *Macromolecular Chemistry and Physics* **2013**, *214*, 236.

9. Kockler, K. B.; Haehnel, A. P.; Junkers, T.; Barner-Kowollik, C. *Macromolecular Rapid Communications* **2016**, *37*, 123.

10. Wenn, B.; Junkers, T. *Macromolecular Rapid Communications* **2016**, *37*, 781.

11. Junkers, T.; Barner-Kowollik, C. *Journal of Polymer Science Part A: Polymer Chemistry* **2008**, *46*, 7585.

12. Junkers, T. *Australian Journal of Chemistry* **2008**, *61*, 646.

13. Willemse, R. X. E.; Herk, A. M. v.; Panchenko, E.; Junkers, T.; Buback, M. *Macromolecules* **2005**, *38*, 5098.

14. Liu, S.; Srinivasan, S.; Grady, M. C.; Soroush, M.; Rappe, A. M. *International Journal of Quantum Chemistry* **2014**, *114*, 345.

15. Hamzehlou, S.; Ballard, N.; Reyes, Y.; Aguirre, A.; Asua, J. M.; Leiza, J. R. *Polymer Chemistry* **2016**, *7*, 2069.

16. Mavroudakis, E.; Cuccato, D.; Moscatelli, D. *Industrial & Engineering Chemistry Research* **2014**, *53*, 9058.

17. Vandenbergh, J.; Junkers, T. *Macromolecules* **2013**, *46*, 3324.

18. Marien, Y. W.; Steenberge, P. H. M. V.; Barner-Kowollik, C.; Reyniers, M.-F.; Marin, G. B.; D'hooge, D. R. *Macromolecules* **2017**, *50*, 1371.

19. Marien, Y. W.; Steenberge, P. H. M. V.; Kockler, K. B.; Barner-Kowollik, C.; Reyniers, M.-F.; D'hooge, D. R.; Marin, G. B. *Polymer Chemistry* **2016**, *7*, 6521.

20. Ballard, N.; Hamzehlou, S.; Asua, J. M. *Macromolecules* **2016**, *49*, 5418.

21. Vandenbergh, J.; Junkers, T. *Macromolecules* **2012**, *45*, 6850.

22. Asua, J. M.; Beuermann, S.; Buback, M.; Castignolles, P.; Cherleux, B.; Gilbert, R. G.; Hutchinson, R. A.; Leiza, J. R.; Nikitin, A. N.; Vairon, J.-P.; van Herk, A. M. *Macromolecular Chemistry and Physics* **2004**, *205*, 2151.

23. Rantow, F. S.; Soroush, M.; Grady, M. C.; Kalfas, G. A. *Polymer* **2006**, *47*, 1423.

24. Sato, E.; Emoto, T.; Zetterlund, P. B.; Yamada, B. *Macromolecular Chemistry and Physics* **2004**, *205*, 1829.

25. Plessis, C.; Arzamendi, G.; Alberdi, J. M.; van Herk, A. M.; Leiza, J. R.; Asua, J. M. *Macromolecular Rapid Communications* **2003**, *24*, 173.

26. Gaborieau, M.; Koo, S. P. S.; Castignolles, P.; Junkers, T.; Barner-Kowollik, C. *Macromolecules* **2010**, *51*, 5492.

27. Wenn, B.; Reekmans, G.; Adriaensens, P.; Junkers, T. *Macromolecular Rapid Communications* **2015**, *36*, 1479.

28. Junkers, T.; Koo, S. P. S.; Stenzel, M. H.; Davis, T. P.; Barner-Kowollik, C. *Macromolecules* **2007**, *40*, 8906.

29. Koo, S. P. S.; Junkers, T.; Barner-Kowollik, C. *Macromolecules* **2009**, *42*, 62.

30. Junkers, T.; Bennet, F.; Koo, S. P. S.; Barner-Kowollik, C. *Journal of Polymer Science Part A: Polymer Chemistry* **2008**, *46*, 3433.

31. Chiefari, J.; Chong, Y. K.; Ercole, F.; Krstina, J.; Jeffery, J.; Le, T. P. T.; Mayadunne, R. T. A.; Meijs, G. F.; Moad, C. L.; Moad, G.; Rizzardo, E.; Thang, S. H. *Macromolecules* **1998**, *31*, 5559.

32. Haven, J. J.; Guerrero-Sanchez, C.; Keddie, D. J.; Moad, G.; Thang, S. H.; Schubert, U. S. *Polymer Chemistry* **2014**, *5*, 5236.

33. Haven, J. J.; Guerrero-Sanchez, C.; Keddie, D. J.; Moad, G. *Macromolecular Rapid Communication* **2014**, *35*, 492.

34. Moad, G.; Rizzardo, E.; Thang, S. H. *Australian Journal of Chemistry* **2009**, *62*, 1402.

35. Moad, G.; Guerrero-Sanchez, C.; Haven, J. J.; Keddie, D. J.; Postma, A.; Rizzardo, E.; Thang, S. H. *ACS Symposium Series* **2014**, *1170*, 133.

36. Haven, J. J.; Vandenbergh, J.; Kurita, R.; Gruber, J.; Junkers, T. *Polymer Chemistry* **2015**, *6*, 5752.

37. Haven, J. J.; Vandenbergh, J.; Junkers, T. *Chemical Communications* **2015**, *51*, 4611.

38. Haven, J. J.; Baeten, E.; Claes, J.; Vandenbergh, J.; Junkers, T. *Polymer Chemistry* **2017**, *8*, 2972.

39. Ferguson, C. J.; Hughes, R. J.; Nguyen, D.; Pham, B. T. T.; Gilbert, R. G.; Serelis, A. K.; Such, C. H.; Hawkett, B. S. *Macromolecules* **2005**, *38*, 2191.

40. http://tools.thermofisher.com/content/sfs/manuals/Man-XCALI-97542-MSFileReader-30-Ref-ManXCALI97542-A-EN.pdf (Accessed March 2017).

41. Haven, J. J.; Zaquen, N.; Rubens, M.; Junkers, T. *Macromolecular Reaction Engineering* **2017**, DOI: 10.1002/mren.201700016.

42. Reyes, Y.; Asua, J. M. *Macromolecular Rapid Communications* **2011**, *32*, 63.

43. Derboven, P.; Van Steenberge, P. H. M.; Vandenbergh, J.; Reyniers, M.-F.; Junkers, T.; D'hooge, D. R.; Marin, G. B. *Macromolecular Rapid Communication* **2015**, *36*, 2149.

44. Postma, A.; Davis, T. P.; Moad, G.; O'Shea, M. S. *Macromolecules* **2005**, *38*, 5371.

45. Hornung, C. H.; Postma, A.; Saubern, S.; Chiefari, J. *Polymer* **2014**, *55*, 1427.

46. Van Steenberge, P. H. M.; Vandenbergh, J.; Reyniers, M.-F.; Junkers, T.; D'hooge, D. R.; Marin, G. B. *Macromolecules* **2017**, *50*, 2625.

CHAPTER 4

High-Throughput Polymer Screening in Microreactors: Boosting the Passerini Three-Component Reaction

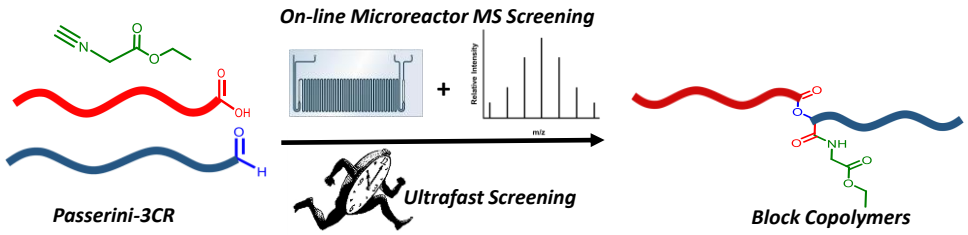

Haven, J. J.; Baeten, E.; Claes, J.; Vandenbergh, J.; Junkers, T. *Polymer Chemistry* **2017**, *8*, 2972.

4.1 Abstract

The Passerini three-component reaction (Passerini 3-CR) is studied via on-line electrospray ionization mass spectrometry (ESI-MS)/microreactor reaction monitoring to demonstrate the high-throughput screening potential of continuous microreactors for macromolecular design. The Passerini 3-CR is an efficient reaction, but generally requires some reagent excesses and comparatively long reactions times to complete. Herein a reaction protocol is proposed for high yields within minute reaction time under equimolar reactant concentrations. The Passerini 3-CR allows for the synthesis of α-acyloxy carboxamides by combining an aldehyde (or ketone), an isocyanide and a carboxylic acid moiety. Carboxylic acid (i, 1300 g mol^{-1}) and aldehyde (ii, 1150 g mol^{-1}) endgroup functionalized low molecular weight poly(*n*-butyl acrylate)s were separately screened with their corresponding Passerini components as follows: (i) with dodecylaldehyde and ethylisocyanoacetate and (ii) with acetic acid and ethylisocyanoacetate. Screened parameters were molarity ratios, residence times, absolute reagent concentrations and reactor temperatures. Equimolar carboxylic acid/aldehyde concentrations give excellent Passerini product yields (> 95%) within 10 minutes reaction time. The established reaction protocol is then transferred to a conventional batch process for the synthesis of the diblock copolymers P(*n*BA)-*b*-P(*n*BA), P(*n*BA)-*b*-P(MMA) and P(*n*BA)-*b*-P(EGMEA) with variable block lengths. All diblock copolymers are synthesized by equimolar carboxylic acid/aldehyde polymer mixtures, showing excellent coupling efficiencies in size-exclusion chromatography analysis.

4.2 Introduction

A classical test that is carried out to investigate how efficient a reaction may be is to use it for the ligation of two polymeric building blocks, hence the formation of block copolymers.[1] This requires stringent reaction conditions and only comparatively few reactions are so far in use for this purpose. Examples for efficient ligation chemistries are multicomponent reactions (MCRs), i.e. reactions that combine at least three different starting materials to yield a single product. MCRs are characterized by their high atom efficiency and straightforward practical synthesis procedures in contrast with tedious multistep synthesis processes.[2-3] MCRs have generally proven to be highly valuable in the field of pharmaceutical and combinatorial chemistry, mainly due to the excessive structural and molecular diversity that can be obtained in the final product.[4-6] However, MCRs were introduced in macromolecular chemistry only recently, yet gaining attention rapidly for the design of new functional polymers.[7-11] The isocyanide based Passerini three-component reaction (Passerini 3-CR, Scheme 4.1, first described in 1921) is, together with the Ugi four-component reaction (Ugi 4-CR), one of the most widely used MCRs in organic chemistry.[12] During the last years different aspects in macromolecular chemistry have been explored via the Passerini 3-CR such as monomer synthesis,[13-17] sequence-regulated polymerizations,[18-25] synthesis of functional polymers,[26-28] postpolymerization functionalizations,[29-30] multiblock copolymers[31-32] and dendritic architectures.[33-35] Nowadays, most reactions are performed in conventional batch reactors and only few examples exist where the Passerini 3-CR was successfully employed as a continuous flow process.[36-37] Despite all the promising features of the Passerini 3-CR, typically some reagent excesses and comparatively long reaction times are required in

order to obtain high product yields (note that in most cases the reactions are performed at or close to room temperature). Tao and coworkers[38] reported on another isocyano based MCR, the Ugi 4-CR, that has been utilized as a green click reaction to efficiently conjugate two polymer chains. No block copolymer formation has yet been reported for the Passerini reaction, despite its other highly efficient outcomes. Step-growth polymerization via Passerini coupling is well known, which hints at a high reaction efficiency also under equimolar conditions (a prerequisite for block copolymer click conjugation).[1] Yet, the ability to undergo step-growth is not indicative for success in block copolymer synthesis as many reactions exist that are well suited for step-growth polymerization, but which fail for block copolymer ligation, e.g. esterification or radical thiol-ene reactions.[1] Being able to drive the Passerini reaction towards quantitative polymer-polymer coupling expand the very high efficiency of the reaction even further.

Firstly, the reaction was tested directly on a polymer support, in order to allow for a quantitative ESI-MS analysis (via the on-line ESI-MS/microreactor coupling described in Chapter 2). To this end, the reaction was approached from two sides; endgroup functionalized low molecular weight poly(*n*-butyl acrylate) (P*n*BA) was individually studied by intensive screening via on-line ESI-MS/microreactor, in one system bearing the required aldehyde moiety and in the other the carboxylic acid group at the chain end. Optimal reaction parameters were investigated to push the limits of the Passerini 3-CR to high product yields (> 95%) in very short reaction times with equimolar carboxylic acid/aldehyde component mixtures.

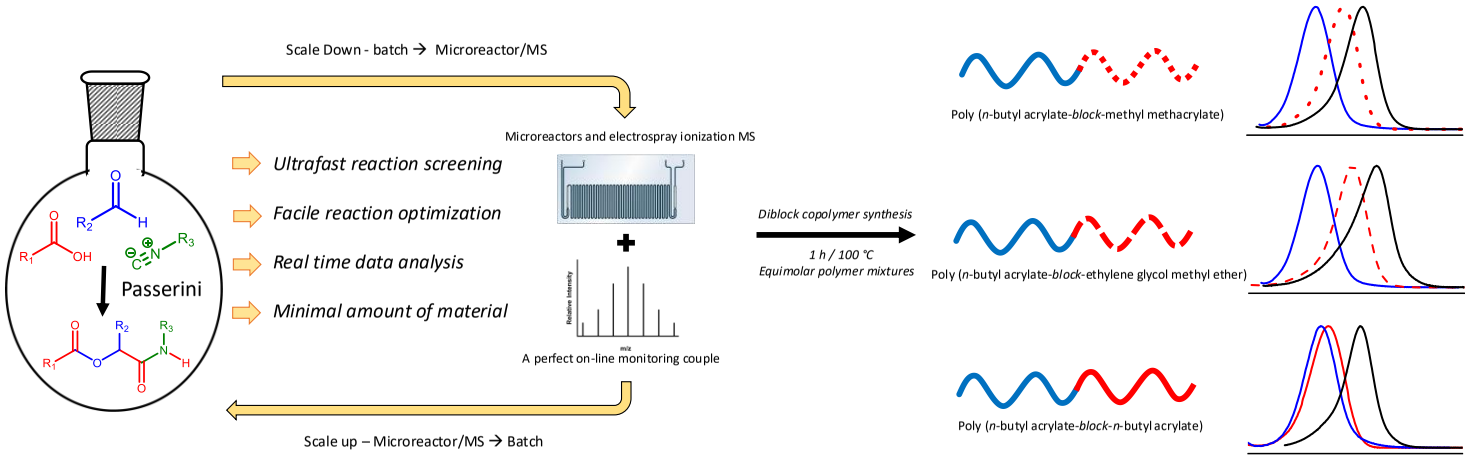

Scheme 4.1. (left) General reaction scheme of the Passerini 3-CR which includes a carboxylic acid, an aldehyde (or ketone) and an isocyanide. ESI-MS/microreactor coupling was utilized as a toolbox to study the Passerini-3CR. Afterwards, the reaction protocol was transferred to a conventional batch process for the synthesis of diblock copolymers. (right) The diblock copolymers P(nBA)$_{10}$-*b*-P(nBA)$_{10}$, P(nBA)$_{10}$-*b*-P(MA)$_{15}$ and P(nBA)$_{10}$-*b*-P(EGMEA)$_{10}$ targeted in 1 h reaction time at a temperature of 100 °C in dichloromethane with equimolar initial polymer reagent mixtures.

Secondly, after a reaction protocol was established for the synthesis of a variety of diblock copolymers as a conventional batch process. The flow chemistry setup served hereby as a mere tool for on-line optimization, not as a synthesis tool *per se*. Details on this choice will be given below. After successful optimization of the individual precursor polymers, diblock copolymers were then synthesized by an equimolar reaction mixture of an aldehyde endgroup functionalized P(*n*BA) and carboxylic acid endgroup functionalized P(*n*BA), poly(methyl acrylate) P(MA) and poly(ethylene glycol methyl ester) P(EGMEA) polymer in the presence of a slight excess of ethylisocyanoacetate.

Flow chemistry has become a progressively more important tool in synthetic chemistry, not only for synthesis purposes, but also as high-throughput screening approach that can be integrated in the daily workflow of classical organic or macromolecular synthesis.[39] Translation back from flow to batch conditions plays thereby an important role. We wished to demonstrate such a strategy using the high synthetic potential of the Passerini reaction for polymer-polymer conjugation.

4.3 Experimental Section

Materials and characterization methods are described in Chapter 8.

4.3.1 Microreactor Setup

Details of the microreactor setup are discussed in Chapter 2 (Experimental Section 2.3.1).

4.3.2 ESI-MS/microreactor Coupling

Details of the ES-MS/microreactor coupling are discussed in Chapter 2 (Experimental section 2.3.2).

4.3.3 Synthetic Procedures

4.3.3.1 Synthesis of DoPAT RAFT Agent

2-(dodecylthiocarbonothioylthio)propionic acid (**DoPAT**) was synthesized according to literature procedure.[40]

4.3.3.2 Synthesis of 3-hydroxybutyl 2-bromo-2-methylpropionate (2)

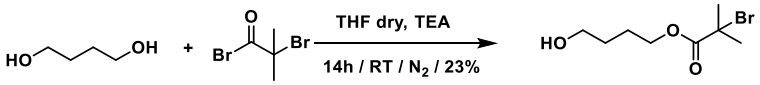

Anhydrous THF (60 mL), 1,4-butanediol (39.7 g, 0.44 mol) and triethylamine (22.2 g, 0.22 mol) were added to a 250 mL round bottom flask under an argon blanket and cooled to 0 °C. To this stirred solution, 2-bromoisobutyryl bromide (46.0 g, 0.20 mol) in anhydrous THF (40 mL) was added drop-wise and the reaction mixture was stirred for 15 h at room temperature. The solvent was removed via rotary evaporation and the residue taken up in diethyl ether (100 mL). The white precipitate was filtered off and the organics were extracted

with 1 N HCl aqueous solution, brine and water. The organic layer was dried ($MgSO_4$), filtered and the volatiles were evaporated to give a colorless oil. The final product was isolated by column chromatography 40/60 diethyl ether/hexane to yield a clear oil (12.7 g, 27%). ^{1}H-NMR ($CDCl_3$): δ (ppm) = 4.16 (t, 2H, CH_2), 3.62 (t, 2H, CH_2), 3.20 (s, 1H, OH), 1.87 (s, 6H, CH_3), 1.78-1.68 (m, 2H, CH_2), 1.67-1.55 (m, 2H, CH_2). ^{13}C-NMR ($CDCl_3$): δ (ppm) = 171.8, 65.9, 62.0, 56.0, 30.7, 28.9, 24.9.

4.3.3.3 Synthesis of 3-butanal 2-bromo-2-methylpropionate (3)

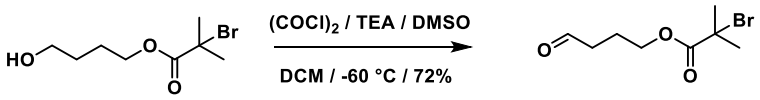

Procedure for the Swern oxidation of product **2**. All glassware was dried before use. Oxalyl chloride (2.20 mL, 25.63 mmol) and CH_2Cl_2 (70 mL) were placed in a 3-necked round bottom flask under inert nitrogen atmosphere equipped with a stirrer. The mixture was cooled to -60 °C (acetone/liquid N_2 bath). Dry DMSO (3.96 mL, 55.77 mmol) was added dropwise while stirring was continued at -60 °C. After *ca* 10 min a solution of 3-HBBMP (**2**) (5.50 g, 23.43 mmol) in CH_2Cl_2 (25 mL) was added dropwise to the reaction mixture. The mixture was stirred for 15 min then Et_3N (16 mL, 115.40 mmol) was added slowly at -60 °C. The cooling bath was removed, water (70 mL) was added and the reaction mixture was stirred for 5 min at room temperature. The organic layer was separated and the aqueous phase twice extracted with CH_2Cl_2 (50 mL). The organic layers were combined and the volume reduced to 50 mL by vacuum distillation. The solution was successively washed with HCl (1 N), water, Na_2CO_3 (1 N) and water, dried with $MgSO_4$ and evaporated to dryness. The final product was isolated by column chromatography

(silica, gradient Et_2O/hexane 20 → 40% Et_2O) to yield a yellowish oil (3.90 g, 72%). ^{1}H-NMR ($CDCl_3$): δ (ppm) = 9.64 (s, 1H, -COH), 4.04 (t, 2H, CH_2), 2.45 (t, 2H, CH_2), 1.92-1.82 (m, 2H, CH_2), 1.76 (s, 6H, CH_3). ^{13}C-NMR ($CDCl_3$): δ (ppm) = 200.9, 171.1, 64.7, 55.8, 40.0, 30.4, 20.8.

4.3.3.4 Synthesis of tris[2-(dimethylamino)ethyl]amine (4)

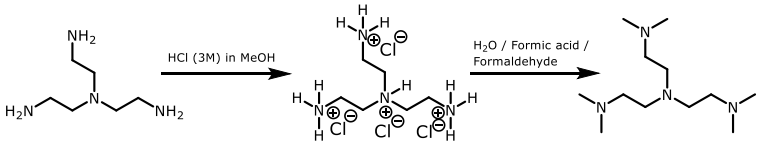

In a 250 mL three-necked flask equipped with a condenser, addition funnel, and stirrer, *tris*(2-aminoethyl)amine (4.0 mL, 0.027 mol) was added in 50 mL of methanol. To this mixture HCl (60 mL, 3N) in methanol was added dropwise and the mixture was stirred at room temperature. After 1 h the precipitate was filtered off and washed thrice with MeOH (50 mL) to yield the product (salt) as a white solid. To this, water (10 mL), formic acid (50 mL) and formaldehyde (aq., 46 mL) was added in a 250 mL round bottom flask. The reaction mixture was stirred under reflux for 6 h. Volatiles were removed by vacuum distillation. The crude product was dissolved in NaOH (aq., 10 wt%) and extracted with diethyl ether (4 x 100 mL). The organic layer was dried over NaOH pellets and the solvent was removed by vacuum distillation to give a yellowish liquid (6.0 g, 89%). ^{1}H NMR ($CDCl_3$): δ (ppm) = 2.56-2.60 (m, 6H, CH_2), 2.33-2.37 (m, 6H, CH_2), 2.12 (s, 18H, CH_3).

4.3.3.5 Synthesis of Poly(*n*-butyl acrylate) via RAFT Polymerization

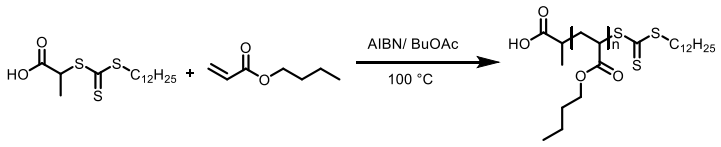

In a typical procedure, 2,2'-azobisisobutyronitrile (AIBN) (0.11 g, 0.70 mmol), 2-(dodecylthiocarbonothioylthio)propionic acid (DoPAT) RAFT agent (5.0 g, 0.014 mol), monomer *n*BA (17.90 g, 0.14 mol) and butyl acetate (20 mL) were added to a 100 mL round bottom flask and stirred until dissolved. The flask was sealed by a rubber septum, the solution was degassed for 30 min by N_2 purging and placed in a thermolysed preheated oil batch of 100 °C. After a reaction time of 5 min, the reaction mixture was cooled down in liquid nitrogen and quenched by a hydroquinone solution in MeOH. The polymer mixture was transferred into an aluminum pan to evaporate all volatiles, yielding 30.0 g of P*n*BA. ^{1}H-NMR ($CDCl_3$) indicated a 92% conversion of *n*BA monomer. SEC (THF): M_n = 1300 g mol^{-1} and PDI = 1.11.

4.3.3.6 Synthesis of Poly(*n*-butyl acrylate) (P*n*BA) via SET-LRP

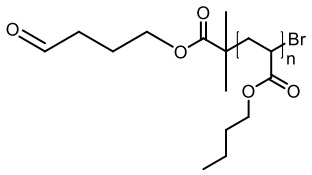

In a typical procedure, 3-butanal 2-bromo-2-methylpropionate (**3**) *(*1 equiv.*)*, monomer *n*BA (10 equiv.), ligand tris[2-(dimethylamino)ethyl]amine (Me_6TREN) (0.16 equiv.) and dimethylformamide (2 mL) were added to a 10 mL glass vial. The glass vial was sealed by a rubber septum, the solution was degassed for 10 min by N_2 purging and subsequently inserted into the glovebox. Copper powder (Cu(0), 0.16 equiv.) and a stirrer bar were added to the glass vial. The glass vial was resealed and the reaction was stirred at room temperature. After 20 min a sample of the reaction was withdrawn for ^{1}H-NMR analysis to determine monomer conversion (76%). The reaction mixture was diluted with THF and passed over silica gel to remove metal complexes. Volatiles were removed by vacuum

distillation and the polymer was dried under vacuum overnight. ^{1}H-NMR ($CDCl_3$): 76% conversion of *n*BA monomer. SEC (THF) M_n = 1050 g mol^{-1}, M_p = 1150 g mol^{-1} and PDI = 1.14.

4.3.3.7 Synthesis of Poly(ethylene glycol methyl ether acrylate) via RAFT Polymerization

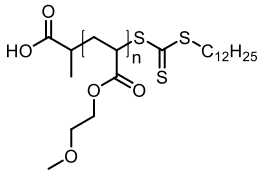

In a typical procedure, 2,2'-azobisisobutyronitrile (AIBN) (8.21 mg, 0.05 mmol), 2-(dodecylthiocarbonothioylthio)propionic acid (DoPAT) RAFT agent (350.60 mg, 1.00 mmol), monomer ethylene glycol methyl ether acrylate (1.48 mL, 8.00 mmol) and butyl acetate (3 mL) were added to a 10 mL glass vial together with a stirrer bar. The glass vial was sealed by a rubber septum, the solution was degassed for 10 min by N_2 purging and subsequently inserted into the glovebox. The glass vial was placed in a preheated copper block at 100 °C. After a reaction time of 5 min the glass vial was quenched by cooling the vial in liquid nitrogen and subjecting the contents to ambient atmosphere. Subsequently the mixture was transferred into an aluminium pan to evaporate the excess of solvent and monomer, yielding 1.750 g of crude product mixture. ^{1}H-NMR ($CDCl_3$): 92% conversion of *n*BA monomer, SEC (THF) M_n = 1650 g mol^{-1}, M_p = 1900 g mol^{-1} and PDI = 1.13.

4.3.3.8 Synthesis of Poly(methyl methacrylate) via RAFT Polymerization

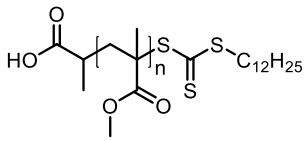

In a typical procedure, 2,2'-azobisisobutyronitrile (AIBN) (0.05 equiv.), 2-(dodecylthiocarbonothioylthio)propionic acid (DoPAT) RAFT agent (1 equiv.), monomer methyl methacrylate (25 equiv.) and butyl acetate (3 mL) were added to a 10 mL glass vial together with a stirrer bar. The glass vial was sealed by a rubber septum, the solution was degassed for 10 min by N_2 purging and subsequently inserted into the glovebox. The glass vial was placed in a preheated copper block at 100 °C. After a reaction time of 5 min the glass vial was quenched by cooling the vial in liquid nitrogen and the content subjected to ambient atmosphere. Subsequently the mixture was transferred into an aluminium pan to evaporate the excess of solvent and monomer. ^{1}H-NMR ($CDCl_3$): 80% conversion of *n*BA monomer, SEC (THF) M_n = 1700 g mol^{-1}, M_p = 2200 g mol^{-1} and PDI = 1.25.

4.3.3.9 Synthesis of Diblock Copolymers

All diblock copolymers were synthesized according to the conditions identified in this thesis. In a typical procedure an equimolar amount of the two corresponding homopolymers (1 equiv.), ethylisocyanoacetate (2 equiv.) and dichloromethane as the reaction solvent were weighted in a glass vial. A magnetic stirrer was added and the reaction mixture was reacted for 1 h at 100 °C in a pre-heated copper heating block on a heating plate. The diblock copolymers were analyzed by SEC and ESI-MS without further purification.

4.4 Results & Discussion

A technique for the continuous on-line monitoring of the Passerini 3-CR is presented by electrospray ionization mass spectrometry (ESI-MS) via coupling with a microreactor system. Thus, analysis of the Passerini reaction products that exit the flow microreactor is achieved directly by on-line by ESI-MS without the requirement of a sampling method. A schematic representation and detailed description of the setup has been given previously in Chapter 2.

Herein, reactions were optimized in a flow reactor and then translated back to batch conditions. In such case, flow reactors are used as pure kinetic tools in a high-throughput experimentation approach. The advantage of such approach is that other researchers can pick up the results without requiring flow synthesis equipment. A disadvantage is that conditions must be found which are not only applicable to flow synthesis, but also for classical batch synthesis (in which case operation windows with regards to temperature and kinetic control are more limited).

For diblock copolymer synthesis via the Passerini reaction the following optimization strategy was applied. Two model reactions as depicted in Scheme 4.2 were screened in the ESI-MS/microreactor setup described above to obtain a comprehensive overview on the kinetics of the reaction. A carboxylic acid (**A**, 1300 g mol^{-1}) and aldehyde (**F**, 1150 g mol^{-1}) endgroup functionalized low molecular weight poly(*n*-butyl acrylate) were separately screened with their corresponding Passerini components; (**A**) was screened with dodecylaldehyde and ethylisocyanoacetate and (**F**) with acetic acid and ethylisocyanoacetate. Screening

of **A** and **F** results in the formation of α-acyloxy carboxamides **D** and **G**, respectively. The carboxylic acid functionalized P*n*BA (**A**, 1300 g mol^{-1}) was synthesized via reversible activation-fragmentation chain transfer (RAFT) polymerization of *n*-butylacrylate (*n*BA) with a carboxylic acid R-group functional RAFT agent 2-(dodecylthiocarbonylthioylthio)propionic acid (DoPAT) and 2-2'-azobisisobutyronitrile (AIBN) as the thermal initiator. The aldehyde functionalized P*n*BA (**F**, 1150 g mol^{-1}) was synthesized by Cu-mediated single electron transfer living radical polymerization (SET-LRP) of *n*-butyl acrylate (*n*BA), Cu(0) with tris(2-(dimethylamino)ethyl)amine (Me_6TREN) as a ligand and 3-butanal 2-bromo-2-methylpropionate (**3**) as the initiator which carries the crucial aldehyde endgroup. Synthetic procedures for all reagents utilized in this study are described in detail in the Experimental Section 4.3. The chemistry of the isocyanide derivative plays a significant role in the Passerini -3CR. The properties, reactivity and synthesis of isocyanides have already been reviewed in the literature and will thus not be discussed in detail here.[2,41] The amount of isocyanide component selected for this study remains unchanged in all screening experiments and is consistently utilized in excess (2 equivalents). In this work, the carboxylic acid/aldehyde component ratio is stressed in the scope of diblock copolymer synthesis. Direct observation of diblock copolymers in ESI-MS is tedious due to a change in overall molecular weight during the reaction, making the quantification of results difficult in mass spectrometry due to mass and chemical ionization bias effects and the complexity of the ESI-MS polymer peak distributions. The model reactions as given below were hence optimized individually (Scheme 4.2).

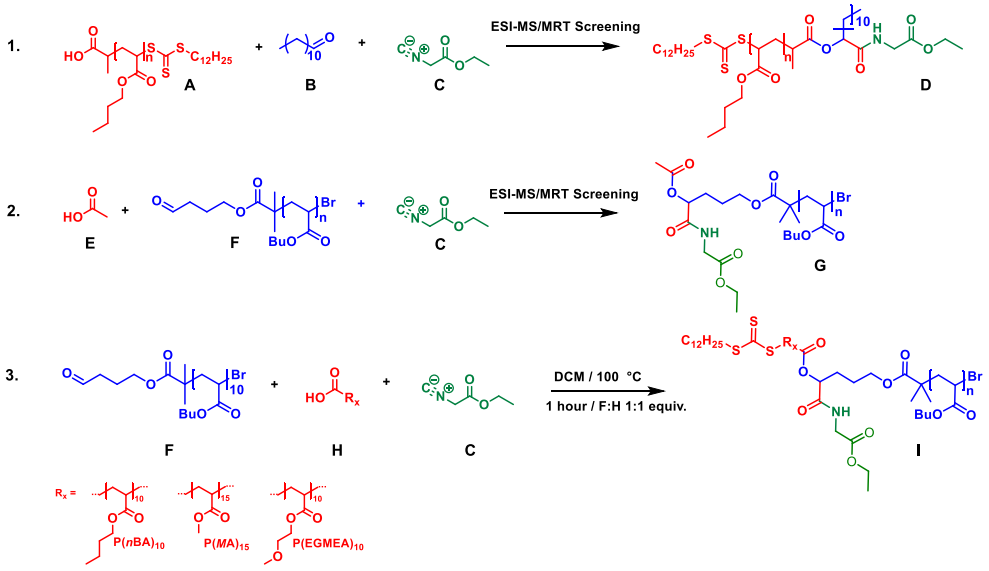

Scheme 4.2. Representation of the Passerini 3-CR reaction schemes with 4.2.1: MRT/ESI-MS screening of a carboxylic acid endgroup functionalized polymer, 4.2.2: MRT/ESI-MS screening of an aldehyde endgroup functionalized polymer and 4.2.3: general reaction scheme for the batch synthesis of P(*n*BA)$_{10}$-*b*-P(*n*BA)$_{10}$, P(*n*BA)$_{10}$-*b*-P(MA)$_{15}$ and P(*n*BA)$_{10}$-*b*-P(EGMEA)$_{10}$ with equimolar initial polymer mixtures (**F** and **H**) for 1 h reaction time at a temperature of 100 °C in dichloromethane as the reaction solvent.

The polymer provides a soluble support for the reaction in question, and allows for a semi-quantitative analysis of results. Herein, to act as a support, the assumption was made that the polymer dominates the ionization and not the endgroup of the polymer, where the reaction takes place. Also, by reaction on a polymer, the (diffusion-controlled) kinetics of the later diblock formation is approximated. For the reactions, the following protocol was used: a solution of ethylisocyanoacetate (**C**) and the polymer P(*n*BA) **A** or **F** in dichloromethane

(DCM) was loaded into a gastight syringe (SGE, 1 mL). A second gastight syringe (SGE, 1mL) was loaded with a solution of the third component (**B** or **E**, respectively). The two gastight syringes were placed in two different syringe pumps (Chemyx N.V.) to control the carboxylic acid/aldehyde ratio in the microreactor. Efficient homogeneous mixing of all components took place in the microreactor staggered oriented ridge (SOR) mixer. All reagent concentrations reported are concentrations after mixing of the two streams. The Passerini 3-CR products were examined under systematic variation of temperature, microreactor residence time and reagent concentration. Passerini product yields (%) were determined by ESI-MS analysis via the equation shown below which determines the MS intensity of the final Passerini polymer product (**D**) obtained in the crude reaction mixture relative to the intensities of both the initial polymer mixture **A** and final product **D**. Yields were determined based on the most intense polymer peak of the corresponding polymer distribution in ESI-MS as follows:

$$\%\ Passerini\ product\ yield = \left[\frac{MS\ peak\ intensity\ \ \boldsymbol{D}}{MS\ peak\ intensity\ (\boldsymbol{D}+\boldsymbol{A})}\right] * 100$$

Figure 4.1.2 shows the Passerini product yield (%) as a function function of the microreactor temperature for the three-component reactions shown in Scheme 4.2. The reaction efficiency for the synthesis of Passerini product **D** (Scheme 4.2.1) was screened for 10 and 20 minutes microreactor residence time, with 2 and 1 equivalent of dodecylaldehyde (**B**) and 2 equivalents of ethylisocyanoacetate (**C**). The formation of product **G** (Scheme 4.2.2) was analyzed for a microreactor residence time of 20 minutes and 1 equivalent of acetic acid (**E**). Both reactions were monitored for a broad temperature range

from 25 – 125 °C in steps of 25 °C. In general the reaction efficiency, in terms of Passerini product yield, increases by ramping up the micro flow reactor temperature for a constant residence time. For all reactions high yields (> 80%) were obtained without high stoichiometric excesses of one or more reagents. At the highest temperature (125 °C), RAFT omega (ω) endgroup thermolysis was observed for the carboxylic acid endgroup derived P(*n*BA) (**A**). Endgroup thermolysis of the RAFT living chain end is comprehensively described in the literature.[42-43] Although the crucial reactive carboxylic acid alpha (α) endgroup for the Passerini 3-CR stays intact in this side reaction, high endgroup fidelity of the polymers is desired in the scope of high value material synthesis by polymer chain extensions or polymer endgroup modifications.[44] Nonetheless, at slightly lower temperature (100 °C) reasonable yields (> 60%) were obtained with an equimolar initial reaction mixture of P*n*BA (**A**) and dodecylaldehyde (**B**) when a higher microreactor residence time of 20 minutes was applied. For efficient diblock copolymer synthesis the aldehyde polymer endgroup (**F**, Scheme 4.2) should show a similar reactivity in terms of endgroup conversion for the formation of the Passerini product **G**. This could be confirmed by screening P*n*BA (**F**) with acetic acid (**E**, 1 equivalent) and ethylisocyanoacetate (**C**, 2 equivalents). The reaction proceeds more rapidly to high conversions (> 80%) but levels off at higher temperature (> 100 °C). Hence, a reactor temperature of 100 °C was used for all further investigations. As outlined above, higher yields are required to favor the diblock copolymer synthesis of equimolar polymer reaction mixtures. Higher reactant concentrations in principle lead to faster overall reactions. Figure 4.1.3 illustrates the Passerini product yield against microreactor concentration (mol L^{-1}) of the P*n*BA (**A**, 1300 g mol^{-1}) polymer precursor in the initial reaction mixture (A+xB+2C, Scheme 4.2). For a fixed set of reaction conditions (100 °C, 20

minutes) it was observed that the initial polymer concentration has a direct effect on the reaction rate and hence final conversion. This effect is more pronounced when utilizing an excess (2 equivalents) of dodecylaldehyde (**B**) relative to P*n*BA (**A**). Thus, the initial polymer concentration was increased (0.38 mol L^{-1}, 44 wt%) and driven to the limits of the microreactor (to prevent clogging of the microreactor channel and inlet tubing when higher concentrations are applied). Figure 4.1.4 shows the Passerini product yield (%) for a high initial polymer concentration (44 wt. %, 0.38 mol L^{-1}) in a microreactor residence time window of 2 to 20 minutes at 100 °C. The reaction reaches nearly full conversion (> 95%) after only 8 minutes microreactor residence time. Note that already after 2 minutes (> 75%) and 4 minutes (> 90%) conversions are obtained as determined by ESI-MS (Figure 4.2).

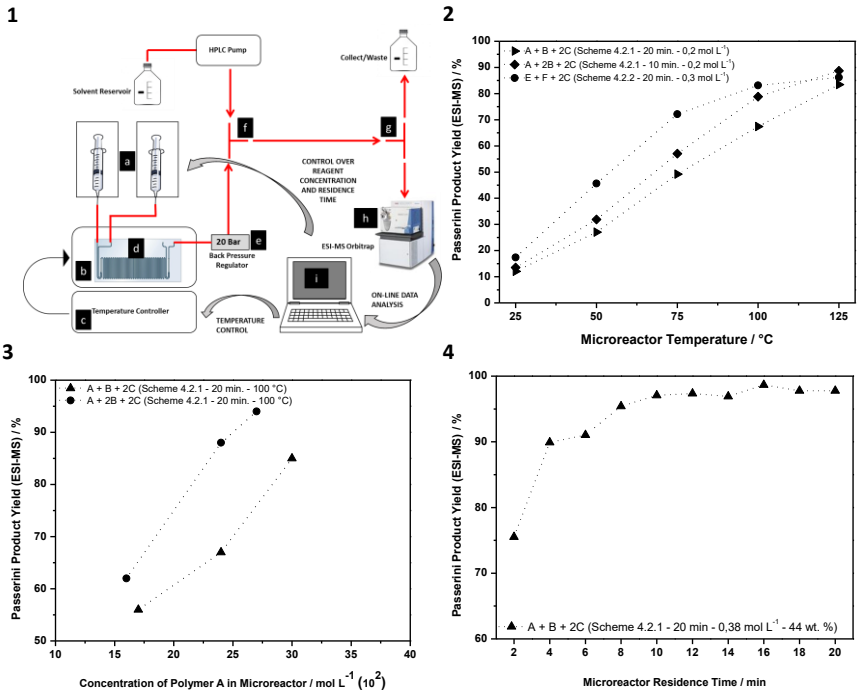

Figure 4.1. (top left 4.1.1) Schematic representation of the on-line ESI-MS/microreactor setup. (A. Syringe pumps, B. Reactor heating unit, C. Temperature controller, D. Microreactor chip, E. Back-pressure regulator, F. Dilution of the reaction mixture, G. Flow rate splitter, H. ESI-MS analysis and I. On-line data analysis). (top right 4.1.2) Screening of the Passerini product yield in function of microreactor temperature for both carboxylic acid polymer **A** and aldehyde polymer **F**. (bottom left 4.1.3) Screening of the Passerini product yield in function of initial polymer concentration in the reaction mixture for carboxylic acid polymer **A** and (bottom right 4.1.4) Screening of the Passerini product yield in function of reaction time for high initial polymer (**A**) concentration and equimolar carboxylic acid/aldehyde mixture at a temperature of 100 °C.

In Figure 4.2 it can be observed that, according to ESI-MS, the Passerini reaction has almost quantitatively taken place after 10 minutes with high (> 99%) endgroup fidelity of the polymer species (however, caution should be applied due to ionization biases). It should be noted that ESI-MS is without further calibration not quantitative. Complete disappearance of peaks can, however, be assumed to prove full conversion. With the conditions identified, continuous flow synthesis of block copolymers could in principle be carried out. As the aim of the study was, however, to optimize the classical batch reaction, direct translation of conditions (back) to batch was carried out. Scheme 4.2.3 shows a general reaction scheme for the diblock copolymer synthesis (**I**) by combining the two model reactions into one polymer-polymer reaction of the aldehyde containing P*n*BA (**F**) and a carboxylic acid-bearing polymer (**H**, poly(*n*-butyl acrylate), poly(methyl methacrylate) and poly(ethylene glycol methyl ester)) and ethylisocyanoacetate (**C**). Table 1 summarizes the synthesis results of the diblock copolymers in batch using the above flow conditions without further optimization. Only few experiments were carried out for the diblock copolymer formation in flow. To stay on the side of caution, and since batch chemistry is less restricted to short reaction times than MRT, the reaction time was extended to 1 h.

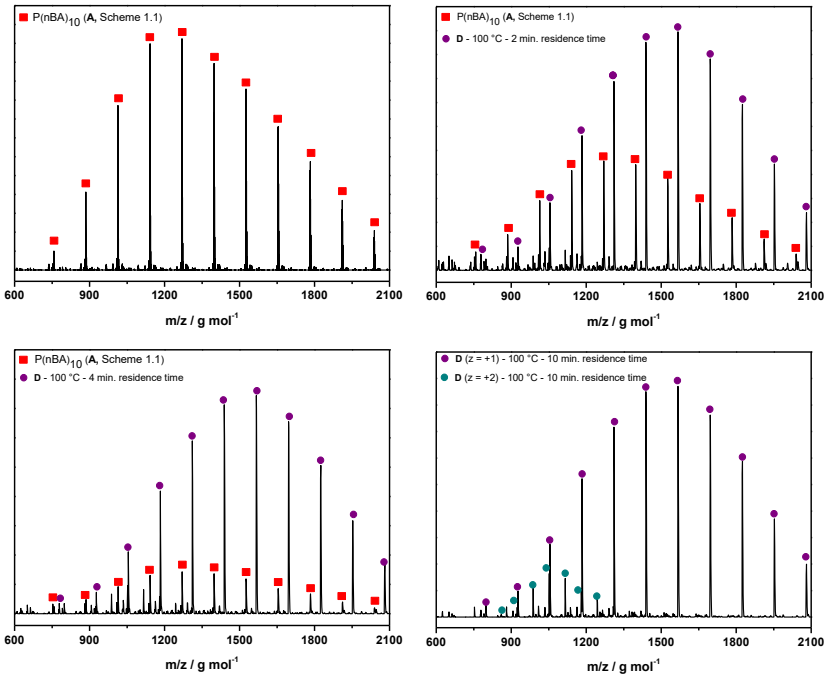

Figure 4.2. Formation of the Passerini product distribution in time in on-line ESI-MS. Spectra are shown at time zero (t_0) (top left), after 2 minutes (top right), 4 minutes (bottom left) and 10 minutes (bottom right) microreactor residence time. At t_0 the initial polymer (**A**) distribution was observed which is then screened with dodecylaldehyde (1 equivalent) and ethylisocyanoacetate (2 equivalents) at different microreactor residence times at a temperature of 100 °C in dichloromethane as the reaction solvent.

Success of the diblock copolymer conjugation was monitored by size-exclusion chromatography (SEC) analysis to determine the molecular weight and polydispersity of the final polymer product **I** (Scheme 4.2.3). In a successful coupling, formation of a monomodal polymer distribution with a M_n representing the sum of the two initial average molecular weights must be found. Table 4.1 shows the molecular weights and dispersities for the initial carboxylic acid (**H**) – and aldehyde (**F**) functionalized endgroup polymer in the reaction mixture as well as the SEC results for the three diblock copolymers (**I**) targeted. In all cases narrow dispersities (≤ 1.27) are obtained in each synthesis. The molar masses at the SEC peak maximum (M_p) are consistently shifted to a peak maximum corresponding to the summed M_p values of the initial polymer components. The corresponding SEC traces for P(*n*BA)$_{10}$-*b*-P(*n*BA)$_{10}$, P(*n*BA)$_{10}$-*b*-P(MA)$_{15}$ and P(*n*BA)$_{10}$-*b*-P(EGMEA)$_{10}$ are shown in Figure 4.3. It must be noted that molar concentrations of the polymer precursors (**F** and **H**, Table 4.1) are lower than previously screened due to solvation limits. Targeting a higher degree of polymerization (DP), so lower molar concentrations of the polymer precursors, caused low molecular weight shoulders in SEC analysis. This indicates that the reaction did not go to completion and increased reaction times are required to reach full conversion. Regardless, similar results were obtained for P(*n*BA)$_{10}$-*b*-P(*n*BA)$_{10}$ formation in batch and in a microreactor.

Table 4.1. Size exclusion chromatography results for the synthesis of P(nBA)$_{10}$-b-P(nBA)$_{10}$, P(nBA)$_{10}$-b-P(MA)$_{15}$ and P(nBA)$_{10}$-b-P(EGMEA)$_{10}$.

	M_p (F) (*g mol^{-1}*)	M_n (F) (*g mol^{-1}*)	*Đ* (F)	Conc. (F) (*wt. %*)	Conc. (F) (*mol L^{-1}*)	M_p (H) (*g mol^{-1}*)	M_n (H) (*g mol^{-1}*)	*Đ* (H)	Conc. H (*wt. %*)	Conc. H (*mol L^{-1}*)	M_p (I) (*g mol^{-1}*)	M_n(I) (*g mol^{-1}*)	*Đ* (I)
P(nBA)$_{10}$-*b*-P(nBA)$_{10}$ (Batch)	1350	1300	1.14	25	0.25	1650	1450	1.11	28	0.25	2900	2400	1.16
P(nBA)$_{10}$-*b*-P(nBA)$_{10}$ (Flow)	1350	1300	1.14	25	0.25	1650	1450	1.11	28	0.25	2900	2400	1.16
P(nBA)$_{10}$-*b*-P(MA)$_{15}$ (Batch)	1150	1050	1.14	17	0.21	2200	1700	1.25	25	0.21	3600	2550	1.27
P(nBA)$_{10}$-*b*-P(EGMEA)$_{10}$ (Batch)	1150	1050	1.14	17	0.24	1900	1650	1.13	29	0.24	2800	2300	1.17

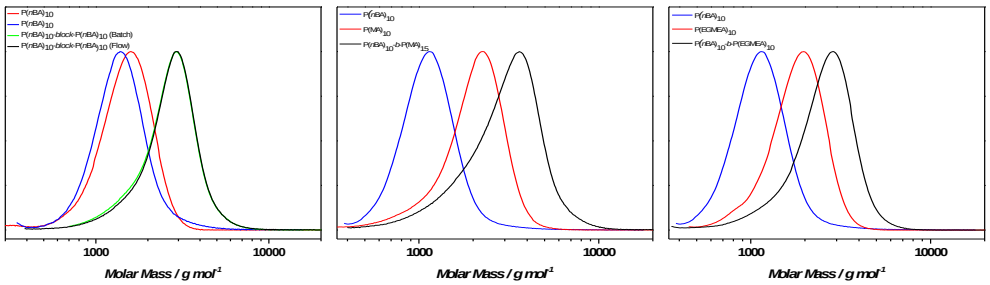

Figure 4.3. Size exclusion chromatography results for the synthesis of P(*n*BA)$_{10}$-*b*-P(*n*BA)$_{10}$, P(*n*BA)$_{10}$-*b*-P(MA)$_{15}$ and P(*n*BA)$_{10}$-*b*-P(EGMEA)$_{10}$ diblock copolymers with starting polymers with DP 10 or higher. It can be observed in SEC analysis that 1 hour reaction time is not sufficient to reach full conversion of the starting materials.

4.5 Conclusions

The Passerini 3-CR is a highly efficient coupling reaction that can be driven to completion within very short reaction times if reaction conditions are chosen carefully. High-throughput flow synthesis optimization showed that the reaction proceeds with ease under equimolar amounts of aldehyde and carboxylic acid moiety. If polymer concentrations are chosen sufficiently high and temperatures around 100 °C are applied, the Passerini reaction fulfills basically all "click" criteria for a polymer reaction (of course it can be debated if application of high temperatures can be seen as "wide in scope"). Various block copolymers have been synthesized to demonstrate the versatility of the reactions. The faster reaction rates found in this study can be rationalized as being due to temperature following Arrhenius kinetics. Yet, as we have shown, application of high temperatures does not lead to degradation, which is why we recommend using higher temperatures for performing Passerini couplings in upcoming works.

Next to unfolding the true potential of the Passerini polymer coupling, this study moreover demonstrates how a combination of on-line monitoring and microreactor flow synthesis can be used as a high-throughput screening device. Within a short time, reactions are optimized with ease without requiring large quantities of reactants. Important to note is that the conditions identified as optimal in the flow reactor are directly translatable back to batch processing. The reaction as described in here can hence be used in conventional approaches without any specific lab equipment. Flow synthesis is – next to its potential in high precision polymer synthesis and upscaling of complex reactions – also an excellent tool for kinetic screenings of polymer reactions.

4.6 References

1. Kowollik, C. B.; Prez, F. E. D.; Espeel, P.; Hawker, C. J.; Junkers, T.; Schlaad, H.; Camp, W. V. *Angewandte Chemie International Edition* **2011**, *50*, 60.

2. Alvim, H. G. O.; da Silva Junior, E. N.; Neto, B. A. D. *RSC Advances* **2014**, *4*, 54282.

3. Cioc, R. C.; Ruijter, E.; Orru, R. V. A. *Green Chemistry* **2014**, *16*, 2958-2975.

4. Dömling, A. *Chemical Reviews* **2006**, *106*, 17.

5. Akritopoulou-Zanze, I. *Current Opinion in Chemical Biology* **2008**, *12*, 257.

6. Weber, L. *Drug Discovery Today* **2002**, *7*, 143.

7. Kakuchi, R. *Angewandte Chemie International Edition* **2014**, *53*, 46.

8. Rudick, J. G. *Journal of Polymer Science Part A: Polymer Chemistry* **2013**, *51*, 3985.

9. Kreye, O.; Tóth, T.; Meier, M. A. R. *Journal of the American Chemical Society* **2011**, *133*, 1790.

10. Sehlinger, A.; Meier, M. A. R. *in Multicomponent and Sequential reactions in Polymer Science,* ed. Patrick, T. *Springer International Publishing, Switzerland,* **2015***, Advances in Polymer Science, Vol. 268,* pp. 61-86.

11. Yang, B.; Zhao, Y.; Y. Wei, C. F.; Tao, L. *Polymer Chemistry* **2015**, *6*, 8233.

12. Passerini, M.; Simone, L. *Gazzetta Chimica Italiana* **1921**, *51*, 126.

13. Pei, Y.; Noy, J.-M.; Roth, P. J.; Lowe, A. B. *Polymer Chemistry* **2015**, *6*, 1928.

14. Sehlinger, A.; Espinosa, L. M. d.; Meier, M. A. R. *Macromolecular Chemistry and Physics* **2013**, *214*, 2821.

15. Sehlinger, A.; Kreye, O.; Meier, M. A. R. *Macromolecules* **2013**, *46*, 6031.

16. Noy, J.-M.; Koldevitz, M.; Roth, P. J. *Polymer Chemistry* **2015**, *6*, 436.

17. Schmidt, S.; Koldevitz, M.; Noy, J.-M.; Roth, P. J. *Polymer Chemistry* **2015**, *6*, 44.

18. Wang, Y.-Z.; Deng, X.-X.; Li, L.; Du, Z.-L.; Li, Z.-C. *Polymer Chemistry* **2013**, *4*, 444.

19. Deng, X.-X.; Cui, Y.; Wang, Y.-Z.; Du, F.-S.; Li, Z.-C. *Australian Journal of Chemistry* **2014**, *67*, 555.

20. Sehlinger, A.; Schneider, R.; Meier, M. A. R. *European Polymer Journal* **2014**, *50*, 150.

21. Solleder, S. C.; Meier, M. A. R. *Angewandte Chemie International Edition* **2014**, *53*, 71.

22. Solleder, S. C.; Zengel, D.; Wetzel, K. S.; Meier, M. A. R. *Angewandte Chemie International Edition* **2016**, *55*, 1204.

23. Oelmann, S.; Solleder, S. C.; Meier, M. A. R. *Polymer Chemistry* **2016**, *7*, 1857.

24. Deng, X.-X.; Li, L.; Li, Z.-L.; Lv, A.; Du, F.-S.; Li, Z.-C. *ACS Macro Letters* **2012**, *1*, 1300.

25. Zhang, J.; Deng, X.-X.; Du, F.-S.; Li, Z.-C. *n Sequence-Controlled Polymers: Synthesis, Self-Assembly, and Properties,* ed. Lutz, J.-F.; Meyer, T. Y.; Ouchi, M.; Sawamoto, M. *American Chemical Society,* **2014***, ACS Symposium Series, Vol. 1170,* Ch. 15*,* pp. 224-235*.*

26. Li, L.; Deng, X.-X.; Li, Z.-L.; Du, F.-S.; Li, Z.-C. *Macromolecules* **2014**, *47*, 4660.

27. Kan, X.-W.; Deng, X.-X.; Du, F.-S.; Li, Z.-C. *Macromolecular Chemistry and Physics* **2014**, *215*, 2221.

28. Li, L.; Lv, A.; Deng, X.-X.; Du, F.-S.; Li, Z.-C. *Chemical Communications* **2013**, *49*, 8549.

29. Sehlinger, A.; Verbraeken, B.; Meier, M. A. R.; Hoogenboom, R. *Polymer Chemistry* **2015**, *6*, 3828.

30. Kakuchi, R.; Theato, P. *ACS Macro Letters* **2013**, *2*, 419.

31. Lv, A.; Deng, X.-X.; Li, L.; L, Z.-L.i; Wang, Y.-Z.; Du, F.-S.; Li, Z.-C. *Polymer Chemistry* **2013**, *4*, 3659.

32. Lin, W.; Guan, X.; Sun, T.; Huang, Y.; X.Jing; Z. Xie, C. S. *Colloids and Surfaces B: Biointerfaces* **2015**, *126*, 217.

33. Deng, X.-X.; Du, F.-S.; Li, Z.-C. *ACS Macro Letters* **2014**, *3*, 667.

34. Kreye, O.; Kugele, D.; Faust, L.; Meier, M. A. R. *Macromolecular Rapid Communications* **2014**, *35*, 317.

35. Jee, J.-A.; Songa, S.; Rudick, J. G. *Chemical Communications* **2015**, *51*, 5456.

36. Steven, C. V. *in Synthesis of Heterocycles via multicomponent reactions I,* ed. Orru, R. V. A.; Ruijter, E*. Springer-Verlag Berlin Heidelberg,* **2010***, Vol. 23,* pp. 161-198.

37. Sharma, S.; Maurya, R. A.; Min, K.-I.; Jeong, G.-Y.; Kim, D.-P. *Angewandte Chemie International Edition* **2013**, *52*, 7564.

38. Yang, B.; Zhao, Y.; Fu, C.; Zhu, C.; Zhang, Y.; Wang, S.; Wei, Y.; Tao, L. *Polymer Chemistry* **2014**, *5*, 2704.

39. Junkers, T. *Macromolecular Chemistry and Physics* **2017**, *218*, DOI: 10.1002/macp.201600421.

40. Ferguson, C. J.; Hughes, R. J.; Nguyen, D.; Pham, B. T. T.; Gilbert, R. G.; Serelis, A. K.; Such, C. H.; Hawkett, B. S. *Macromolecules* **2005**, *38*, 2191.

41. Domling, A.; Ugi, I. *Angewandte Chemie International Edition* **2000**, *39*, 3169.

42. Postma, A.; Davis, T. P.; Moad, G.; O'Shea, M. S. *Macromolecules* **2005**, *38*, 5371.

43. Hornung, C. H.; Postma, A.; Saubern, S.; Chiefari, J. *Polymer* **2014**, *55*, 1427

44. Vandenbergh, J.; Junkers, T. *Macromolecules* **2014**, *15*, 5051.

CHAPTER 5

Efficiency Assessment on Single Unit Monomer Insertion Reactions for Monomer Sequence-Control: Kinetic Simulations and Experimental Observations

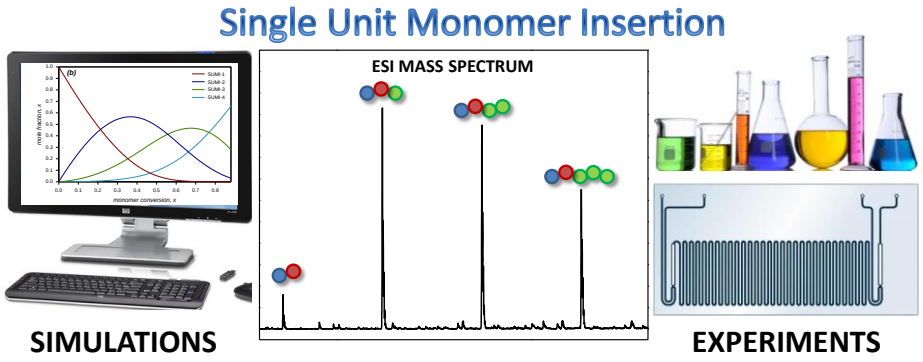

Haven, J. J.; Vandenbergh, J.; Kurita, R.; Gruber, J.; Junkers, T. *Polymer Chemistry* **2015**, *6*, 5752.

5.1 Abstract

The reaction efficiency of single unit monomer insertion (SUMI) reactions via the reversible addition-fragmentation chain transfer (RAFT) method is investigated in detail by determination of obtained product yields of optimized batch and microflow synthesis procedures in combination with kinetic simulations of the radical insertion process. A method is developed to obtain exact concentration information of different SUMI products from calibration of the corresponding electrospray ionization (ESI) mass spectra recorded on-line during synthesis. Experimental data show that isolated yields decrease for each subsequent SUMI reaction. This effect is investigated via kinetic modelling to understand which parameters have a beneficial or negative influence on the reaction outcome. Although most reaction conditions (such as monomer concentration or radical flux) do not play a considerable role in the obtainable yield of the insertion reaction, the model clearly shows that the propagation rate coefficient must display a strong chain-length dependency in order to explain the experimental observations. When this aspect is taken into account, the simulations fit the experimental data obtained from optimized micoreactor flow synthesis and recommendations for SUMI reactions can be formulated. Finally, the optimized SUMI conditions obtained from microreactor experiments and kinetic modelling insights are applied to upscale the SUMI synthesis reactions in a mesoflow reactor. This demonstrates the simple upscalability of continuous flow reactions and opens the pathway towards future synthesis of longer sequence-controlled oligomers.

5.2 Introduction

Single unit monomer insertion (SUMI) reactions via controlled radical polymerization pathways feature several advantages. Monomers can be chosen independent of their characteristic reactivity. At the same time, a broad range of monomers are available. By employing acrylate esters, a virtually infinite number of functional groups can be introduced into the sequence. These monomers are either commercially available, or can be synthesized easily by esterification. RAFT shows at the same time a high tolerance towards functional groups, allowing polar, unpolar or ionic monomers. The clear disadvantage of this method is the reaction yield, which is limited by the reaction statistics and by product isolation. With each growth iteration step, separation on a preparative column becomes more difficult, thus limiting the maximum chain length of the sequence-defined oligomer. A general reaction scheme of a SUMI reaction of a random acrylate is shown in Scheme 5.1, wherein a tetramer (4-mer) is isolated with 6 functionalities in the monodisperse oligomer chain.

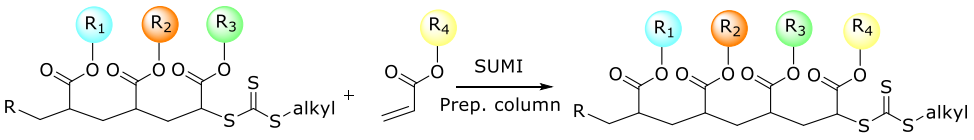

Scheme 5.1. Schematic representation of a single unit monomer insertion reaction using the RAFT process.

Obviously, isolated yields (after column separation) can be increased when the theoretical yields in the crude product mixtures are maximized. Recently, we have shown how such optimization can be carried out in a facile fashion using on-line

ESI-MS reaction monitoring in combination with continuous flow reactions in a microreactor device.[1] In this Chapter, we extract some of the previously described data as well as new optimization results for additional SUMI reactions in combination with kinetic simulations in order to provide an efficiency assessment on the SUMI process, taking differences between theoretical yields in crude reaction mixtures and isolated yields into account. In this way, a deeper understanding of the reaction processes is achieved, which is indispensable for future endeavors towards monomer sequence-defined oligomers with longer chain segments. Moreover, we describe the therefore used mass spectrometric data analysis in detail, giving examples on how exact concentration profiles can be obtained from polydisperse SUMI crude mixtures by on-line mass spectrometry. Further, optimized reaction procedures were used to upscale the synthesis of SUMI products, by changing from the micro- to the mesoscale employing chip-based flow reactors. Concomitantly, the SUMI reactions are modelled via the program package Predici® to shine light on the underpinning processes and to elucidate which reaction conditions are optimal to carry out monomer insertions with highest efficiency.

Note that throughout this Chapter, we will use the following systematic naming of the SUMI products: the initial digit always refers to the SUMI iteration, thus *1* to the first monomer insertion reaction, *2* for the second, etc. The letters represent the monomer sequence that is obtained in the respective iteration. *SUMI-2ABB* thus hypothetically refers to the second SUMI reaction side product (with *SUMI-1A* as starting material), in which two monomers *B* were built in.

5.3 Experimental Section

5.3.1 Flow Reactor Setups

Microreactor setup and **on-line ESI-MS coupling** are described in Chapter 2. The applied **mesoreactor setup** (Figure 5.1) consisted of a custom built reactor system (Uniqsis Ltd, UK), fitted with a glass chip reactor (**A**, internal volume = 2 mL, channel internal diameter = 1 mm) with active mixing geometry channels and an in-line back-pressure regulator (**B**, BPR, 17 bar). The reactant solution (**C**) was degassed *in situ* by nitrogen purging and introduced into the reactor through a Knauer HPLC pump (**D**) capable of delivering a solution at flow rates between 0.001 and 10 $mL \cdot min^{-1}$. The reactor temperature was controlled via a conventional hotplate (**E**) with a temperature controller (**F**, IKA Laboratory Equipment, RCT basic, temperature range 20 °C to 150 °C). The solution that exits the mesoreactor was collected while being cooled in an ice-bath (**G**).

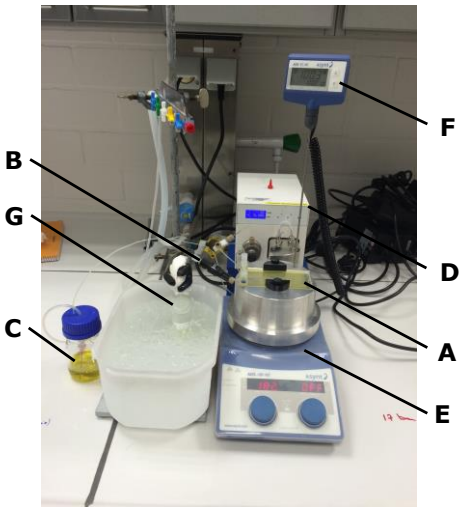

Figure 5.1. Mesoreactor setup with **A** glass chip – **B** BPR – **C** reactant solution – **D** HPLC pump – **E** hotplate – **F** temperature controller – **G** ice-batch.

5.3.2 Synthetic Procedures

Materials and characterization methods are described in Chapter 8.

The synthetic batch procedures towards SUMI-1A, SUMI-2AB and SUMI-3ABC have been described in in literature previously.[2]

The on-line ESI-MS/microreactor procedure towards screening SUMI-2AB has been described previously.[1]

5.3.2.1 Mesoreactor Flow Procedure Towards SUMI-2AB

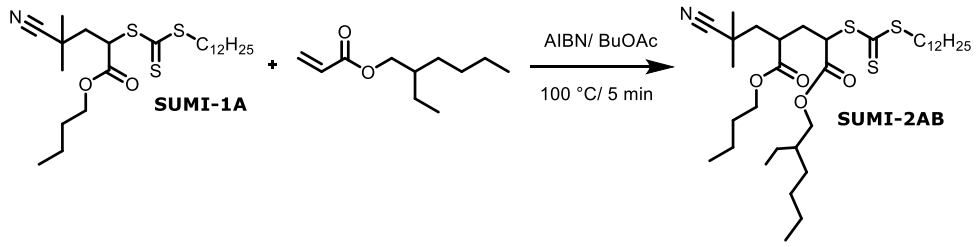

A 39 mL solution of 14.194 mmol (2.610 g, 5 equiv.) of the monomer 2-ethylhexyl acrylate (EHA), 2.838 mmol (1.345 g, 1 equiv.) of macroRAFT agent *SUMI-1A* and 0.113 mmol (0.0186 g, 0.04 equiv.) of AIBN was prepared with butyl acetate as the reaction solvent. Chemicals were weighted in a glass vial, dissolved in butyl acetate and via a measuring cylinder transferred into a schott bottle connected to the Knauer HPLC pump. The solution was degassed by nitrogen purging for 30 min to remove oxygen and subsequently employed with the mesoreactor setup. The conditions applied to the mesoreactor were 100 °C and 5 minutes residence time with a HPLC pump flow rate of 0.4 mL min^{-1}. The reaction mixture that exits the mesoreactor was collected in an ice-bath after the in-line back-pressure regulator (BPR, 17 bar) and transferred into an aluminum pan to evaporate excess solvent and monomer. The crude product mixture was purified via recycling preparative SEC to obtain **SUMI-2AB** as yellowish oil in 48% yield (0.889 g). ^{1}H-

NMR (300 MHz, $CDCl_3$, δ): 4.98−4.82 (m, 1H, CHCOO, backbone, EHA unit), 4.20−3.94 (br, 4H, $CH_2OC=O$, side chains), 3.35 (t, *J* = 7.5 Hz, 2H, $CH_2SC=S$, chain end), 2.82−2.66 (br, 1H, CHCOO, backbone, *n*BA unit), 2.50−1.82 (br, 4H, $C\underline{H_2}CHC\underline{H_2}CH$, backbone), 1.75−1.50 (m, 2H, CH_2, *n*BA side chain + 1H, CH, EHA side chain + 2H, CH_2, chain end), 1.46−1.15 (br, 10H, CH_2, side chains + 18H, CH_2, chain end + 6H, CN-C-$(CH_3)_2$), 0.94 (t, *J* = 7.4 Hz, 3H, CH_3, *n*BA side chain), 0.91−0.80 (br, 3H, CH_3, chain end + 6H, CH_3, EHA side chain). ^{13}C-NMR (75 MHz, $CDCl_3$, δ): 221.27, 221.02, 174.30, 170.30, 170.17, 124.18, 68.37, 65.43, 50.55, 49.79, 42.66, 40.63, 40.29, 38.77, 37.62, 35.22, 34.71, 32.02, 31.74, 31.67, 30.59, 30.53, 30.40, 30.37, 29.74, 29.67, 29.55, 29.46, 29.21, 29.01, 27.98, 27.00, 26.96, 26.87, 26.75, 24.97, 23.83, 23.78, 23.09, 22.81, 19.31, 14.25, 14.19, 13.88, 11.10. ESI-MS (m/z): 680.38 ($M+Na^+$).

5.3.2.2 On-Line Microreactor Flow Procedure Towards Screening of SUMI-3ABC

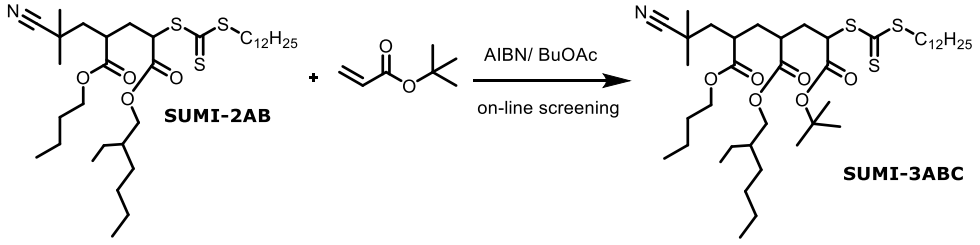

A 0.20 mL solution of 0.0881 mmol (58 mg, 1 equiv.) of macroRAFT agent **SUMI-2AB** and 0.0070 mmol (1.2 mg, 0.08 equiv.) of AIBN with butyl acetate was prepared. A second 1 mL solution of 0.440 mmol (56 mg, 1 equiv.) of the monomer *tert*-butyl acrylate with butyl acetate was prepared. Chemicals were weighted in a glass vial with a stirring bar and inserted into the glovebox, where butyl acetate was added. The solution was stirred for 15 min to remove the

residual oxygen. The two solutions were transferred to two gas-tight 1 mL syringes (SGE) and subsequently employed with the microreactor setup. The conditions applied to the microreactor and screened by the on-line ESI-MS/microreactor setup are summarized in Table 5.3 and Table 5.4.

5.3.2.3 Mesoreactor Flow Procedure Towards SUMI-3ABC

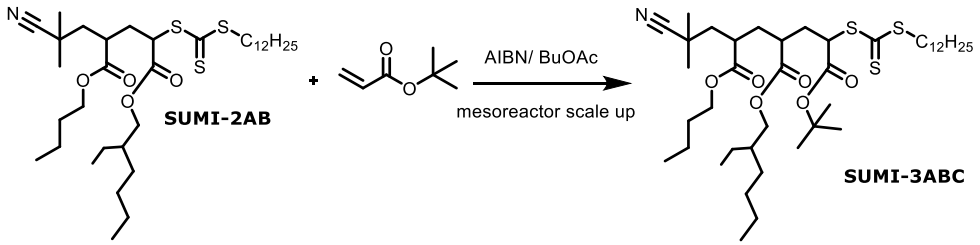

A 18 mL solution of 1.299 mmol (0.166 g, 1 equiv.) of the monomer *tert*-butyl acrylate (*t*BA), 1.299 mmol (0.855 g, 1 equiv.) of macroRAFT agent **SUMI-2AB** and 0.104 mmol (0.017 g, 0.08 equiv.) of AIBN was prepared with butyl acetate as the reaction solvent. Chemicals were weighted in a glass vial, dissolved in butyl acetate and via a measuring cylinder transferred into a schott bottle connected to the Knauer HPLC pump. The solution was degassed by nitrogen purging for 30 min to remove oxygen and subsequently employed with the mesoreactor setup. The conditions applied to the mesoreactor were 100 °C and 8 minutes residence time with a HPLC pump flow rate of 0.25 $mL \cdot min^{-1}$. The reaction mixture that exited the mesoreactor was collected in an ice-bath after the in-line back-pressure regulator (BPR, 17 bar) and transferred into an aluminum pan to evaporate excess solvent and monomer. The crude product mixture was purified via recycling preparative SEC to obtain **SUMI-3ABC** as a yellowish oil in 20% yield (0.204 g). ^{1}H-NMR (300 MHz, $CDCl_3$, δ): 4.79−4.63 (m, 1H, CHCOO, backbone, *t*BA unit), 4.20−3.90 (m, 4H, $CH_2OC=O$, side chains), 3.38−3.15 (d t, *J* = 7.5 Hz, 2H,

$CH_2SC=S$, chain end), 2.65−2.41 (b, 2H, CHCOO, backbone, *n*BA and EHA units), 2.42−1.80 (b, 6H, $C\underline{H_2}CHC\underline{H_2}CHC\underline{H_2}CH$, backbone), 1.72−1.52 (m, 2H, CH_2, *n*BA side chain + 1H, CH, EHA side chain + 2H, CH_2, chain end), 1.46−1.41 (tr s, 9H, $OC(CH_3)_3$, *t*BA), 1.42−1.20 (b, 10H, CH_2, side chains + 18H, CH_2, chain end + 6H, CN-C-$(CH_3)_2$), 0.97−0.83 (b, 3H, CH_3, chain end + 3H, CH_3, *n*BA side chain + 6H, CH_3, EHA side chain). ^{13}C-NMR (75 MHz, $CDCl_3$, δ): 221.73, 221.88, 221.44, 221.29, 174.82, 174.35, 174.31, 174.08, 169.17, 169.12, 169.05, 168.97, 124.34, 124.28, 82.79, 67.67, 67.61, 65.23, 65.16, 52.14, 52.04, 51.49, 43.48, 42.57, 42.35, 41.58, 41.17, 41.06, 40.68, 40.60, 40.48, 40.43, 38.86, 37.55, 36.63, 36.36, 36.14, 34.67, 34.26, 33.78, 33.03, 32.09, 31.79, 31.66, 30.64, 30.51, 29.80, 29.74, 29.63, 29.52, 29.28, 29.11, 28.02, 27.14, 27.04, 26.90, 26.85, 26.81, 26.76, 23.86, 23.17, 22.87, 19.35, 14.31, 13.94, 11.14. ESI-MS (m/z): 808.25 ($M+Na^+$).

5.4 Results & Discussion

5.4.1 Single Unit Monomer Insertions via RAFT Polymerization

The RAFT process can be used for consecutive single unit monomer insertions (SUMI), successfully leading to monodisperse acrylate oligomers with precisely defined structure.[3-4] The synthetic pathway and the exact monomer sequence for the materials under investigation in this contribution is given in Scheme 5.2. In a first reaction, the initial cyanoisopropyl-functional trithiocarbonate RAFT agent (CPD-TTC RAFT) was reacted with *n*BA to form the *SUMI-1A* product. After purification (see below), *SUMI-1A* was used as macroRAFT agent for subsequent insertion of 2-ethylhexyl acrylate (EHA) into *SUMI-2AB* which in turn was reacted with *t*BA to obtain *SUMI-3ABC*.

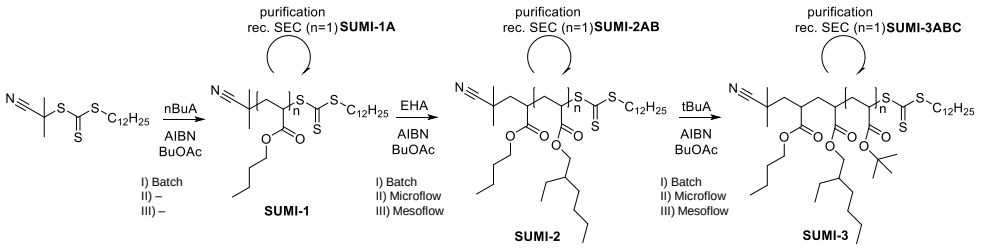

Scheme 5.2. Synthetic pathway towards sequence-defined *SUMI-1A*, *SUMI-2AB* and *SUMI-3ABC* using SUMI via RAFT polymerization.

In our first study, all reactions were carried out in batch and were not fully optimized for maximum product yields. In Chapter 2, we also introduced the on-line coupling of a microreactor with soft ionization mass spectrometry (ESI-MS) to optimize reaction conditions (monomer to macroRAFT agent ratio, reaction temperature and residence time) of the *SUMI-2* reaction.[1] Herein, we extend this

concept to the optimization of the *SUMI-3* reaction and upscale the synthesis of *SUMI-2* and *SUMI-3* using a mesoflow reactor with an internal volume 100 times larger than the volume of the microreactor. Flow reactors serve hereby not only as a tool to upscale the SUMI reactions; but in combination with on-line monitoring, allows for facile kinetic screening and fast optimization of reactions. At the same time, a better definition of products can be reached in such reactors. The reaction exotherm is quickly dissipated in the microfluidic devices, thus leading to a significant reduction in side reactions. In consequence, reaction conditions are more reproducible, batch-to-batch variations are significantly smaller, and overall better microstructures can be expected. Thus, employing continuous flow by itself increases the obtainable yield of the SUMI reaction. At the same time, it can also be assumed that microreactions are – due to their ideal thermal behaviour – much closer to most kinetic modelling studies as no exothermicity and thus temperature change must be considered for this type of reactions. Exactly for this reason, microreactors are often described as ideal kinetic tools, besides their high synthetic potential.

Before discussing the experimental results (and how they were derived), the focus is first on the kinetic modelling of the SUMI reactions, as a thorough understanding of the reaction is required to discuss the observed experimental results.

5.4.2 Modelling of SUMI Reactions

Single unit monomer insertions are limited in their reaction yield due to the statistical nature of the radical insertion process applied. It is important to differentiate the conversion of successive SUMI to the desired monomer inserted product (theoretical yield) from the isolated yield of the reaction, which might be

significantly different from each other. Obviously, yields must be kept high in order to allow for most efficient product separations as column chromatography works the more efficient the less by-products are present in the crude mixture. While these considerations are part of the reaction optimization (see below), it appears worthwhile to investigate SUMI reactions also using a kinetic modelling approach to determine limitations and best operation windows of the insertions. Thus, the reactions as described in the experimental section were modelled using the program package Predici® (Simulations have been carried out with Predici® (CIT) version. 7.1.0). Simulations were performed by Prof. Tanja Junkers. Therefore, only simulation results rather than the full model discription are described in this Chapter. Also, recommendations are given for the SUMI experiments. More theoretical details on the model can be found in the corresponding manucript.[5]

5.4.2.1 Simulation Results

Figure 5.2 depicts the simulation outcome for the model as described above for an initial [monomer]:[*SUMI-1A*] concentration ratio of 3:1, assuming chain-length independent propagation and RAFT addition for Figure 5.2a, while considering chain-length effects in Figure 5.2b. For the chain-length independent model, consumption of all starting material is only achieved upon reaching full monomer conversion. The concentration of *SUMI-2AB* and thus of the desired product, reaches a maximum at around one equivalent of monomer consumption compared to *SUMI-1A*, which is in line with expectations. Yet, also significant amounts of *SUMI-2ABB* are present at the same stage already. The high accumulation of *SUMI-2ABBB* at the end of the reaction is indicative that the system under such conditions would feature also species with much higher chain lengths (product

SUMI-2ABBB represents an accumulation of *SUMI-2ABBB* and all higher chain length derivates). This simulation outcome is not in line with the experimental observation, where higher fractions of *SUMI-2AB* are found alongside faster conversion of *SUMI-1A* (as can be seen in Figure 5.2a, *SUMI-1A* has not yet fully depleted even at 90 % of monomer conversion, a fact that can not be confirmed in experiments) and only small amounts of higher chain length species.

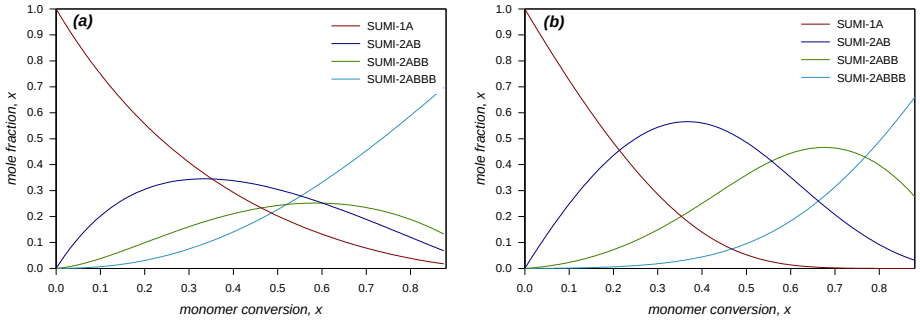

Figure 5.2. Modelling of the evolution of SUMI products during polymerization assuming (a) a chain-length independent propagation and RAFT addition reaction and (b) under consideration of chain-length effects. For the simulations, a [monomer]:[SUMI-1] ratio of 3:1 was assumed for a reaction at 100 °C. *SUMI-2ABBB* represents an accumulation of *SUMI-2ABBB* and all higher chain length derivates.

Further model refinement was thus required to match the experimental results. Interestingly, changing key parameters such as termination rate coefficients, RAFT addition or intermediate radical fragmentation rate coefficients, monomer concentration (at fixed ratio to *SUMI-1*) or radical flux has very little influence on the outcome of the simulation as shown in Figure 5.2a and only affects the overall rate of polymerization. The reason why the influence is rather small is because all

shifts are in such case constant and do not lead to a differentiation between the various SUMI products. The distribution between species of different chain lengths is purely given by statistics and in principle a Poisson distribution is obtained. The only way how a deviation from such statistic distribution can be achieved is by implementing a chain-length dependency for the reactions and assigning individual rate parameters to the individual elemental reactions. The key reaction in this respect is a chain-length dependency on the propagation reaction which has already been discussed. [6-11] Compared to termination, where the change in rate parameters can be essentially assigned to a change in diffusion coefficients,[12-13] a less clear theoretical understanding of propagation is available. However, a chain-length dependency of the termination rate cannot play a significant role in a well-controlled RAFT system with low AIBN concentrations. Additionally, experiments have shown that any chain-length dependency of propagation is in all likelyhood limited roughly to the first 10 propagation steps and thus hard to follow in polymerizing systems where much higher chain lengths dominate. For the sake of the present study, the reason for the effect is not relevant, only the question if a dependency exists. Nevertheless, Heuts *et al.* had proposed that the rate coefficient for propagation should follow:

$$k_p(i) = k_p(SPR)\left[1 + C_1 \cdot exp\left(-\frac{ln2}{i_{1/2}}\right)(i-1)\right]$$

where k_p(SPR) marks the long-chain limit of k_p (as measured by pulsed-laser polymerization techniques), i the chain length and where C_1 and $i_{½}$ are scaling parameters.[14] Adopting (arbitrary choice) C_1=10 and $i_{½}$=1, the individual rate parameters for $k_p(i)$ (see Table 5.1) are derived.

Table 5.1. Individual propagation rate coefficients used in the modelling of the SUMI reactions following Eq. 1 with C_1=10 and $i_{½}$= 1. Note that the addition of monomer to the radical fragment R-M· was considered to proceed with $k_p(2)$.

$k_p(1)$	**770 000 L·mol^{-1}·s^{-1}**
$k_p(2)$	420 000 L·mol^{-1}·s^{-1}
$k_p(3)$	245 000 L·mol^{-1}·s^{-1}
$k_p(4)$	157 500 L·mol^{-1}·s^{-1}
$k_p(5)$	113 750 L·mol^{-1}·s^{-1}
$k_p(6)$	91 875 L·mol^{-1}·s^{-1}
$k_p(\infty)$	70 000 L·mol^{-1}·s^{-1}

As can be seen, the predicted variation of the rate is dramatic for the first few reaction steps. Implementation of these coefficients into the model (note that a radical fragment as released from *SUMI-1*, consisting of the original leaving group and one monomer unit, is considered to be of chain length 2) improves the modelling outcome. However, only when also the radical addition rate (and the according intermediate radical fragmentation rate) to the macroRAFT is likewise defined with the same chain-length dependency, a modelling result is obtained which is close to the experimental observation (see Figure 5.2b). While the choice of individual rate parameters is here somewhat arbitrary, the in this way derived results in Figure 5.2b nicely demonstrate that chain-length effects must clearly play a role in the SUMI reactions when comparing these results with the experimentally derived theoretical yields (Table 5.2). Starting material is consumed at a much higher rate compared to the chain-length independent case,

and also a better relation between conversion and progressive chain addition is seen. It must be stressed that a similar modelling result as in Figure 5.2b cannot be reached with the present model if no chain-length dependency is assumed. While on first glance also alternative explanations – such as non-idealities of the RAFT process itself, any type of termination (including cross-termination of the RAFT intermediate), involvement of AIBN-derived cyanoisopropyl radicals, a chain-length dependent RAFT intermediate fragmentation rate or a chain-length dependent macroradical addition rate – may cause a similar effect, only chain-length dependent propagation can really serve as a viable origin of the effect. Moreover, no experimental evidence was observed for the previously named alternative explanations. A more detailed discussion can be found in the corresponding manuscript.[5]

While of course the different SUMI products coexist at any given point in time, better separation of the different concentration profiles is observed. In the example given in Figure 5.2b (where *SUMI-1A* is used as the starting macroRAFT agent), a theoretical yield of 56% (at exactly x = 0.33, note that the absolute maximum is reached slightly above this monomer conversion) is obtained for the desired *SUMI-2AB*. If instead of *SUMI-1A*, *SUMI-2AB* or *SUMI-3ABC* is chosen as starting macroRAFT material, yields of resulting *SUMI-3ABC* and *SUMI-4ABCD* insertion products decrease, respectively, as the chain-length effect between the different species becomes less pronounced ($k_p(2)/k_p(4)$=2.66 vs. ($k_p(4)/k_p(6)$=1.71). For the first single unit monomer insertion starting from *SUMI-2AB*, a theoretical yield of 50% (for obtaining *SUMI-3ABC*) and starting from *SUMI-3ABC*, a theoretical yield of 46% (for *SUMI-4ABCD*) was calculated. The trend of this observed decrease in SUMI efficiency was also observed

experimentally, but of course more reliable information on the chain-length dependent k_p would be required to make more accurate theoretical predictions. For the moment, the given numbers only present a trend. Still, the significant change of $k_p(i)$ is in its order of magnitude required to create the effect and certainly a change in individual propagation rate coefficients in a similar order of magnitude would be realistic. Importantly, as the described product distributions are a direct consequence of the individual rate coefficients rather than the control methodology employed, the herein derived results should be transferable to other polymerization techniques, such as nitroxide-mediated polymerization[15] or atom transfer radical polymerization.[16] Results from ATRP-like SUMI reactions in our laboratories confirm this assumption.[4]

5.4.2.2 Recommendations for the SUMI Experiments

The given product distribution does not change much with the experimental conditions and is thus independent of most reaction parameters. This means for the experiment that monomer and RAFT agent concentrations can be chosen freely. Temperature and initiator concentrations may be chosen accordingly to the desired reaction time, whilst keeping in mind the need to avoid backbiting and β-scission side reactions which are more pronounced at high temperatures. It is therefore noteworthy to add that in the modelling roughly 2-3% termination products are predicted, which is in good agreement to the amount of AIBN used in the model. Hence, the initiator concentration plays no significant role for the reaction yield unless extreme concentrations were considered.

An important remaining question is which monomer to macroRAFT agent ratio is most beneficial for carrying out SUMI reactions. An equimolar range is often

proposed as this supposedly leads to a maximum yield of the insertion. As shown above, the theoretical yield is governed mostly by the individual rate parameters, and less by monomer concentration. In fact, when reactions are always stopped at monomer conversions identical to consumption of one equivalent of monomer, very similar product patterns are observed when the initial equivalents of monomer are varied between 1 and 10 (see Table 5.2).

Table 5.2. Simulated effect of monomer to *SUMI-1* ratio on the yields of individual products at consumption of one equivalent of monomer.

[Monomer]:[SUMI-1]	1:1	2:1	3:1	4:1	5:1	10:1
x(SUMI-1A)	21%	22%	23%	23%	24%	31%
***x*(SUMI-2AB)**	**58%**	**58%**	**56%**	**55%**	**53%**	**46%**
x(SUMI-2ABB)	17%	18%	18%	19%	19%	18%
x(SUMI-2ABBB)	2%	2%	3%	3%	3%	5%

While indeed equimolar conditions result in the highest absolute yield of the first SUMI product, only a very small decrease with increasing monomer equivalents is seen (represented in bold in table 5.2). Only at a ratio of 10:1, a significant reduction of the product yields must be expected. Larger equivalents of monomer are thus recommended for the SUMI reactions as higher monomer concentrations directly translate to increased overall polymerization rates. An additional advantage is given by the fact that truly optimal conditions for maximized yields are not obtained at consumption of one monomer equivalent, but systematically at slighty higher conversions, thus giving a slight advantage to the 2:1 or 3:1 condition over equimolar ratios.

5.4.3 Experimental Observations

5.4.3.1 ESI-MS Analysis and Isolation of Obtained SUMI Products

As described above the radical insertion of monomers into a macroRAFT agent is a statistical process, so not only the desired SUMI product is formed, but also multiple insertion by-products. When the crude SUMI products (obtained by RAFT polymerization in batch) are analyzed by ESI-MS, the different insertion products can clearly be observed (see Figure 5.3, left side). Therefore purification using automated recycling size exclusion chromatography (SEC) was required.[17] In recycling SEC, the SUMI product mixture was recycled over columns with size exclusion limits from 1000 to 5000 Da. With each additional cycle, the products with different sizes (hydrodynamic volumes) are further separated. The process is fully computer controlled, followed by UV and RI signal detection, and resulting pure product fractions are collected automatically. Separation of SUMI products becomes more tedious upon increasing number of monomer units in the oligomer chain. Because the hydrodynamic volume of the SUMI species does not increase linearly with increasing chain length, more recycling cycles are required for separation of *SUMI-2* and *SUMI-3* than for *SUMI-1*. After purification, the pure SUMI products are again analyzed with ESI-MS (see Figure 5.3, right) to confirm the purity of the final monodisperse products. Currently, flash column chromatography is utilized in our labs for the purification of oligomer mixtures (up to 11-mers).[3] However, up to oligomer chain length 4 or 5, recycling SEC is an excellent technique to purify the oligomer mixtures.

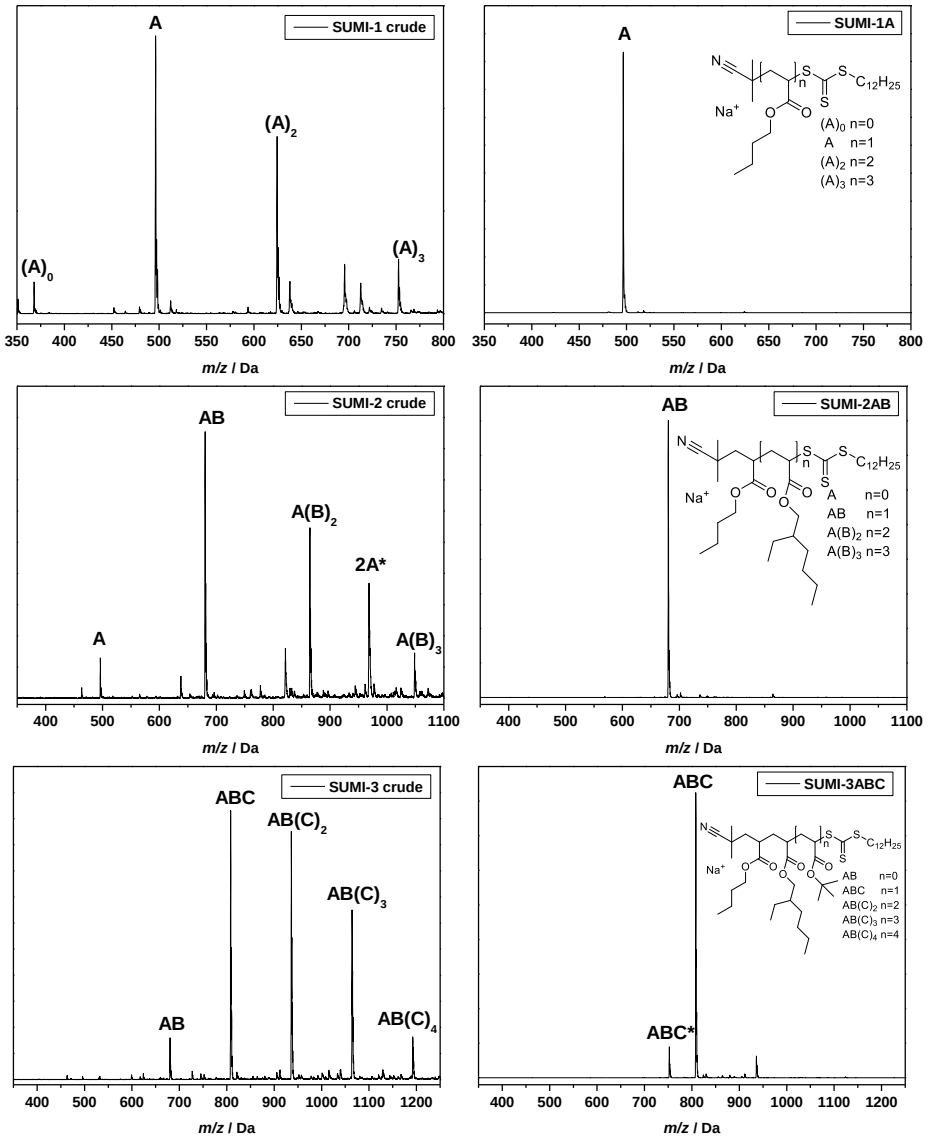

Figure 5.3. ESI-MS spectra of *SUMI-1*, *SUMI-2* and *SUMI-3* before (left) and after (right) purification with recycling SEC. The species marked with asterisks correspond to an aggregate of 2 A molecules or to an ABC molecule with a hydrolyzed *t*BA unit, respectively.

5.4.3.2 Concentration Calibration of ESI Mass Spectra

The following isolated yields were obtained for the monodisperse batch products: 55% for *SUMI-1A*, 46% for *SUMI-2AB* and 20% for *SUMI-3ABC*. The decreasing yield can be attributed to the predicted loss of efficiency of the SUMI reactions with increasing chain length, but also to the increasing difficulty in separation of the different product species. The question thus arises how the isolated yield relates to the theoretical yield in the crude product mixture. As seen in Figure 5.3, the crude mixture is conveniently analyzed by ESI-MS. Mass spectrometry thus offers the opportunity to obtain information on the composition of individual species and hence to directly optimize the reaction parameters towards maximum theoretical yields for each consecutive SUMI reaction.

However, in order to use ESI-MS to determine the yield of the desired SUMI product (species A, AB and ABC in Figure 5.3) before final isolation, the peak intensities of the different insertion species need to be related to their true molar fractions in the crude SUMI mixtures. Peak intensities in ESI-MS suffer from mass and ionization bias effects, so they cannot be considered quantitative. In this specific system, it is observed that species containing more acrylate units (hence more polarizable ester moieties) ionize easier than species containing fewer acrylate units, as also observed previously in Chapter 2. In this case, AB ionizes more readily than A, and ABC ionizes more readily than AB, resulting in apparently increasing peak intensities for equal concentrations. In order to correlate the peak ratios with the true molar fractions, calibration files were prepared for the *SUMI-2* and *SUMI-3* reactions. The *SUMI-1* reaction was left out of consideration for the same reason as why it was excluded from the kinetic simulations, namely because

the pre-equilibrium stage alters the kinetic scenario significantly, thus making it difficult to derive clear conclusions from the analysis of this reaction.

In a first step to make the calibration file for *SUMI-2*, pure *SUMI-1A* and *SUMI-2AB* were mixed systematically in well-known ratios and the mixtures were measured by ESI-MS. For all molar ratios tested throughout the calibration, the total concentration of the samples was kept constant. Regardless, in the range of concentrations used in this study, no significant impact of the sample solution on the residual mass spectrum was expected.[18-19] Based on the obtained peak abundances in the mass spectra, calibration curves for species A and AB were determined (Figure 5.4.1). As can be seen from Figure 5.4.1, species A is underestimated relatively to AB, which is in agreement with the fact that AB ionizes more readily due to its extra acrylate unit. In the calibration file, any measured peak abundance for species A or AB can now directly be related to the true molar fraction. It was further tested if the A:AB peak ratio changed significantly if a certain amount of species $A(B)_2$ was present. But as can be seen from Figure 5.4.3, the experimentally measured peak abundances for A and AB stay comparatively constant, regardless of the mole fraction of $A(B)_2$ present. Therefore, the use of the calibration curve in Figure 5.4.1 for the more complex SUMI product mixtures, containing several insertion products, appears to yield a good approximation.

For calibration of *SUMI-3*, the same procedure was repeated (Figure 5.4.2), using mixtures of *SUMI-2AB* and *SUMI-3ABC*. Experimentally observed peak abundances were compared to true molar AB:ABC ratios and the calibration curves

were determined. Again, the presence of $AB(C)_2$ did not alter the measured peak intensities of AB and ABC too much (Figure 5.4.4).

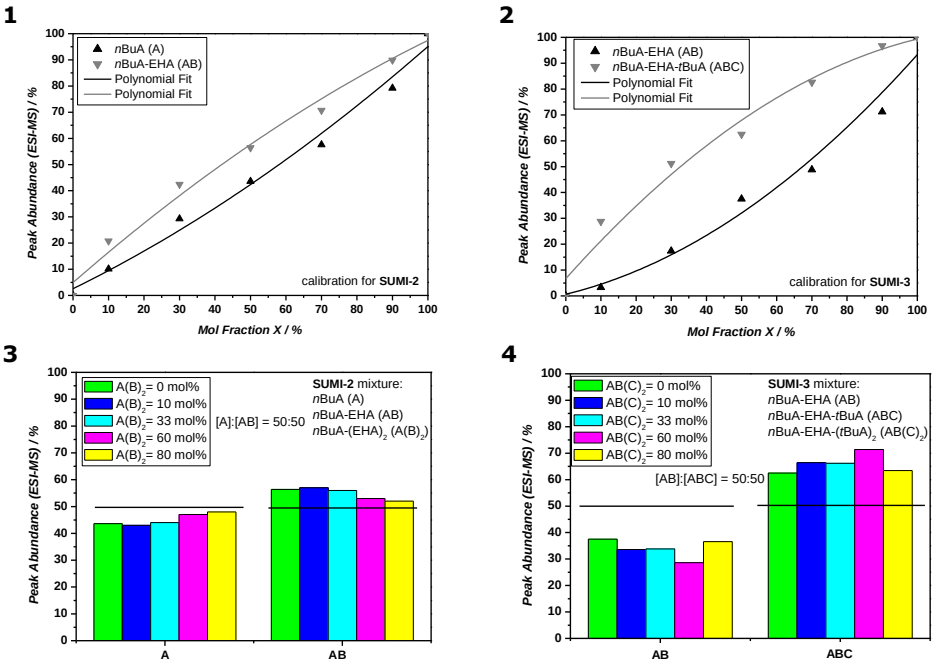

Figure 5.4. ESI-MS calibration curves for *SUMI-2* and *SUMI-3*, correlating peak abundances of products A, AB and ABC with their true molar ratio.

When comparing calibration curves for *SUMI-2* and *SUMI-3*, the deviation of the measured peak intensities from their true molar fractions is more severe for the *SUMI-3* calibration. This effect can be explained by the nature of the acrylate unit inserted in the different SUMI reactions. In the case of *SUMI-2*, EHA is used as the insertion monomer, which is more apolar than *t*BA, used as the model monomer in the *SUMI-3* reaction. Due to this difference in polarity, it is plausible to assume that the ionization bias effect for *t*BA insertions is more pronounced

than for EHA insertions, causing this effect in the resulting calibration curves. Another reason for this different ionization behavior might be the lower molar mass of *t*BA compared to EHA. At the same time, this ionization difference also demonstrates that calibrations as shown here are highly sequence-dependent and cannot be used for other monomer combinations. It must also be noted that during optimization experiments (Table 5.3 and 5.4), the microflow in-situ injected into the ESI chamber, is of higher concentration (10x-50x) than the manually injected SUMI product mixtures prepared for calibration. However, in this concentration range no additional concentration related bias effects were observed; the only concentration dependent parameters are the total ion count as well as the maximum injection time to fill the trap.

5.4.3.3 Optimization via an On-Line ESI-MS/microreactor Coupling

After the calibration files were established the main focus shifted towards on-line ESI-MS/microreactor reactions as the microflow reactions were expected to yield more stable and reproducible results. The synthesis and optimization of a *SUMI-2* product had been demonstrated before and the description of this step is thus kept short in here (experimental data is given in Chapter 2). By coupling a microreactor system to an ESI-MS spectrometer, chemical (polymerization) processes can be monitored in real time and thus allow for rapid and efficient high-throughput optimization by screening a broad range of reactor residence times, reaction temperatures and reagent ratios (by mixing monomer and macroRAFT solutions from two syringes with individual flow rates). A picture and schematic representation of the on-line monitoring setup is shown in Chapter 2 (section 2.3.2). Optimization results for the *SUMI-2* reaction are given in Tables 2.2-2.4 (Chapter 2). Optimized reaction conditions were identified with 100 °C, a

monomer to *SUMI-1A* ratio of 5:1 and a reaction time of 5 minutes. It should be noted that a slightly better result was seen for reaction at 110 °C, but for reasons of consistency and in order to reduce the likelihood of thermal elimination reactions, 100 °C was chosen. For this case, a total theoretical yield of 59% for the desired *SUMI-2AB* was identified after ESI calibration, with 11% remaining starting material, 26% of *SUMI-2ABB* and 4% *SUMI-2ABBB* product. The values are in astonishingly good agreement with the simulation results as given in Table 5.2. This underpins that (*i*) the assumption of chain-length dependent k_p is very valid (without it the experimental results could not be explained, see section 5.4.2) and (*ii*) that the microflow reactor indeed provides close to ideal reaction conditions that are well represented by simulations. At the same time, it also became evident that the monomer to *SUMI-1* ratio has only little effect on the maximum yield of the product, but only on the rate of the reaction (and to some extent distribution of the by-products), which is also well in line with the simulations.

SUMI-3ABC was again synthesized in flow by insertion of a *tert*-butyl acrylate monomer into the *SUMI-2AB* macroRAFT agent. Reaction products are depicted in Scheme 5.3. Results for the various screening conditions are summarized in Table 5.3 (ESI-MS peak abundances) and Table 5.4 (molar ratios from calibration). The temperature was kept constant at 100 °C throughout the optimization experiment since this temperature had been identified as optimal in the *SUMI-2* reactions. Reactor residence times were varied from 2-10 minutes and molar ratios [*t*BA]:[*SUMI-2AB*] from 1:1 to 10:1. Again, only a small variation in product yields was observed when changing the monomer feed ratios, being in good agreement with the theoretical expectations. However, an absolute maximum yield for this

reaction was obtained for equimolar ratios between monomer and the starting *SUMI-2AB* product. After 8 minutes reaction time, 34% of *SUMI-3ABC* was reached, with a significant proportion of unreacted *SUMI-2AB* being left over (41%). By increasing the monomer concentration, the amount of unreacted starting material could be reduced, but concomitantly larger amounts of the higher insertion products were obtained. The first case is from a synthetic point of view more attractive as remaining starting material is more easily separated from the product and can be reused in following reactions while the higher insertion products usually must be seen as waste. The reason for the slight difference in reactivity of the *SUMI-3* reaction compared to *SUMI-2* can be explained by the difference in reactivity between EHA and *t*BA, but also by the decreasing chain length dependency. The rather low yield and fast equilibration over the different products in fact hints to the fact that the chain-length dependency of k_p reduces faster with chain length than anticipated in Table 5.1. Further investigations on this observation are desirable, but could at present not be carried out due to the large experimental efforts that are required for each ESI calibration step. Regardless, in principle the present SUMI experiments allow – provided a broad data basis can be gathered over time – for an assessment of the exact $k_p(i)$ dependency.

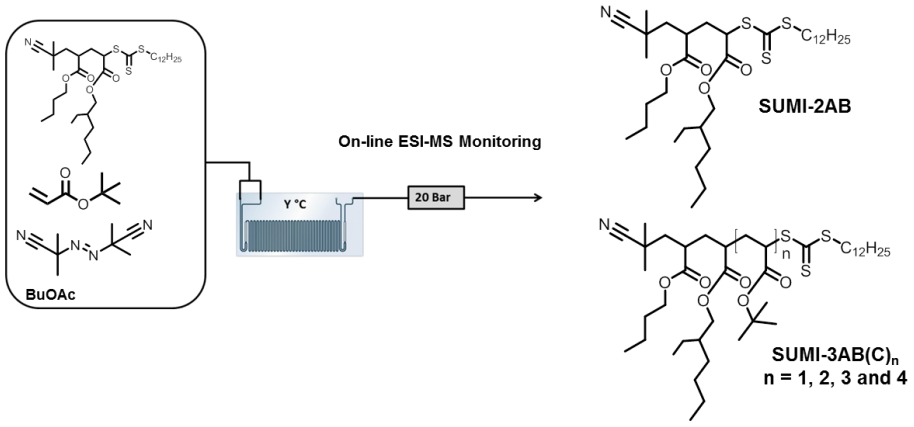

Scheme 5.3. Schematic representation of the *SUMI-3* insertion reaction in a glass-chip microreactor at 100 °C.

Table 5.3. Microreactor screening conditions and ESI-MS peak abundances for the synthesis of *SUMI-3ABC*.

Condition	Temp. (°C)	[*t*BA] : [**SUMI-2AB**]	Residence Time (min)	AB (%)	ABC (%)	$AB(C)_2$ (%)	$AB(C)_3$ (%)	$AB(C)_4$ (%)
1	100	10:1	5	8	30	30	22	10
2	100	5:1	5	17	38	30	17	0
3	100	2:1	5	25	43	25	7	0
4	**100**	**1:1**	**8**	**28**	**47**	**21**	**4**	**0**
5	100	2:1	8	16	42	30	10	2
6	100	3:1	8	11	36	32	17	4
7	100	3:1	3	23	45	25	6	1
8	100	5:1	3	18	40	28	11	3
9	100	10:1	2	20	38	26	13	3
10	100	1:1	10	27	48	21	4	0

Table 5.4. Microreactor screening conditions and molar ratios for all insertion products for the synthesis of *SUMI-3ABC*.*

Condition	Temp. (°C)	[*t*BA] : [**SUMI-2AB**]	Residence Time (min)	AB (%)	ABC (%)	$AB(C)_2$ (%)	$AB(C)_3$ (%)	$AB(C)_4$ (%)
1	100	10:1	5	14	24	30	22	10
2	100	5:1	5	27	28	30	17	0
3	100	2:1	5	37	31	25	7	0
4	**100**	**1:1**	**8**	**41**	**34**	**21**	**4**	**0**
5	100	2:1	8	27	31	30	10	2
6	100	3:1	8	19	28	32	17	4
7	100	3:1	3	35	33	25	6	1
8	100	5:1	3	28	30	28	11	3
9	100	10:1	2	30	28	26	13	3
10	100	1:1	10	41	34	21	4	0

* It is assumed that peak abundances of $AB(C)_2$, $AB(C)_3$ and $AB(C)_4$ match the true molar ratio.

5.4.3.4 Upscaling of Optimized Microflow Procedures

In the following section, the hypothesis that microscale reactions can be easily scaled up was tested. On one hand, upscaling is required to obtain more significant amounts of product, but also with respect to the determination of isolated yields, an increase in reactant volume is desired. Preparative SEC is associated with considerable dead volume so significant proportions of material are lost if injection loadings are too small thereby reducing the isolated yield. Thus, by upscaling the reaction, more reliable isolated yields can be determined. Additionally, in Table 5.5 theoretical and isolated yields for *SUMI-2* and *SUMI-3* products, synthesized with different setups (batch, micro and mesoflow) are summarized. It was shown that optimized reaction conditions could easily be transferred from one setup to another, each time resulting in comparable yields. It was observed

that regardless of the employed setup, a theoretical yield in the range of 50-59% is obtained for *SUMI-2AB* and a range of 22-34% for *SUMI-3ABC*.

Table 5.5. Theoretical and isolated yields for *SUMI-2* and *SUMI-3* products, synthesized with different setups (parts of the experimental results were already previously published).[1-2]

Setup	Desired SUMI	Theoretical Yield (%)	Isolated Yield (%)
Batch	*SUMI-2AB*	50	46
Batch	*SUMI-3ABC*	30	20
Batch	*SUMI-2AC*	n.a.	50
Batch	*SUMI-3ACB*	n.a.	20
Microflow	*SUMI-2AB*	59	43
Microflow	*SUMI-3ABC*	34	n.a.
Mesoflow	*SUMI-2AB*	53	48
Mesoflow	*SUMI-3ABC*	22	20

Upscaling was achieved by increasing the reactor volume of the flow chips from 19.5 µL to 2 mL, thus by a volume increase of roughly a factor of 100. Also, for the larger reactor volume, eluents are fed by HPLC pumps rather than syringe pumps. The setup is shown in Figure 5.1 (Experimental section 5.3.1). *SUMI-1A* was again obtained from classical batch experiments, since no further optimization of that reaction was required (high yield reaction and facile separation by SEC). The *SUMI-2* and *SUMI-3* mesoflow reactions were performed under identical conditions as described above for the microreactions. *SUMI-2AB* (condition 11, Chapter 2, Table 2.4) was obtained in 48% (0.889 g) isolated yield after

purification by automated rec-SEC whereas *SUMI-3ABC* was obtained with 20% (0.204 g) isolated yield. It should be noted that the runtime of the flow reactions was kept short and samples were collected quickly after reactor stabilization, thus much larger amounts are readily obtained by operation of the flow reactors for several hours. Both crude and pure SUMI products were analyzed by ESI-MS (Figure 5.5). Although some higher insertion products are observed compared to the on-line experimental data for the synthesis of *SUMI-3ABC*, the ESI-MS spectra are overall in good agreement with the earlier ESI-MS spectra (peak abundances) acquired during the on-line microreactor optimization experiment. The theoretical yields have thus remained in a similar range after upscaling. Especially for *SUMI-2AB* MS results of on-line screening and upscaling are very analogous. The isolated yield (48%) for *SUMI-2AB* corresponds quite well to the ESI-derived theoretical yield of 59% (see above). *SUMI-3ABC* was isolated in 20% yield which is in relatively good agreement with the predicted yield of 34% (Table 5.4). Isolated yields were thus in both cases somewhat lower than the theoretical yields, which is easily explained by loss of material during purification. Obviously, separation becomes more and more difficult with increasing number of monomer units as SEC scales logarithmically with size. Base-line separation of peaks becomes increasingly difficult with each subsequent monomer addition and more and more shoulders in the mass distributions must be cut off to provide pure products. 20% isolated yield may on first glance be low, but given that only 34% theoretical yield could be reached, this is still a rather satisfying result. Also, the ability to upscale the reaction in flow should not be underestimated. A significant scale-up of the reaction is required in order to allow for synthesis of sufficient amounts of *SUMI-3* products. To date, *SUMI-4* products have only been obtained in minute amounts, preventing the push forward to longer oligomer sequences. Batch reactions cannot

readily be upscaled due to the relatively high exothermicity of the reactions, and thus continuous flow provides an elegant and easily accessible pathway towards larger product volumes. Recycling SEC can – up to several grams – be used to isolate the various SUMI products and the bottleneck is thus not yet reached, however, for longer sequences flash column chromatography is highly promising as discussed in Chapter 6.

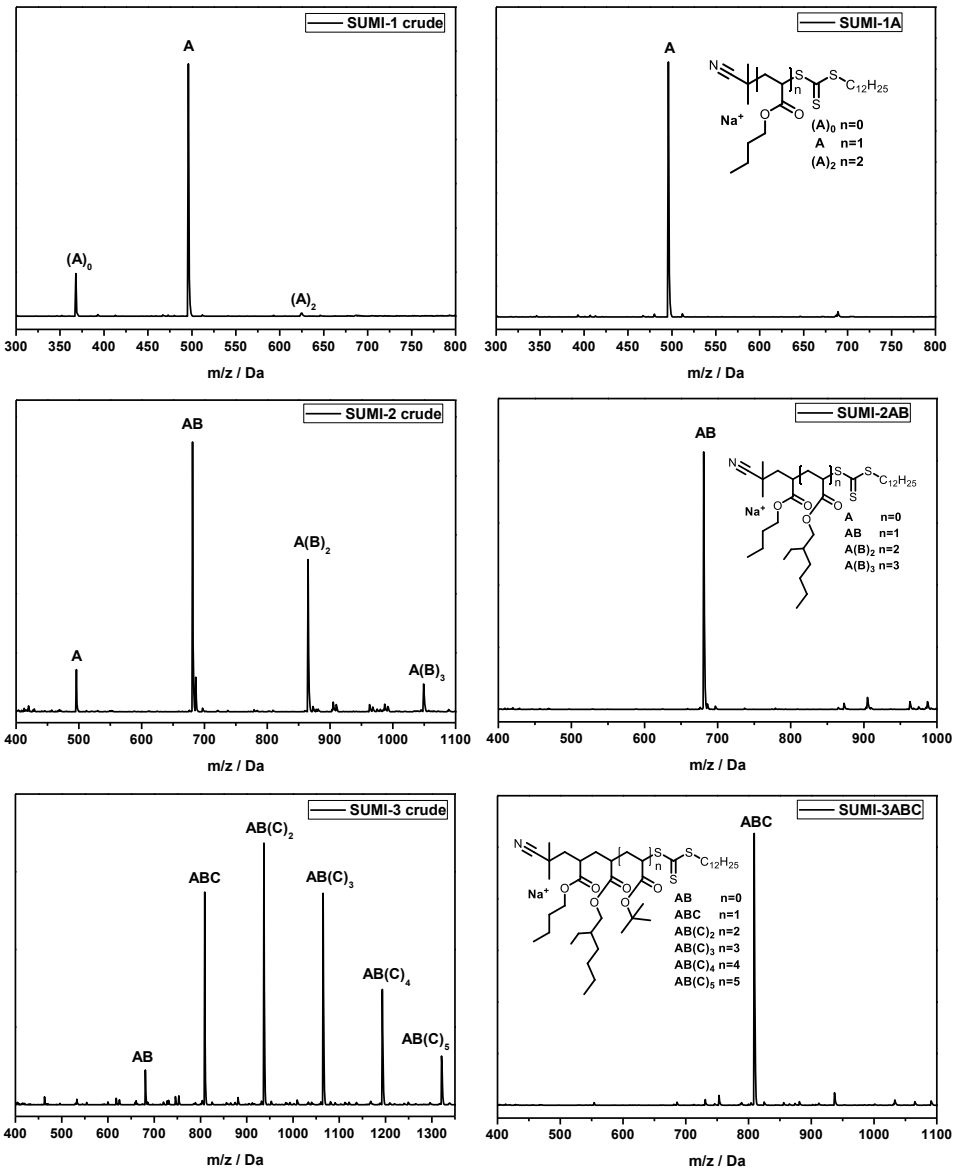

Figure 5.5. ESI-MS spectra of *SUMI-1A*, *SUMI-2AB* and *SUMI-3ABC* synthesized in mesoflow via RAFT polymerization before (left) and after (right) purification with recycling SEC.

5.5 Conclusions

Single unit monomer insertion reactions have a high potential to provide a variety of sequence-defined oligomers. Elucidation of obtainable yields as presented herein is a crucial step in the development of these reactions since without a good understanding of the involved processes, no meaningful optimization of the reactions may be carried out. At the same time, it is obvious that especially SUMI reactions require a thorough optimization. Isolated yields are – as we have demonstrated by modelling and experiments – comparatively low when going beyond the third monomer insertion. Even lower yields can and must be expected for *SUMI-4* or *SUMI-5* reactions due to the decreasing gap of the individual propagation rate coefficients with each further reaction.

Modelling of the SUMI reactions has shown that most reaction conditions play only a minor role for the success of the insertions. This is a positive result as it opens up a broad range of reaction conditions for SUMI reactions and allows performing SUMIs with short reaction times. Neither monomer concentrations nor radical flux have a distinct impact on the product distributions. On the other hand, it also underpins that SUMIs must be carried out with a somewhat fatalistic attitude. Significant side products must be tolerated and a work-around is difficult if not impossible to achieve.

Furthermore, we demonstrated that chain-length dependency effects play a crucial role in the SUMI reactions. If equal propagation rate coefficients for each monomer addition step were assumed, much lower theoretical yields of the desired SUMI products are predicted than observed experimentally. In fact, by

assuming a strong chain-length dependency (variation of k_p over a factor of 10 within the first 7 propagation steps), simulation results are obtained which are in very good agreement with experimental data from microflow synthesis.

Microreactions can be efficiently used to optimize the SUMI reactions and the scale-up of the reactions is quickly realized by applying the optimized microreactor conditions to mesoflow reactions in a 2 mL glass chip reactor. This is a nice confirmation for the generally assumed simple upscalability of lab-scale continuous flow reactions and certainly shows the pathway towards future developments in the synthesis of longer sequence-defined oligomers. At this point in time, significant efforts still had to be made to push the technique to a level where also oligomers with chain length above 5 would be available, yet in Chapter 6 the synthesis of 20-mer oligoacrylates is discussed which proves the fast growing character and potential of this research field.

5.6 References

1. Haven, J. J.; Vandenbergh, J.; Junkers, T. *Chemical Communications* **2015**, *51*, 4611.

2. Vandenbergh, J.; Reekmans, G.; Adriaensens, P.; Junkers, T. *Chemical Communications* **2013**, *49*, 10358.

3. Haven, J. J.; De Neve, J. A.; Junkers, T. *ACS Macro Letters* **2017**, *6*, 743.

4. Vandenbergh, J.; Reekmans, G.; Adriaensens, P.; Junkers, T. *Chemical Science* **2015**, *6*, 5753.

5. Haven, J. J.; Vandenbergh, J.; Kurita, R.; Gruber, J.; Junkers, T. *Polymer Chemistry* **2015**, *6*, 5752.

6. Olaj, O. F.; Zoder, M.; Vana, P.; Kornherr, A.; Schnoll-Bitai, I.; Zifferer, G. *Macromolecules* **2005**, *38*, 1944.

7. Olaj, O. F.; Vana, P.; Zoder, M.; Kornherr, A.; Zifferer, G. *Macromolecular Rapid Communications* **2000**, *13*, 913.

8. Willemse, R. X. E.; Staal, B. B. P.; Herk, A. M. v.; Pierik, S. C. J.; Klumperman, B. *Macromolecules* **2003**, *36*, 9797.

9. Heuts, J. P. A.; Russell, G. T. *European Polymer Journal* **2006**, *42*, 3.

10. Moad, G.; Rizzardo, E.; Solomon, D.; Beckwith, A. J. *Polymer Bulletin* **1992**, *29*, 647.

11. Fisher, H.; Radom, L. *Angewandte Chemie International Edition* **2001**, *40*, 1340.

12. Derboven, P.; D'hooge, D. R.; Reyniers, M.-F.; Marin, G. B.; Barner-Kowollik, C. *Macromolecules* **2015**, *48*, 492.

13. Barner-Kowollik, C.; Russell, G. T. *Progress in Polymer Science* **2009**, *23*, 1211.

14. Heuts, J. P. A.; Russell, G. T.; Smith, G. B.; van Herk, A. M. *Macromolecular Symposia* **2007**, *248*, 12.

15. Nicolas, J.; Guillaneuf, Y.; Lefay, C.; Bertin, D.; Gigmes, D.; Charleux, B. *Progress in Polymer Science* **2013**, *38*, 63.

16. Matyjaszewski, K.; Xia, J. *Chemical Reviews* **2001**, *101*, 2921.

17. Zeng, L.; Burton, L.; Yung, K.; Shushan, B.; Kassel, D. B. *Journal of Chromatography A* **1998**, *794*, 3.

18. Gründling, T.; Guilhaus, M.; Barner-Kowollik, C. *Analytical Chemistry* **2008**, *80*, 6915.

19. Barner-Kowollik, C.; Falkenhagen, J.; Weidner, S. *Mass Spectrometry in Polymer Chemistry* 2011, Wiley-VCH, ISBN-10: 3527329242.

CHAPTER 6

Versatile Approach for the Synthesis of Sequence-Defined Monodisperse 18- and 20-mer Oligoacrylates

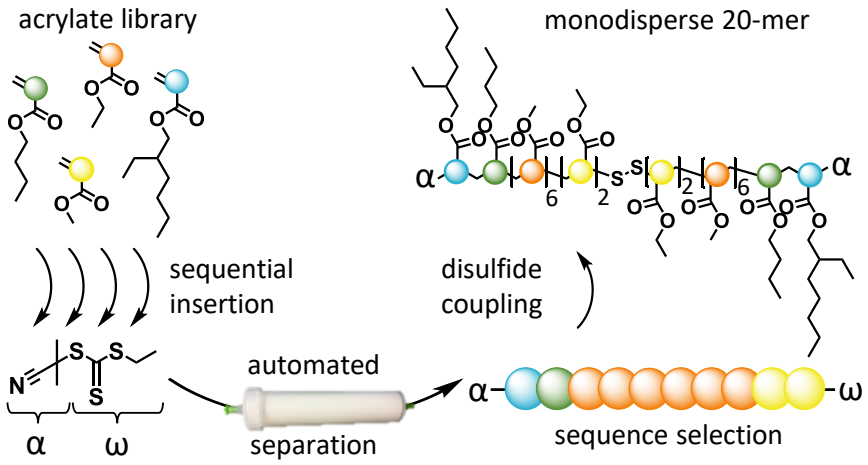

Haven, J. J.;‡ De Neve, J.A.;‡ Junkers, T. *ACS Macro Letters* **2017**, *6*, 743.

‡These authors contributed equally.

6.1 Abstract

Linear monodisperse 18- and 20-mer acrylates are obtained via consecutive synthesis of two sequence-defined acrylate 9- and 10-mers followed by disulfide coupling utilizing reversible addition-fragmentation chain transfer (RAFT) endgroup chemistry. The sequence-defined oligoacrylates are accessed via consecutive single (SUMI) and multiple (MUMI) unit monomer insertions through RAFT polymerization, using an acrylate monomer library as functional building blocks. Aminolysis of the trithiocarbonate macroRAFT endroup and *in situ* oxidation of the thiols to form a disulfide bridge leads to the formation of an 18- and 20-mer. In this approach, one or multiple acrylate building blocks can be inserted in each step by chain extension to form a stable carbon-carbon backbone. Isolation of the targeted monodisperse oligomers, from the statistical mixtures obtained at first, was performed by flash column chromatography with high efficiency. It was shown that the SUMI and MUMI strategy, when combined with flash chromatography separation, was highly efficient and allows construction of monodisperse materials of very considerable length starting from cheap and very versatile building blocks.

6.2 Introduction

Biopolymers such as proteins and DNA have highly selective and complex functions based fundamentally on their primary structure encoded by the specific order of repeating units. Concomitantly, there is a high need for specialized, sustainable materials produced via synthetic routes. Therefore, the synthesis of precision polymers with unprecedented control over the primary monomer sequence is currently widely investigated.[1-3] In polymer chemistry, the versatility of monomer building blocks are endless compared to nature where DNA uses only 4 nucleotides and proteins/peptides only have a library of 20 amino acids to encode. Regulation of the monomer sequence in polymerizations – so called sequence-controlled multiblock copolymers having a polydisperse nature – is of high interest to mimic biological materials in their functionality.[4-14] Truly following the concept of nature, thus to synthesize monodisperse materials – so called sequence-defined polymers – broadens the functionality of these materials further, and opens new perspectives for e.g. biological and information storage applications.[15-22] Iterative and orthogonal growth via non-radical chemical strategies have been reported in this area. A binary encoded polyphosphate oligomer with a degree of polymerization above 100 was synthesized by iterative Merrifield-based chemistry by Lutz and coworkers,[23-24] this method being inspired by solid-phase peptide synthesis.[25-26] More non-radical iterative approaches up to 10-mers are known in the literature.[27-33] Meier and coworkers recently reviewed this field.[22] However, orthogonal and iterative growth strategies can only couple one building block at a time and in many cases require protection/deprotection strategies of the growing oligomer chain, which makes it an expensive and time-consuming approach. While some of these methods are

able to yield products with high efficiencies, typically monomer building blocks need to be pre-synthesized, which must be taken into account when assessing the economy of the transformations. In this Chapter, the synthesis of an acrylate monomer based sequence-defined 18- and 20-mer is reported via a radical growth strategy in homogeneous liquid-phase. The family of acrylate monomers is of high interest due to their commercial availability and tunability through post polymerization modification, e.g. transesterification. Specifically for SUMI reactions, they are known for their high propagation rate thus insertions are fast, typically on the timescale of tens of minutes or faster. Due to the radical process, oligomer growth is not limited to one unit at a time and a rather chemically inert carbon-carbon backbone is grown, making SUMI sequence-defined materials considerable more stable than most counterparts made from iterative strategies, which practically always require heteroatom incorporation in the main chain. Moreover, chain extension can, after purification, be either mono- or polydisperse and a large versatility of building blocks and functionalities are available. Yet careful purification is required (which is, however, also the case for many other techniques) and overall product yields are low due to the separation of products out of statistical mixtures. It must be noted though that isolation of oligomers often results in a library of monodisperse compounds, which can be used for further purposes. This, in combination with the very simple synthesis procedure itself and the broad availability of cheap monomers, leads to an overall very economic synthesis process. It must be noted that the terminology used for all sequences refers to the amount of acrylate monomers incorporated in the sequence. Herein, oligomers were prepared in a two-step approach. Telechelic monodisperse 9- and 10-mers are produced which were then orthogonally coupled via aminolysis of the RAFT endgroup followed by *in situ* oxidation for the formation

of a disulfide bridge. Coupling allows an increase in the chain length of the oligomers, but also serves as an ideal tool to demonstrate another advantage of using the well-known controlled radical polymerization (CRP) methods for sequence-defined oligomer synthesis: For CRP, a plethora of click-like coupling techniques have been developed in previous years, which are directly available for the SUMI products without any further modification. Counting functional groups per chain, one would need to take polymer endgroups into account, yielding 20- and 22-mers as products. However, no clear terminology exists on this matter. Counting only the inserted functionalities, in this case acrylate monomers, gives a more conservative number for the sequence length, and has been implemented throughout this Chapter.

6.3 Experimental Section

Materials and characterization methods are described in Chapter 8.

6.3.1 Synthetic Procedures

6.3.1.1 Synthesis of 2-cyano-2-propyl ethyl trithiocarbonate (1)

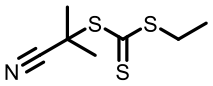

Ethanethiol (4.71 g, 75.99 mmol) was added over 10 min to a stirred suspension of sodium hydride (60 wt % in oil, 3.15 g, 78.7 mmol) in diethyl ether (150 mL) while the reaction was cooled in an ice-bath. The gray sodium hydride was converted to a thick white slurry of sodium ethanethiolate. Carbon disulfide (6.0 g, 78.9 mmol) was added. The resulting thick yellow precipitate was isolated by filtration to give sodium ethyl trithiocarbonate in quantitative yield.

Iodine (6.3 g, 0.025 mol) was added portionwise to a suspension of sodium ethyl trithiocarbonate (14.6 g, 0.049 mol) in diethyl ether (100 mL). The resultant mixture was then stirred at room temperature for 1 h when the white sodium iodide which settled was removed by filtration. The yellow-brown filtrate was washed with aqueous sodium thiosulfate, to remove excess iodine, and water, dried over sodium sulfate and evaporated to leave a residue of *bis*(ethylsulfanylthiocarbonyl) disulfide in quantitative yield.

A solution of AIBN (4.93 g, 0.03 mol) and *bis*(ethylsulfanylthiocarbonyl)disulfide (5.5 g, 0.020 mol) in ethyl acetate (100 mL) was heated at 70 °C overnight. After evaporation of the volatiles, the crude mixture was purified by silica column

chromatography with petroleum ether:ethyl acetate (49:1) as eluent to obtain CPE-TTC as an orange liquid (7.2 g, 88% yield).^{1}H-NMR ($CDCl_3$, ppm): 1.35 (t, 3H, C*H*$_3$CH$_2$); 1.28 (s, 6H, (CH$_3$)$_2$CCN); 3.33 (q, 2H, CH$_3$C*H*$_2$S). ^{13}C-NMR ($CDCl_3$, ppm): 218.2, 121.0, 43.0, 31.9, 27.7, 13.4. ESI-MS: [227.994]$^{Na+}$

6.3.1.2 General Synthesis Procedure for RAFT Polymerizations

In a typical procedure, the acrylate monomer, 2,2'-azobisisobutyronitrile (AIBN), 2-cyano-2-propyl ethyl trithiocarbonate RAFT agent **1** and butyl acetate as a reaction solvent were added into a glass vial together with a magnetic stirring bar. The glass vial was sealed by a rubber septum. The solution was degassed for 15 min by N_2 purging, and subsequently inserted into the glovebox with inert atmosphere. The reaction mixture was heated in a copper heat block and quenched by cooling in liquid nitrogen. After evaporation of the volatiles (monomer and solvent) the reaction mixture was analyzed by ESI-MS to observe the oligomer distribution and endgroups before purification with flash column chromatography. Isolated oligomers were analyzed by ESI-MS. ESI-MS spectra are included and discussed in Results & Discussion section 6.4.

6.3.1.3 Synthesis of α-[EHA]$_1$-ω MacroRAFT Agent (2)

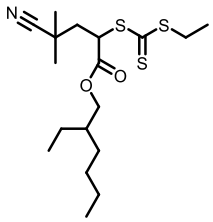

Synthesis of macroRAFT **2** is performed according to the general procedure discussed above. 13.17 mmol (2.24 g, 1 equiv.) of the monomer EHA, 0.61 mmol (0.1 g, 0.05 equiv.) of AIBN, 12.17 mmol (2.5 g, 1 equiv.) of RAFT agent **1** and

2.5 mL of butyl acetate were added into a glass vial. The mixture was reacted at 100 °C for 30 min. ESI-MS: $[412.140]^{Na+}$

6.3.1.4 Synthesis of α-[EHA]$_1$-[*n*BA]$_1$-ω MacroRAFT Agent (3)

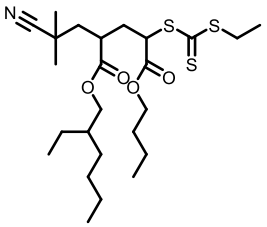

Synthesis of macroRAFT **3** is performed according to the general procedure discussed above. 2.35 mmol (0.3 g, 1 equiv.) of the monomer nBA, 0.12 mmol (0.02 g, 0.05 equiv.) of AIBN, 2.35 mmol (0.92 g, 1 equiv.) of macroRAFT agent **2** and 1 mL of butyl acetate were added into a glass vial. The mixture was reacted at 100 °C for 30 min. ESI-MS: $[540.223]^{Na+}$.

6.3.1.5 Synthesis of α-[EHA]$_1$-[*n*BA]$_1$-[MA]$_6$-ω MacroRAFT Agent (4)

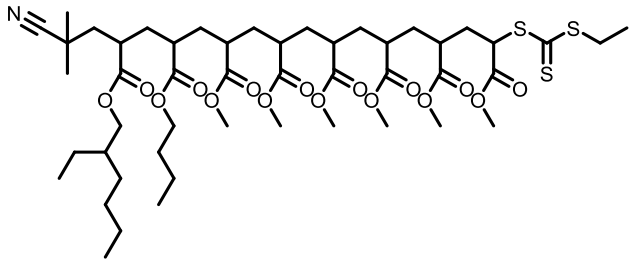

Synthesis of macroRAFT **4** is performed according to the general procedure discussed above. 3 mmol (0.26 g, 3 equiv.) of the monomer nBA, 0.05 mmol (0.082 g, 0.05 equiv.) of AIBN, 1 mmol (0.52 g, 1 equiv.) of macroRAFT agent **3** and 0.5 mL of butyl acetate were added into a glass vial. The mixture was reacted at 100 °C for 30 min. ESI-MS: $[1056.446]^{Na+}$.

6.3.1.6 Synthesis of α-[EHA]$_1$-[*n*BA]$_1$-[MA]$_6$-[EA]$_2$-ω MacroRAFT Agent (5)

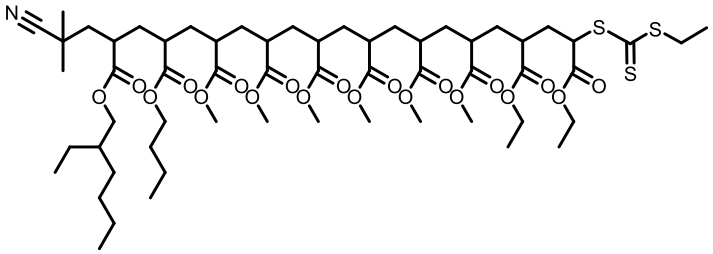

Synthesis of macroRAFT **5** is performed according to the general procedure discussed above. 0.1 mmol (0.010 g, 2 equiv.) of the monomer EA, 0.002 mmol (0.5 mg, 0.05 equiv.) of AIBN, 0.05 mmol (0.053 g, 1 equiv.) of macroRAFT agent **4** and 0.25 mL of butyl acetate were added into a glass vial. The mixture was reacted at 85 °C for 2.5 h. ESI-MS: $[1256.551]^{Na+}$.

6.3.1.7 Synthesis of α-[EHA]$_1$-[*n*BA]$_1$-[MA]$_6$-[EA]$_2$-S-S-[EA]$_2$-[MA]$_6$-[*n*BA]$_1$-[EHA]$_2$-α 20-mer (6)

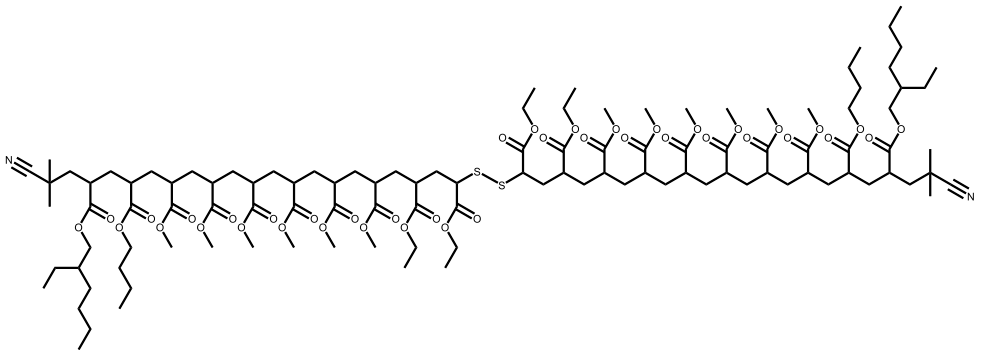

MacroRAFT **5** (5 mg, 1 equiv.) and hexylamine (15 µL, 5 equiv.) were dissolved in 0.2 mL $CHCl_3$ as reaction solvent. The reaction was performed under ambient atmosphere at room temperature and stirred for 48 h. The 20-mer oligoacrylate was isolated by silica column chromatography and analyzed by ESI-MS: $[2280.141]^{Na+}$.

6.3.1.8 Synthesis of α-[EHA]$_1$-[*n*BA]$_1$-[MA]$_6$-[EA]$_1$-S-S-[EA]$_1$-[MA]$_6$-[*n*BA]$_1$-[EHA]$_1$-α 18-mer.

Synthesis of the 18-mer oligoacrylate is identical to the synthesis of the 20-mer oligoacrylate **6**. The starting macroRAFT agent is α-[EHA]$_1$-[nBA]$_1$-[MA]$_6$-[EA]$_1$-ω (8 mg). ESI-MS: $[2080.030]^{Na+}$.

6.3.2 Flash Column Chromatography

Figure 6.1 shows the Büchi sepacore system equipped with GRACE Resolve normal phase silica cartridges (40 gram). Crude oligomer mixtures were embedded on normal-phase silica (dry loading) and loaded into a pre-column cartridge and placed on top of the GRACE resolve normal-phase silica cartridges.

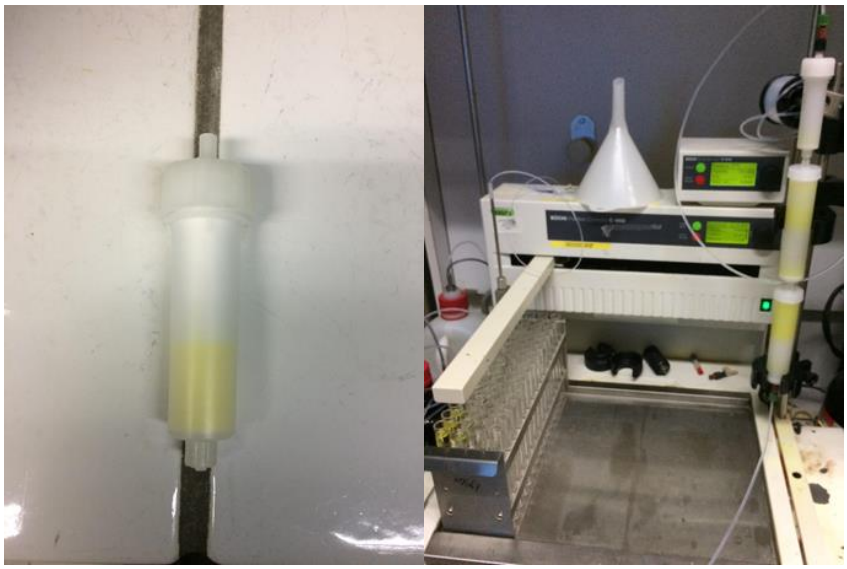

Figure 6.1. (left) Precolumn cartridge for dry loading crude reaction products on normal-phase silica and (right) Flash column chromatography system (Büchi sepacore) photographed during a separation run of a crude oligomer mixture.

6.4 Results & Discussion

6.4.1 Synthesis Approach for 18- and 20-Mer Oligoacrylates

In this study, four different acrylate monomer building blocks were selected, being 2-ethylhexyl acrylate (EHA), *n*-butyl acrylate (*n*BA), methyl acrylate (MA) and ethyl acrylate (EA). Any acrylate monomer that is compatible with RAFT could in principle be chosen for this purpose with an adaptation of the separation protocol. Scheme 6.1 shows a general reaction scheme for the synthesis of a 20-mer and its assembly via a disulfide coupling reaction. Virtually any other oligomer sequence can likewise be synthesized by varying type and length of each monodisperse building block. In short, to demonstrate the scope of the reaction, single monomer insertions were first carried out using EHA and *n*BA, respectively. In the next step, a chain length extension of six MA units was performed. Finally, two further EA units were built into the sequence to yield a 10-mer. Monodisperse sequences of the targeted oligomer length were every time isolated via flash column chromatography. Flash column chromatography is a straightforward and scalable technique which Hawker and coworkers recently employed for the separation of homopolymer insertion products.[34] In previous studies we had used recycling (preparative) GPC to purify mixtures.[19-21] Flash chromatography has proven not only faster (with separation of the products taking roughly 1 hour), but also to be able to separate higher sequence lengths compared to GPC when polar monomers are employed. The flash column chromatography setup and procedure is described in the Experimental Section (section 6.3.2). Finally, the RAFT ω-endgroups of the obtained oligomers were aminolyzed and *in situ* oxidized for disulfide bridge formation. Via this approach, selected sequences could be coupled to form custom-made precision polymers.

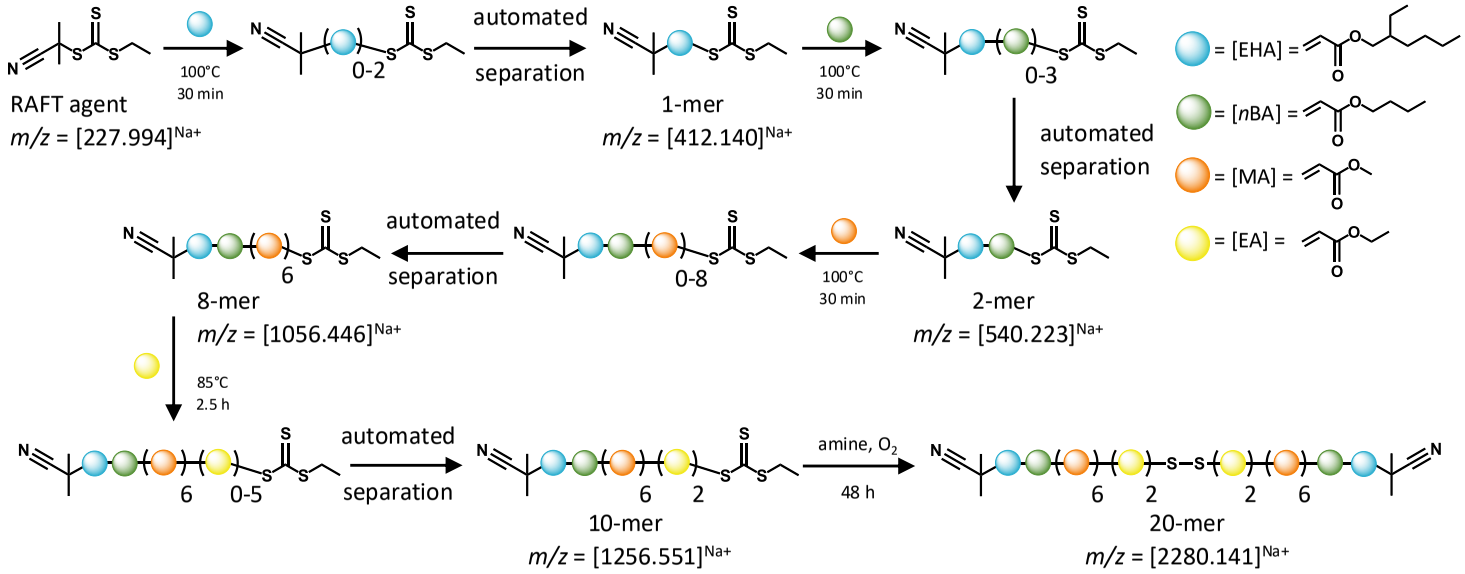

Scheme 6.1. General reaction scheme for the synthesis of a 20-mer. Four RAFT polymerizations were performed, with purification steps in between via automated separation through flash column chromatography, to obtain a 10-mer. All RAFT polymerizations were thermally initiated at elevated temperatures by 2,2'-azobis(2-methylpropionitrile) (AIBN). The 10-mers were then orthogonally coupled via aminolysis of the RAFT endgroup followed by in situ oxidation for the formation of a disulfide bridge to yield 20-mers.

6.4.2 Synthesis of α-[EHA]$_1$-ω AND α-[EHA]$_1$-[*n*BA]$_1$-ω

Without going into detail on the exact synthesis procedures here (see Experimental Section 6.3.1), it is important to discuss reaction efficiencies. The first SUMI reaction yielded 1.9 g (58% isolated yield) of the monodisperse α-[EHA]$_1$-ω 1-mer. Figure 6.2 shows the ESI-MS analysis of the crude and purified product after chain extension with a SUMI of 2-ethylhexyl acrylate (EHA) as a first building block into the RAFT agent. A mixture of one and two insertions of EHA in CPE-TTC is observed (Figure 6.2 left). ESI-MS analysis shows > 99% endgroup fidelity of the obtained SUMI product after automated purification via flash chromatography (Figure 6.2 right). The small peak, seen in the crude and pure ESI-MS spectrum at $[300{,}016]^{Na+}$, can be assigned to hydrolysis of the α-[EHA]$_1$-ω macroRAFT agent which is generated *in situ* in the ESI-MS nozzle. The UV detector trace (λ = 305 nm, blue trace Figure 6.3) during oligomer purification of α-[EHA]$_{0\text{-}2}$-ω macroRAFT agent via flash chromatography is shown in Figure 6.3. The system could be easily operated under UV detection due to the high absorption of the trithiocarbonate RAFT living chain end at λ = 305 nm. The gradient eluent mixture used during purification was petroleum ether:ethyl acetate, and the red trace indicates the percentage of ethyl acetate polar solvent fraction utilized in time. It can be observed that both the 1st and 2nd insertion of EHA into CPE-TTC RAFT agent is baseline separated, therefore almost no product losses are encountered during purification of the crude polymerization mixture. It has to be noted that, in contrast to previous Chapters in this thesis, ESI-MS spectra were recorded off-line. Reactions were performed in batch and samples were taken manually.

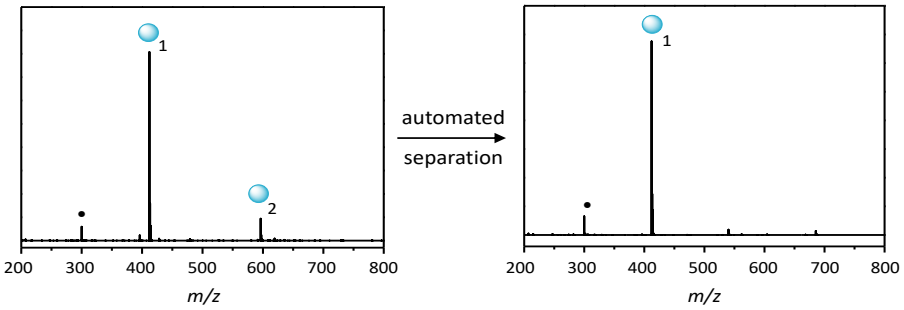

Figure 6.2. Electrospray ionization mass spectrometry (ESI-MS) analysis after single unit monomer insertion (SUMI) of EHA into the CPE-TTC RAFT agent. (left) Crude reaction mixture (right) ESI-MS of the isolated targeted α-$[EHA]_1$-ω macroRAFT agent species after purification via flash column chromatography. The small $[300{,}016]^{Na+}$ peak can be assigned to hydrolysis of the EHA generated *in situ* in the ESI-MS nozzle.

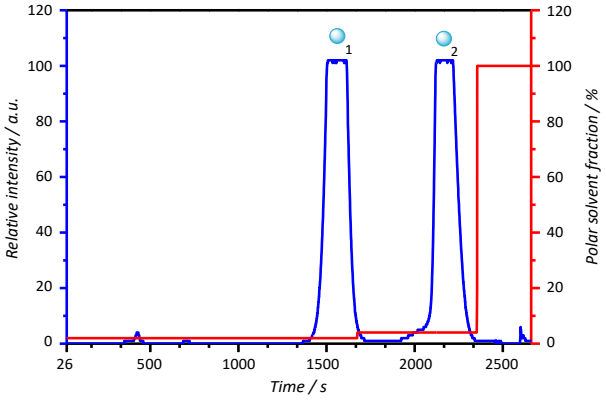

Figure 6.3. UV detector trace (λ = 305 nm, blue trace) during oligomer purification of α-$[EHA]_{0\text{-}2}$-ω macroRAFT agent. Gradient eluent mixture was petroleum ether:ethyl acetate, the red trace indicates the percentage of ethyl acetate polar solvent fraction utilized in time.

In the next step, a SUMI with *n*-butyl acrylate (*n*BA) (Scheme 6.1) into the 1-mer α-[EHA]$_1$-ω macroRAFT agent yielded again a monodisperse macroRAFT α-[EHA]$_1$-[*n*BA]$_1$-ω 2-mer (540 mg, 45% isolated yield). RAFT polymerization was performed at 100 °C and quenched after 30 minutes reaction time. Figure 6.4 shows the ESI-MS analysis of the crude oligomer mixture obtained after RAFT polymerization. A mixture of starting material (α-[EHA]$_1$-ω) along with one, two and three insertions was observed (Figure 6.4 left). ESI-MS analysis shows > 99% endgroup fidelity of the obtained SUMI product after automated purification via flash chromatography (Figure 6.4 right). The UV detector trace (λ = 305 nm, blue trace Figure 6.5) during oligomer purification of the α-[EHA]$_1$-[nBA]$_{0\text{-}3}$-ω macroRAFT agent via flash chromatography is shown in Figure 6.5. The procedure and eluent mixture are similar to the previous SUMI step. It can be observed that all oligomer chain lengths are baseline separated. Purity is also confirmed by ESI-MS (Figure 6.4 right), and therefore only minimal products losses due to sample preparation and analysis are encountered. From the 2nd insertion on, UV traces show bimodal peaks due to the separation of diastereoisomer mixtures of a monodisperse oligomer chain length.

Although purification of the oligomer mixtures is inevitable, reactions can be optimized to obtain maximum yields of the targeted oligomer length, as described previously in Chapter 5 (close to 45% was identified to be the maximum achievable crude yield, only for the first insertion higher yields are achievable due to the difference in pre-equilibrium kinetics).[19] In principle, from here on several SUMIs could be performed as a follow up, each time adding exactly one unit, or from another approach multiple units can be inserted in just one step, as discussed below.

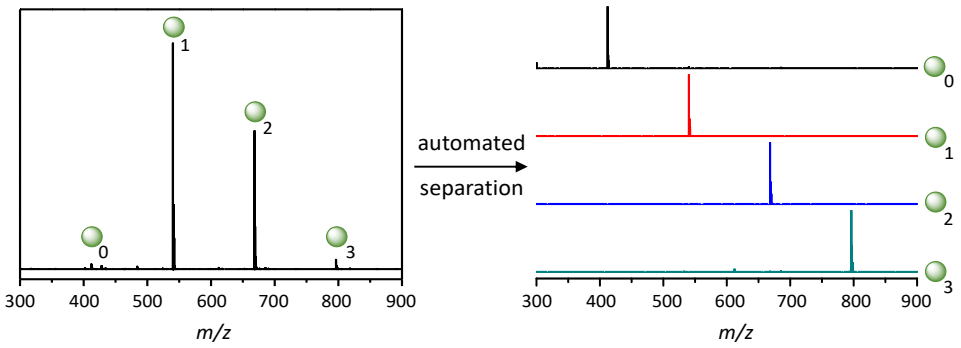

Figure 6.4. ESI-MS analysis after single unit monomer insertion (SUMI) of *n*BA into α-[EHA]$_1$-ω. (left) Crude reaction mixture (right) ESI-MS of the isolated oligomers (1-, 2-, 3- and 4-mers) after flash chromatography.

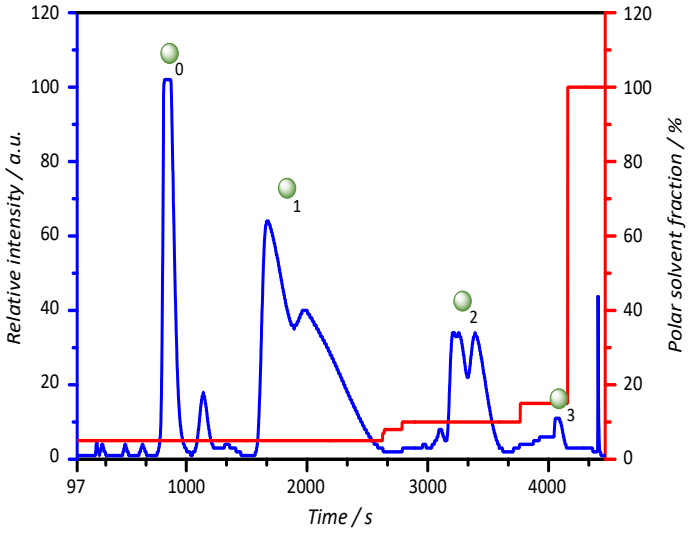

Figure 6.5. UV detector trace (λ = 305 nm, blue trace) during oligomer purification of α-[EHA]$_1$-[*n*BA]$_{0\text{-}3}$-ω macroRAFT agent. The gradient eluent mixture was petroleum ether:ethyl acetate, the red trace indicates the percentage of ethyl acetate polar solvent fraction utilized in time.

6.4.3 Synthesis of α-[EHA]$_1$-[*n*BA]$_1$-[MA]$_6$-ω (8-mer)

In the following step, to use the power of RAFT, a multiple unit monomer insertion (MUMI) was performed adding 6 acrylate units at a time. Many sequence-defined natural materials contain homo-sequences of several units, and a direct insertion of a larger (yet monodisperse) block can be of advantage. After polymerization of the macroRAFT agent α-[EHA]$_1$-[*n*BA]$_1$-ω with MA, 750 mg crude reaction product was loaded on the flash column to isolate 53 mg (5% isolated yield) of the monodisperse 8-mer α-[EHA]$_1$-[*n*BA]$_1$-[MA]$_6$-ω (all other yields are given in Figure 6.6). The more units that are inserted per step, the lower the overall achievable yield due to the resulting Poisson distribution of products. The polydisperse ESI-MS spectrum directly after polymerization of MA shows a chain length distribution from 0 to 8 insertions of MA. ESI-MS of the crude oligomer spectrum shows that higher insertions (> 6) are only present in very small amounts. However, insertions 7 and 8 were also isolated and analyzed by ESI-MS, as shown in the supporting information of the corresponding manuscript.[35] Via this technique almost no product losses are encountered during purification since monomer insertions were baseline separated according to the UV detection signal as seen in Figure 6.7. Isolated yields shown in Figure 6.6 are calculated based on the initial amount (mol%) of macroRAFT agent. For 0 to 6 insertions of MA > 85 mol% of the crude material could be isolated in total, so only minor losses are encountered via this approach, taking into account the higher insertion products and little losses due to sample preparation, analysis and purification. Thus, while the individual yield of a single oligomer sequence may be low, the overall yield of all isolated oligomers is rather high.

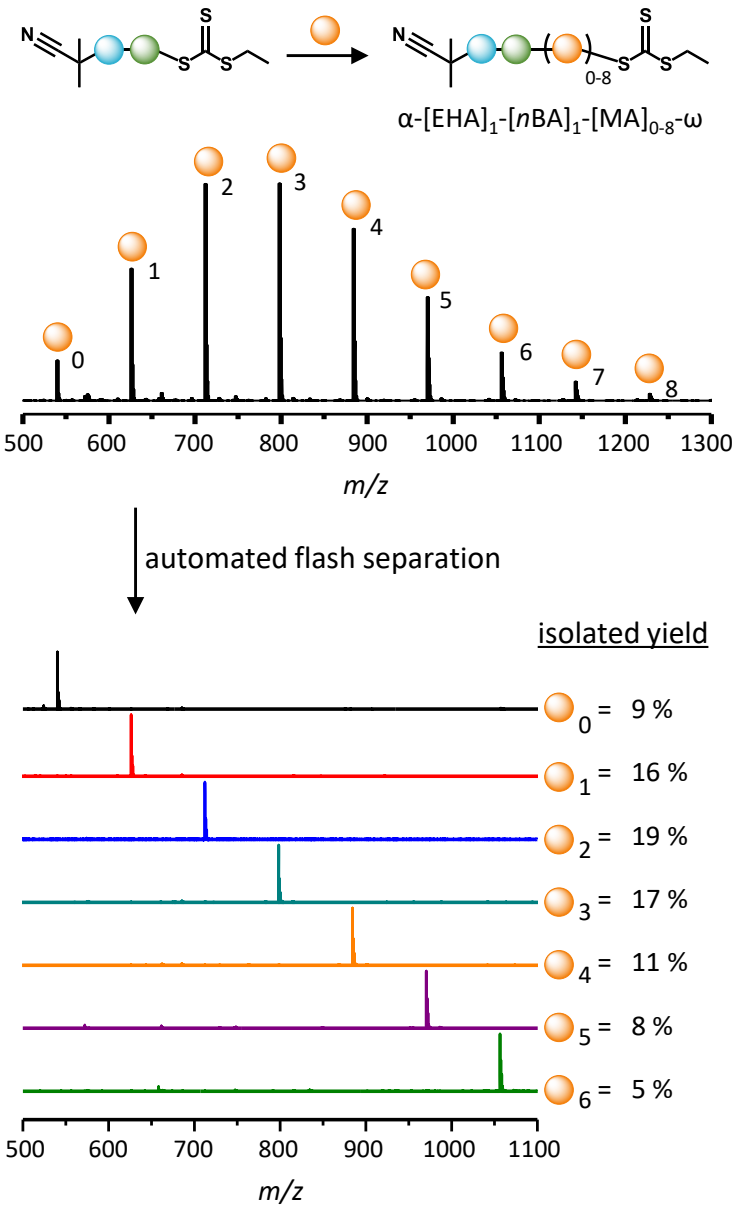

Figure 6.6. ESI-MS analysis of the oligomer chain extension with six methyl acrylate (MA) units. ESI-MS shows the isolated oligomers after purification via flash column chromatography. The corresponding isolated yields are given at the side.

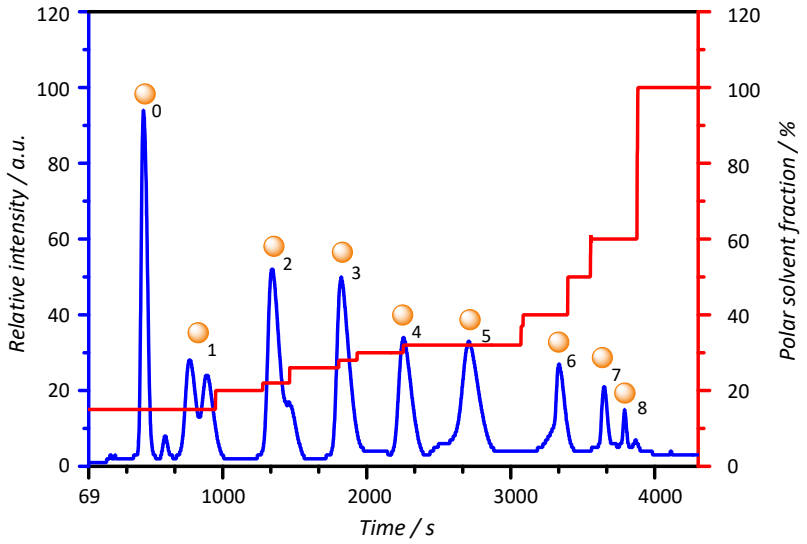

Figure 6.7. UV detector trace (λ = 305 nm, blue trace) during oligomer purification of the α-[EHA]$_1$-[*n*BA]$_1$-[MA]$_{0\text{-}8}$-ω macroRAFT agent. The gradient eluent mixture was petroleum ether:ethyl acetate, and the red trace indicates the percentage of ethyl acetate polar solvent fraction utilized in time.

6.4.4. Synthesis of α-[EHA]$_1$-[*n*BA]$_1$-[MA]$_6$-[EA]$_{1\text{-}2}$-ω (9- and 10-mer)

Figure 6.8 shows the final RAFT polymerization step where the sequence was chain extended with ethyl acrylate (EA) as a fourth monomer building block to obtain α-[EHA]$_1$-[*n*BA]$_1$-[MA]$_6$-[EA]$_{0\text{-}5}$-ω. One, two and three insertions of EA could be isolated as monodisperse sequences yielding 8 mg of 9-mers (14% isolated yield), 7 mg 10-mers (11% isolated yield) and 6 mg 11-mers (8% isolated yield). It was observed that more losses are encountered, which can be explained by mixed insertion fractions obtained after column chromatography and the beginning loss of separation resolution with increasing chain lengths (Figure 6.9). Overall yields obtained for the 8-, 9- and 10-mers, after 4 chain extensions, are in the range of a few percent. However, the synthesis of the targeted oligomer sequences is still

economically feasible since starting materials are cheap and commercially available. Moreover, purification of the polydisperse oligomer mixtures via flash chromatography is fast, which limits eluent consumption. More precisely, purification of the final 10-mer sequence was performed in less than 1 hour (Figure 6.9). Overall, synthesis is fast and sequences can be built up rapidly without the use of solid-phase synthesis strategies, even if product amounts are low when compared to Merrifield synthesis approaches.

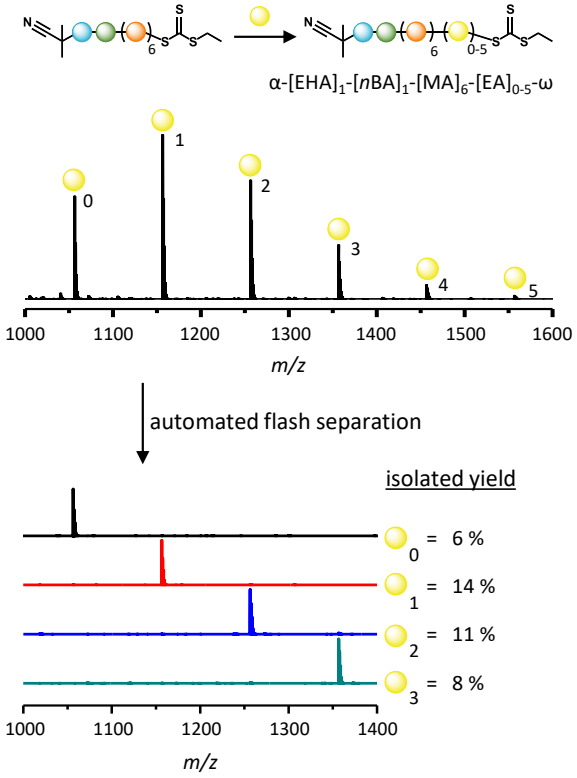

Figure 6.8. ESI-MS analysis of the oligomer chain extension with up to three ethyl acrylate (EA) units. The ESI-MS spectra show the isolated oligomers after purification via flash column chromatography. The corresponding yields are given at the side.

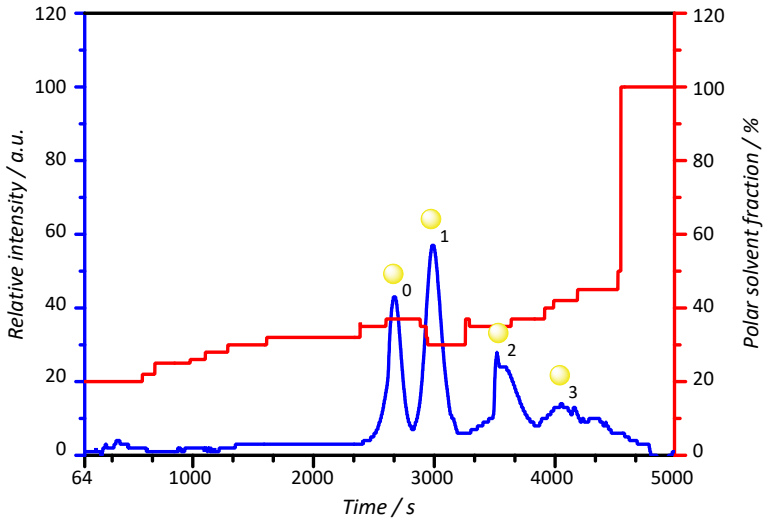

Figure 6.9. UV detector trace (λ = 305 nm, blue trace) during oligomer purification of the α-[EHA]$_1$-[nBA]$_1$-[MA]$_6$-[EA]$_{0\text{-}5}$-ω macroRAFT agent. The gradient eluent mixture was petroleum ether:ethyl acetate, and the red trace indicates the percentage of ethyl acetate polar solvent fraction utilized in time.

6.4.5 Synthesis of 18- and 20-mer Oligoacrylates

Figure 6.10 demonstrates the disulfide coupling towards the final 18- and 20-mers as an example of how RAFT SUMI reactions can be combined with post oligomerization reactions. RAFT chemistry allows for numerous click-like reactions, ranging from azide-alkyne coupling over Diels-Alder cycloadditions to thiol-ene chemistry. Disulfide coupling was chosen herein to demonstrate the synthetic potential as disulfide bridges are a common motif in biomolecule conjugation, and because we see the future of the SUMI-made sequence-defined materials in this field. To carry out the coupling, the trithiocarbonate RAFT endgroup is reduced via aminolysis, a fast and quantitative reaction. Disulfide bridges form under oxidative conditions of the residual thiol endgroups in air. The

coupling products were purified by manual silica column chromatography (to remove ethane-thiol coupling side products) and analyzed by ESI-MS. The mass spectra (Figure 6.10) exhibit a double and single sodium charged species of the 18- (2057.05 g·mol^{-1}) and 20-mer (2257.15 g·mol^{-1}). Some small side products can also be identified in the 20-mer oligoacrylate, these can be assigned to single and double sodium charged 21-mers (< 10%) due to coupling of a 10- and 11-mer trace left from the starting material. These side products occur only at very low abundancy.

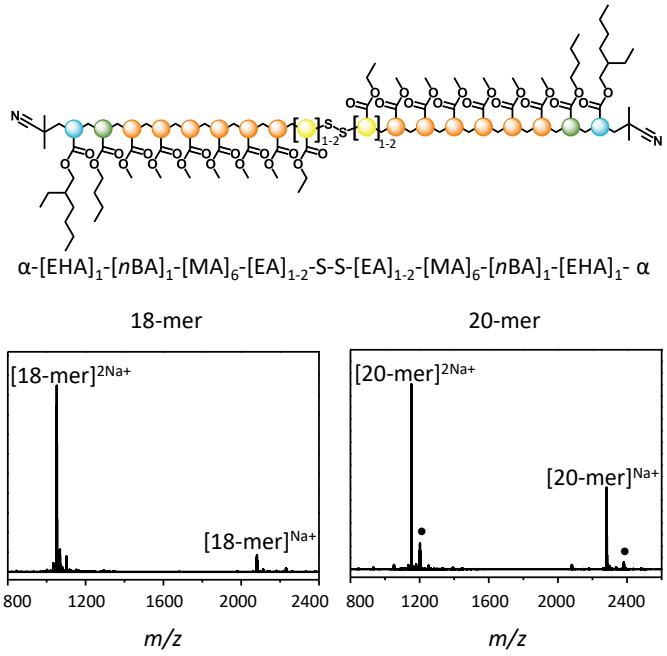

Figure 6.10. Representation of the synthesized 18- and 20-mer. Monodisperse oligomers were obtained, as shown by ESI-MS. The marked signals are assigned to a single and double sodium charged 21-mer (< 10%) due to coupling of a 10- and 11-mer trace left from the starting material.

6.4.6 Linear Oligoacrylates

As widely investigated in the literature, so called midchain radicals can be formed via backbiting during acrylate propagation due to the formation of a more stable tertiary radical. These radicals can undergo propagation and cause branched polymer structures, a phenomenon that is well known.[36-38] Obviously, branching would disturb the pristine sequence desired. While ESI-MS shows the monodisperse nature of the isolated oligomers, it does not give any information on the exact macromolecular architecture since structural branched isomers have exactly the same mass-to-charge signal in ESI-MS (isobaric structures). To exclude branching and to prove a linear growth of the oligomers without defects in the structure, ^{13}C and attached proton test (APT) carbon NMR spectra were recorded confirming the complete absence of any branched structure in the final products. For this purpose, the isolated oligomer α-$[EHA]_1$-$[n BA]_1$-$[MA]_4$-ω was utilized as described below. It can be speculated that branched structures are associated with considerably different polarities and are hence separated out in the chromatography process. In principle, it would be interesting to use MS^2 techniques for sequencing of the structures, yet side chain fragmentation would likely occur before backbone fragmentation, blocking this pathway of analysis.

The isolated oligomer α-$[EHA]_1$-$[n BA]_1$-$[MA]_4$-ω (Figure 6.11) was utilized to investigate the effects of midchain radical formation and chain branching. This process is likely to happen after 3 consecutive monomer insertions and hence might influence the product from the 4th insertion onwards. To exclude branching – which would lead to defects in the encoded information of the oligomer structure – and to prove a linear growth of the oligomers without defects in the structure, carbon (^{13}C) nuclear magnetic resonance (NMR) and APT ^{13}C-NMR were studied

to determine the chemical structure of the α-[EHA]$_1$-[*n*BA]$_1$-[MA]$_4$-ω macroRAFT agent (Figure 6.12). All peaks can be neatly assigned to the linear structure of the macroRAFT agent. It can thus safely be assumed that backbiting did not occur during the RAFT insertion reactions revealing no branching and thus a linear growth of the oligomer chains. Typical resonances for branched structures are not present:

- No resonances typical for quaternary carbons in the polymer backbone are present. Typically APT ^{13}C-NMR would show a positive resonance peak around 49 ppm.[36,38]
- If a branched structure was formed, then the CH_2 carbon next to the resulting methacrylate-like quaternary substituted carbon would give rise to a positive resonance around 52-54 ppm.[21]
- In the case of branching, three carbonyl resonance peaks are expected around 170 ppm. Only two are observed, which indicates a linear macroRAFT structure.

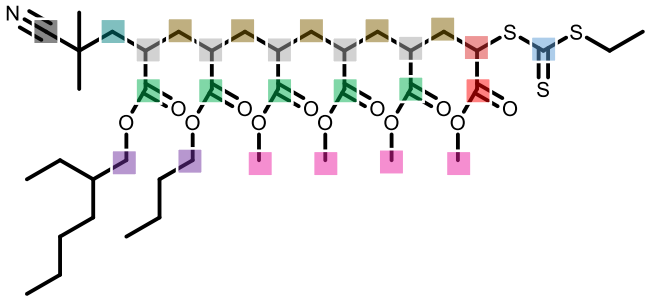

Figure 6.11. Linear structure of the α-[EHA]$_1$-[*n*BA]$_1$-[MA]$_4$-ω macroRAFT agent.

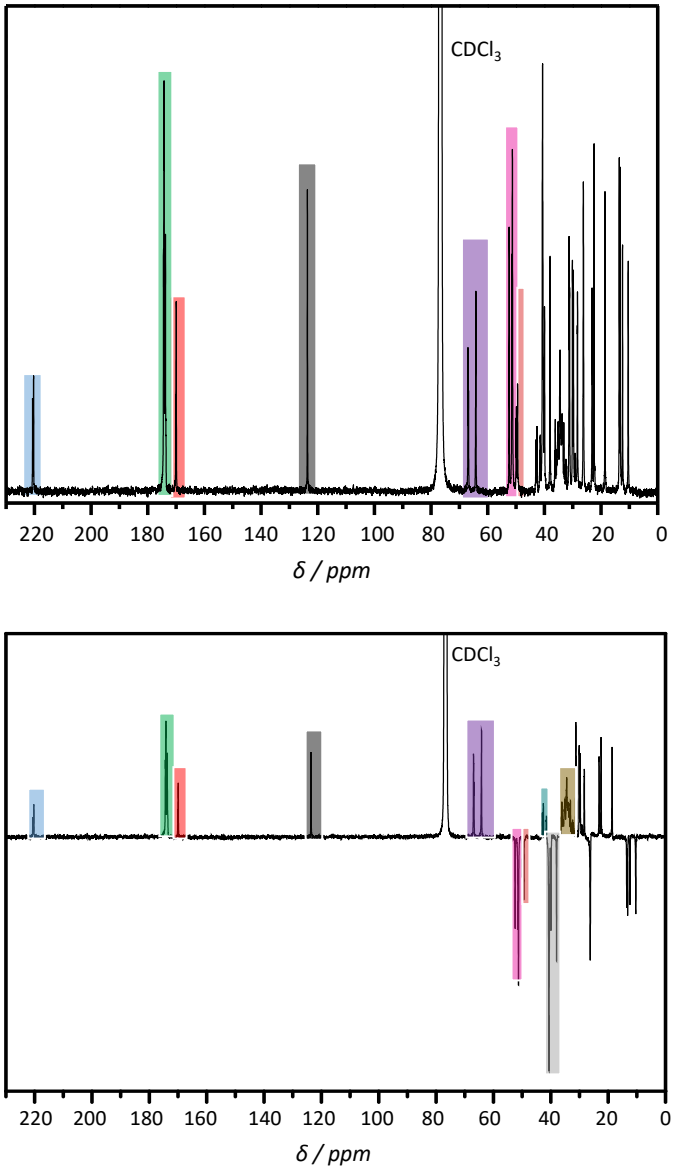

Figure 6.12. (top) Assigned ^{13}C-NMR spectrum of the macroRAFT agent and (bottom) Assigned APT ^{13}C-NMR spectrum of the macroRAFT agent.

6.5 Conclusions

An effective and flexible route towards the synthesis of sequence-defined oligomers was established. Using flash chromatography has significantly advanced the reachable sequence length of the materials, now unfolding the full potential of using RAFT for the synthesis of sequence-defined materials. 18- and 20-mers with a precisely defined monomer order could be synthesized, stemming from single monomer insertions and insertion of several monomer units at a time with a large tolerance towards functional groups. Separation of the various insertion products via flash chromatography resulted in the fast (< 1 h) and elegant purification of reaction mixtures. The materials described herein mark an unprecedented length for sequence-defined materials made from radical reactions, and are highly competitive with iterative synthesis strategies. Individual yields of the different sequences are relatively low, yet in each step a library of compounds is obtained. This plethora of sequences – each with a varying structure – can be of significant interest to study property differences. Furthermore, a simple and fast synthesis process has been presented. All monomers used are cheap and commercially available and synthesis time is minimal. Also purifications typically do not consume much time (typically 60 min per separation), allowing for comparatively fast oligomer separation. ESI-MS and APT ^{13}C-NMR confirmed the high structural integrity of the products. Furthermore, the successful coupling of two monodisperse blocks of a specified length has been demonstrated, resulting in 18- and 20-mers. This straightforward synthesis of such sequence-defined block copolymers truly pushes the boundaries of such materials and paves the way to numerous innovations in the field of material chemistry with the possibility to create new, highly-customizable materials.

6.6 References

1. Lutz, J.-F. *Polymer Chemistry* **2010**, *1*, 55.

2. Lutz, J.-F.; Ouchi, M.; Liu, D. R.; Sawamoto, M. *Science* **2013**, *341*, 628.

3. Lutz, J.-F. *Macromolecules* **2015**, *48*, 4759.

4. Gody, G.; Maschmeyer, T.; Zetterlund Per, B.; Perrier, S. *Nature Communications* **2013**, *4*, 2505.

5. Boyer, C.; Soeriyadi, A. H.; Zetterlund, P. B.; Whittaker, M. R. *Macromolecules* **2011**, *44*, 8028.

6. Engelis, N. G.; Anastasaki, A.; Nurumbetov, G.; Truong, N. P.; Nikolaou, V.; Shegiwal, A.; Whittaker, M. R.; Davis, T. P.; Haddleton, D. M. *Nature Chemistry* **2016**, *9*, 171.

7. Nurumbetov, G.; Engelis, N.; Godfrey, J.; Hand, R.; Anastasaki, A.; Simula, A.; Nikolaou, V.; Haddleton, D. M. *Polymer Chemistry* **2017**, *8*, 1084.

8. Chuang, Y.-M.; Ethirajan, A.; Junkers, T. *ACS Macro Letters* **2014**, *3*, 732.

9. Anastasaki, A.; Nikolaou, V.; Nurumbetov, G.; Wilson, P.; Kempe, K.; Quinn, J. F.; Davis, T. P.; Whittaker, M. R.; Haddleton, D. M. *Chemical Reviews* **2016**, *116*, 835.

10. Haven, J. J.; Guerrero-Sanchez, C.; Keddie, D. J.; Moad, G.; Thang, S. H.; Schubert, U. S. *Polymer Chemistry* **2014**, *5*, 5236.

11. Haven, J. J.; Guerrero-Sanchez, C.; Keddie, D. J.; Moad, G. *Macromolecular Rapid Communication* **2014**, *35*, 492.

12. Gody, G.; Barbey, R.; Danial, M.; Perrier, S. *Polymer Chemistry* **2015**, *6*, 1502.

13. Baeten, E.; Haven, J. J.; Junkers, T. *Polymer Chemistry* **2017**, *8*, 3815.

14. Kuroki, A.; Martinez-Botella, I.; Hornung, C. H.; Martin, L.; Williams, E. G. L.; Locock, K. E. S.; Hartlieb, M.; Perrier, S. *Polymer Chemistry* **2017**, *8*, 3249.

15. Lutz, J.-F.; Lehn, J.-M.; Meijer, E. W.; Matyjaszewski, K. *Nature Reviews Materials* **2016**, *1*, 16024.

16. Roy, R. K.; Meszynska, A.; Laure, C.; Charles, L.; Verchin, C.; Lutz, J.-F. *Nature Communications* **2015**, *6*, 7237.

17. Houshyar, S.; Keddie, D. J.; Moad, G.; Mulder, R. J.; Saubern, S.; Tsanaktsidis, J. *Polymer Chemistry* **2012**, *3*, 1879.

18. Haven, J. J.; Baeten, E.; Claes, J.; Vandenbergh, J.; Junkers, T. *Polymer Chemistry* **2017**, *8*, 2972.

19. Haven, J. J.; Vandenbergh, J.; Kurita, R.; Gruber, J.; Junkers, T. *Polymer Chemistry* **2015**, *6*, 5752.

20. Vandenbergh, J.; Reekmans, G.; Adriaensens, P.; Junkers, T. *Chemical Science* **2015**, *6*, 5753.

21. Vandenbergh, J.; Reekmans, G.; Adriaensens, P.; Junkers, T. *Chemical Communications* **2013**, *49*, 10358.

22. Solleder, S. C.; Schneider, R. V.; Wetzel, K. S.; Boukis, A. C.; Meier, M. A. R. *Macromolecular Rapid Communication* **2017**, *38*, 1600711.

23. Al Ouahabi, A.; Kotera, M.; Charles, L.; Lutz, J.-F. *ACS Macro Letters* **2015**, *4*, 1077.

24. Al Ouahabi, A.; Charles, L.; Lutz, J.-F. *Journal of American Chemical Society* **2015**, *137*, 5629.

25. Caruthers, M. H. *Science* **1985**, *230*, 281.

26. Merrifield, R. B. *Journal of the American Chemical Society* **1963**, *85*, 2149.

27. Solleder, S. C.; Schneider, R. V.; Wetzel, K. S.; Boukis, A. C.; Meier, M. A. R. *Macromolecular rapid communications* **2017**, 1600711.

28. Solleder, S. C.; Zengel, D.; Wetzel, K. S.; Meier, M. A. R. *Angewandte Chemie, International Edition* **2016**, *55*, 1204.

29. Solleder, S. C.; Wetzel, K. S.; Meier, M. A. R. *Polymer Chemistry* **2015**, *6*, 3201.

30. Martens, S.; Van den Begin, J.; Madder, A.; Du Prez, F. E.; Espeel, P. *Journal of the American Chemical Society* **2016**, *138*, 14182.

31. Espeel, P.; Carrette, L. L. G.; Bury, K.; Capenberghs, S.; Martins, J. C.; Du Prez, F. E.; Madder, A. *Angewandte Chemie International Edition* **2013**, *125*, 13503.

32. Zydziak, N.; Konrad, W.; Feist, F.; Afonin, S.; Weidner, S.; Barner-Kowollik, C. *Nature Communications* **2016**, *7*, 13672.

33. Zydziak, N.; Feist, F.; Huber, B.; Mueller, J. O.; Barner-Kowollik, C. *Chemical Communications* **2015**, *51*, 1799.

34. Lawrence, J.; Lee, S.-H.; Abdilla, A.; Nothling, M. D.; Ren, J. M.; Knight, A. S.; Fleischmann, C.; Li, Y.; Abrams, A. S.; Schmidt, B. V. K. J.; Hawker, M. C.; Connal, L. A.; McGrath, A. J.; Clark, P. G.; Gutekunst, W. R.; Hawker, C. J. *Journal of the American Chemical Society* **2016**, *138*, 6306.

35. Haven, J. J.; De Neve, J. A.; Junkers, T. *ACS Macro Letters* **2017**, *6*, 743.

36. Wenn, B.; Reekmans, G.; Adriaensens, P.; Junkers, T. *Macromolecular Rapid Communications* **2015**, *36*, 1479.

37. Gaborieau, M.; Koo, S. P. S.; Castignolles, P.; Junkers, T.; Barner-Kowollik, C. *Macromolecules* **2010**, *51*, 5492.

38. Wenn, B.; Junkers, T. *Macromolecular Rapid Communications* **2016**, *37*, 781.

CHAPTER 7

Synthesis of Artificial Peptides and Their Applicability as Polymeric Drug Transporters

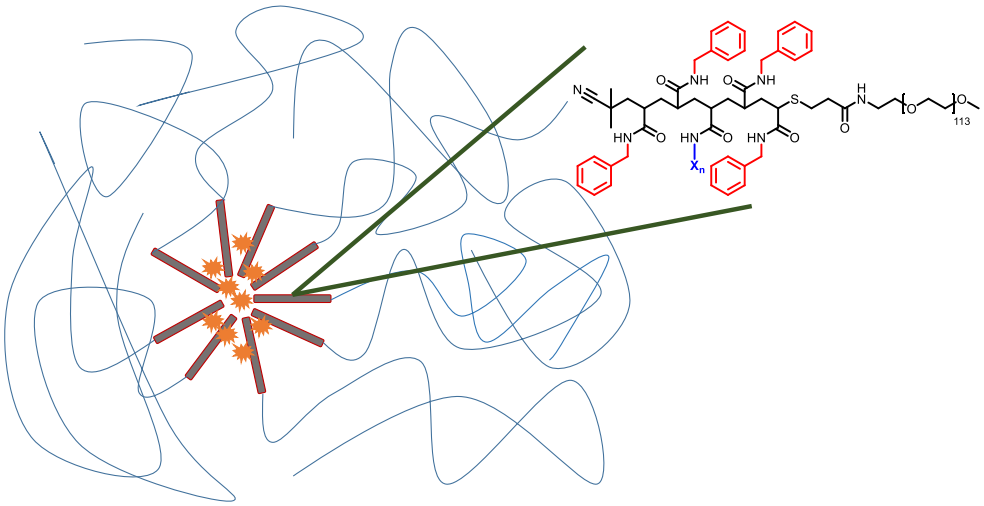

In collaboration with Prof. Dr Hans Börner and drs Eva Maron from Humboldt-Universität zu Berlin.

7.1 Abstract

Precision polymer-based drug transporters are synthesized to study their drug solubilization and drug release kinetics. More specifically, a set of three monodispere sequence-defined oligo(acrylamide) pentamers are synthesized for their use as a drug carrier systems. A promising peptide sequence, namely [Gln-Phe-Phe-Leu-Phe-Phe-Gln], is mimicked. Amino acids phenylalanine (Phe) and leucine (Leu) are replaced by their synthetic counterparts *N*-benzyl acrylamide and *N*-isobutyl acrylamide, respectively. Monodisperse pentamer sequences, so-called artificial peptides, are PEGylated to realize water soluble polymeric drug transporters for solubilization and release of tetra(hydroxyphenyl)chlorin (*m*-THPC), which is a partially approved drug for photodynamic cancer therapy (PDT). Variations on the oligo(acrylamide) pentamer sequence are introduced by structurally changing the middle leucine-mimicking building block. For this purpose, *N*-isopropyl acrylamide and *N*-methyl acrylamide, synthetic counterparts of valine and alanine, are synthesized and tested.

7.2 Introduction

Sequence-defined macromolecules such as proteins or nucleic acids are largely responsible for the complexity and diversity of the biological world as we know it today. One can predict that their synthetic analogues could play an important role in applied materials science. Tremendous efforts have been undertaken to gain control over the primary polymer structure, as already discussed throughout this thesis (Chapter 1, 2, 5 and 6). As the ability to control the monomer sequence of synthetic polymers increases, new relationships between the sequence, polymer structure and functional properties are being discovered.[1-3] Thus, bioinspired materials are attracting increasing attention due to significant advantages over their natural counterparts. The ability to precisely tune their structure with an expanded source of building blocks and increased stability leads to a broad range of chemical and physical properties and improved processability.

A major difficulty in pharmacological drug development results from poor water solubility of the lead compounds, from which uncontrolled drug partitioning and severe adverse effects can result.[4-6] Börner and coworkers reported on strategies to overcome these properties of problematic drugs such as combinatorial screening of structurally derived compound libraries (Figure 7.1).[7-8]

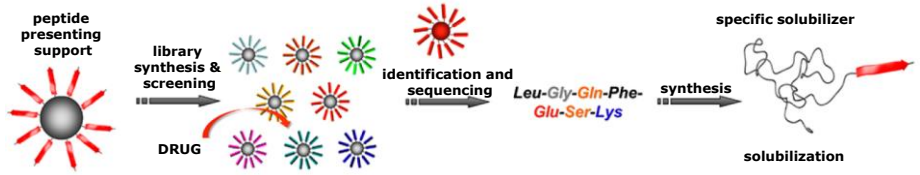

Figure 7.1. Schematic representation of the combinatorial screening method. Figure reproduced from H. G. Börner and coworkers 2013.[7]

Synthetic polymers already proved their potential by enabling stealth delivery, active drug release, improved biobarrier translocation or passive targeting.[9-10] Block copolymers have been used as solubilization agents. However, compound-specific interaction as occurring in protein-based transporters is still difficult to realize.[11-17] Core-designed dendrimers or macrocycles have been employed to bind drugs specifically via supramolecular host/guest complexes. Nevertheless, the synthetic efforts required for modifications limits their application as transporter platform.[18-20] In recent years, peptide-polymer conjugates have shown great potential for material science and biomedical applications.[21-24] Short peptide sequences offer precisely adjustable interaction capabilities as a key parameter to realize specific drug solubilizers.[25]

In this Chapter, it is the aim to replace the short peptide segments by synthetically sequence-defined pentamers (5-mers), so-called artificial peptides, which consist out of acrylamide monomer units (peptide analogues). These newly synthesized materials were tested on their drug loading and release capacities to act as a drug transporter and compared to their natural counterparts. For this purpose, a promising drug for photodynamic cancer therapy (PDT), *m*-tetra(hydroxyphenyl)chlorin (*m*-THPC, Figure 7.2), was chosen. *m*-THPC has proven its use in effective photosensitization of singlet oxygen ($^1O_2$) and has been partially approved for use against head and neck squamous cell carcinoma.[26] Despite its promising properties it has a very limited solubility in water due to intermolecular aggregation. Ideally, the drug transporter should solubilize *m*-THPC well. But even more important is an effective release of the drug which is often too slow, in e.g. micellar carriers, making patients suffer from light sensitivity over days.[26] Thus, there is a high need for tailor-made solubilizers

that improve the solubility of *m*-THPC and allow for adjustment of drug-release kinetics.

First, appropriate peptide sequences were selected for solubilization of *m*-THPC via solid-phase supported split-and-mix procedures, as described by Börner and coworkers.[7] Three peptide sequences were selected that should provide high affinity to bind *m*-THPC (Figure 7.2). In previous work,[7] peptide-PEG conjugates were tested on their *m*-THPC solubilization and release kinetics. The peptide-PEG conjugate II (Figure 7.2) showed highest performance and thus represents an excellent starting point to develop a drug transporter for *m*-THPC.

Figure 7.2. (left) *m*-tetra(hydroxyphenyl)chlorin (*m*-THPC) photosensitizer and (right) sequences of the most promising peptide-PEG conjugates. Figure reproduced from H. G. Börner and coworkers 2013.[7]

The research described in this Chapter was performed in collaboration with prof. dr. Hans Börner and drs. Eva Maron from Humboldt-Universität zu Berlin. Three oligo(acrylamide) pentamer-polymer conjugates were synthesized at Hasselt University and tested for their biomedical potential by drs. Eva Maron. This research project is still ongoing and only initial results are presented herein.

7.3 Experimental Section

Materials and characterization methods are described in Chapter 8.

7.3.1 Monomer Synthesis

N-isopropyl acrylamide (97%, Sigma-Aldrich) was used as received.

7.3.1.1 Synthesis of *N*-benzyl acrylamide (A)

Dry THF (300 mL), benzylamine (4.3 g, 40 mmol) and trimethylamine (6.6 mL, 48 mmol) were added into a 500 mL round bottom flask and cooled in an ice-bath. Acryloyl chloride (3.8 mL, 48 mmol) dissolved in 10 mL dry THF was added dropwise at 0 °C under inert (N_2) atmosphere while stirring the mixture. After addition, the flask was sealed and the mixture was allowed to react at room temperature overnight. The precipitate was removed by filtration and residual solvent in the filtrate was evaporated under reduced pressure. The crude product was purified by silica gel column chromatography (EtOAc:Hexane 1:3 → 1:1 v/v) to obtain a white crystalline solid (4.1 g, 66%). ^{1}H-NMR (300 MHz, $CDCl_3$, δ): 7.37-7.28 (m, 5H, benzyl), 6.33 (dd, 1H, -C*H*=CH_2), 6.10 (dd, 1H, -CH=C*H*$_2$), 5.85 (brs, 1H, -NH), 5.67 (dd, 1H, -CH=C*H*$_2$), 4.53 (d, 2H, -CH_2).

7.3.1.2 Synthesis of *N*-isobutyl acrylamide (B)

Dry THF (80 mL), isopropylamine (4 mL, 40 mmol), trimethylamine (6.6 mL, 48 mmol) and acryloyl chloride (3.8 mL, 48 mmol) were used. The procedure is identical as in 7.3.1.1. A colorless oil was obtained (3.9 g, 76%). ^{1}H-NMR (300 MHz, $CDCl_3$, δ): 6.28 (dd, 1H, -C*H*=CH_2), 6.10 (dd, 1H, -CH=C*H*$_2$), 5.65 (dd, 1H, -CH=C*H*$_2$), 3.17 (t, 2H, -C*H*$_2$CH), 2.00 (brs, 1H, -NH), 1.82 (m, 1H, -C*H*(CH_3)$_2$), 0.93 (d, 6H, -CH(C*H*$_3$)$_2$).

7.3.1.3 Synthesis of *N*-methyl acrylamide (D)

Dry DCM (100 mL), methylamine (2 M solution in THF, 150 mL, 300 mmol), trimethylamine (7 mL, 50 mmol) and acryloyl chloride (4 mL, 50 mmol) were used. The procedure is identical to that in 7.3.1.1. ^{1}H-NMR (300 MHz, $CDCl_3$, δ): 6.25 (dd, 1H, -C*H*=CH_2), 6.10 (dd, 1H, -CH=C*H*$_2$), 6.05 (brs, 1H, -NH), 5.60 (dd, 1H, -CH=C*H*$_2$), 2.86 (d, 3H, -CH_3).

7.3.2 Synthesis of Artificial Peptides

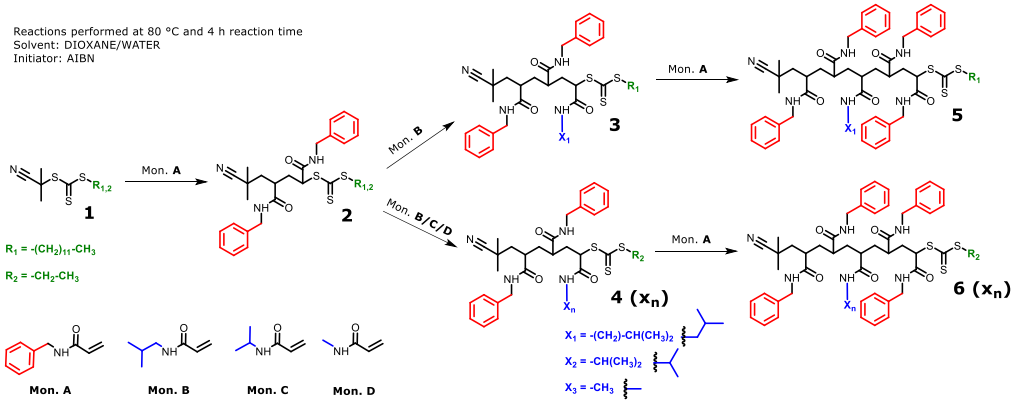

Scheme 7.1. General scheme for the synthesis of monodisperse pentamers (5-mers).

7.3.2.1 Synthesis of RAFT Agents (1)

The synthesis of reversible addition-fragmentation chain transfer (RAFT) agents 2-cyano-2-propyl dodecyl trithiocarbonate (**CPD-TTC**) and 2-cyano-2-propyl ethyl trithiocarbonate (**CPE-TTC**) is described in Chapter 2 and 6, respectively.

7.3.2.2 General Procedure for the Synthesis of Artificial Peptides (2-6)

In a typical procedure, 2,2'-azobisisobutyronitrile (AIBN) (0.1 equiv.), RAFT agent (**1**, 1 equiv.), monomer (**A**, **B**, **C** or **D** in 1 or 2 equiv.) and reaction solvent dioxane/water (1:1 v/v) were added to a glass vial with stirring bar. The glass vial

was sealed by a rubber septum. The solution was degassed for 10 min by N_2 purging, and subsequently inserted into the glovebox. The glass vial was placed in a preheated copper-block at 80 °C. After 4 h reaction time the mixture was quenched by cooling the vial in liquid nitrogen and subjecting the contents to an ambient atmosphere. Subsequently the mixture was transferred into an aluminium pan to evaporate volatiles. The crude mixture was purified via flash column chromatography in combination with preparative HPLC for the pentamers **5** and **6 (x_n)** to yield the monodisperse products **2-6 (x_n)**. The monodisperse character was confirmed by ESI-MS.

7.3.2.3 Synthesis of Oligo(acrylamide) Dimers (2)

2,2'-azobisisobutyronitrile (AIBN) (0.08 g, 0.4 mmol), CPE-TTC RAFT agent (**1**, 0.95 g, 4.6 mmol), *N*-benzyl acrylamide (**A**, 1.5 g, 9.3 mmol) and dioxane/water as reaction solvent were used. The general procedure as described in 7.3.2.2 was followed. The oligomer was isolated via flash column chromatography (petroleum ether:ethyl acetate 4:1 → 1:1 v/v) to yield the dimer **2** in 0.89 g (37%) as a yellowish oil. ESI-MS (m/z): 550.16 ($M+Na^+$).

7.3.2.4 Synthesis of Oligo(acrylamide) Trimers (3 and 4 (x_n))

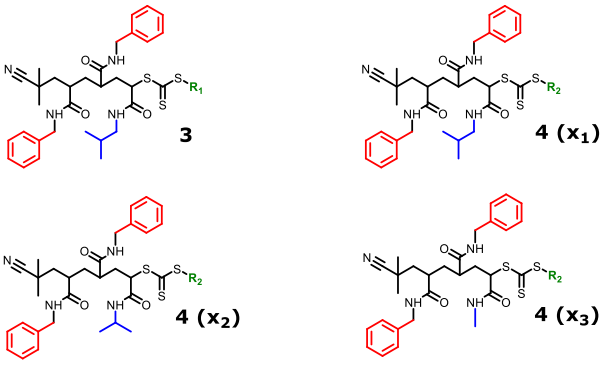

The general procedure as described in 7.3.2.2 was followed. 2,2'-Azobisisobutyronitrile (AIBN) (0.1 equiv.), dimer **2** (1 equiv.) and dioxane/water were used with the monomers:

- **B** (1 equiv., 0.4 M) to yield 0.14 g (30%) of trimer **3**. ESI-MS (m/z): 817.42 ($M+Na^+$).
- **B** (1 equiv., 0.5 M) to yield 0.35 g (25%) of trimer **4 (x_1)**. ESI-MS (m/z): 677.26 ($M+Na^+$).
- **C** (1 equiv., 0.5 M) to yield 0.20 g (32%) of trimer **4 (x_2)**. ESI-MS (m/z): 663.24 ($M+Na^+$).
- **D** (1 equiv., 0.50 M) to yield 0.18 g (30%) of trimer **4 (x_3)**. ESI-MS (m/z): 635.21($M+Na^+$).

7.3.2.5 Synthesis of Oligo(acrylamide) Pentamers (5 and 6 (x_n))

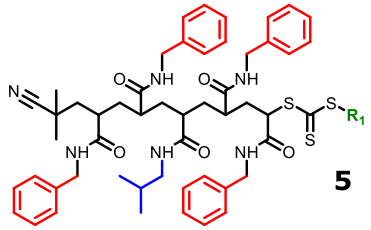

5

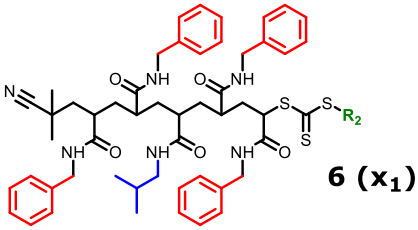

6 (x_1)

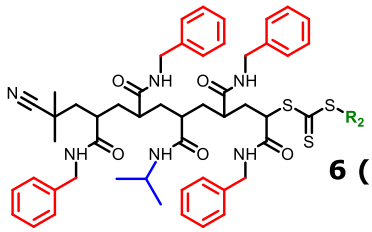

6 (x_2)

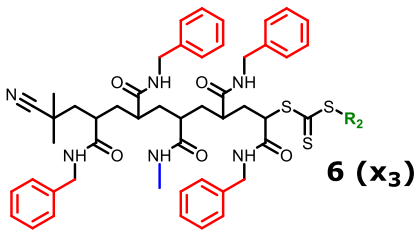

6 (x_3)

R_1 = $-(CH_2)_{11}-CH_3$

R_2 = $-CH_2-CH_3$

The general procedure as described in 7.3.2.2 was followed. 2,2'-Azobisisobutyronitrile (AIBN) (0.1 equiv.), monomer **A** (2 equiv.) and dioxane/water were used with the trimers:

- **3** (1 equiv., 0.10 M) to yield 20 mg (18%) of pentamer **5**. ESI-MS (m/z): 1139.59 ($M+Na^+$).
- **4 (x_1)** (1 equiv., 0.30 M) to yield 52 mg (21%) of pentamer **6 (x_1)**. ESI-MS (m/z): 999.43 ($M+Na^+$).
- **4 (x_2)** (1 equiv., 0.30 M) to yield 51 mg (19%) of pentamer **6 (x_2)**. ESI-MS (m/z): 985.41 ($M+Na^+$).
- **4 (x_3)** (1 equiv., 0.30 M) to yield 42 mg (16%) of pentamer **6 (x_3)**. ESI-MS (m/z): 957.38 ($M+Na^+$).

7.3.3 Synthesis of Functionalized Poly(ethylene glycol) (7)

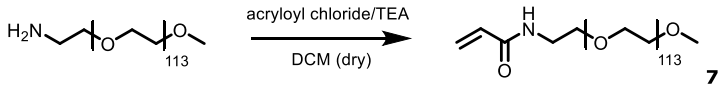

7

Poly(ethylene) glycol (PEG_{5000}) amine (1 g, 0.2 mmol) and TEA (34 µL, 0.24 mmol) were dissolved in 2 mL DCM (dry). Acryloyl chloride (23 µL, 0.24 mmol) was dissolved in 0.3 mL DCM (dry) and added slowly to the mixture while stirring at 0 °C. The mixture was stirred for 3 h at room temperature. The crude mixture was purified by preparative SEC (rec-SEC) and the functionalized PEG_{5000} was precipitated in cold diethyl ether (Et_2O) and separated from the solution by centrifugation. The precipitate was extensively washed with Et_2O. 85% of the PEG_{5000}-amine was functionalized (determined by integration of the acrylic protons after functionalization relative to the PEG backbone in ^{1}H-NMR).

7.3.4 General Synthesis of Pentamer-PEG$_{5000}$ Conjugates

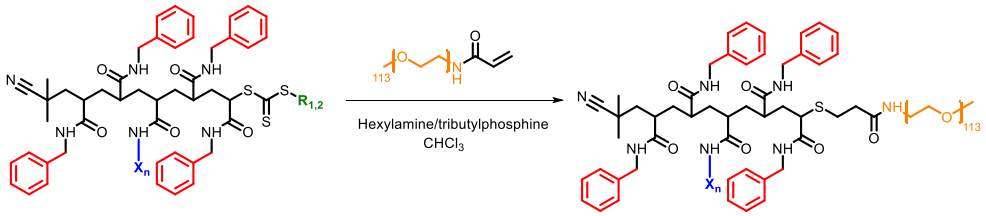

A mixture of synthesized pentamer (**5** or **6** ($\mathbf{x_n}$), 1 equiv., 0.04 M), functionalized PEG$_{5000}$-amine (**7**, 2.2 equiv.), hexylamine (10 equiv.) and tributylphosphine (0.5 equiv.) were dissolved in chloroform ($CHCl_3$, 0.3 mL/10 mg pentamer) and added to a glass vial and subsequently inserted in the glovebox under inert atmosphere. The mixture was stirred at room temperature overnight. The pentamer-PEG$_{5000}$ conjugate was precipitated by the addition of cold diethyl ether (Et_2O) and separated from the solution by centrifugation. The precipitate was extensively washed with Et_2O. ^{1}H-NMR shows 35% for **6** ($\mathbf{x_1}$), 39% **6** ($\mathbf{x_2}$) and 37% for **6** ($\mathbf{x_3}$) of the oligo(acrylamide) pentamer-PEG$_{5000}$ in the resulting white solid (discussed in more detail in section 7.4).

7.4 Results & Discussion

7.4.1 Oligo(acrylamide) Pentamer-PEG_{5000} Derivatives

Small peptide sequences for solubilization of *m*-THPC were selected via solid-phase supported split-and-mix procedures, which is not discussed in this Chapter.[7] Five artificial peptides (monodisperse oligo(acrylamide) pentamers) were synthesized according to their peptide analogues. Acrylamides were selected for their use as synthetic building blocks mainly due to the similarities in their chemical structure compared to peptides. Another advantage is the improved solubility in water compared to other synthetic monomers. Generally, the synthesis of monodisperse oligo(acrylamides) also extends the field of sequence-defined materials discussed throughout this thesis where only acrylates were investigated so far. These monodisperse oligo(acrylamide) sequences were PEGylated (5000 g mol^{-1}) to realize polymeric drug transporters for solubilization and release of *m*-THPC, which is a partially approved drug for photodynamic cancer therapy (PDT). Conceptually the synthetic pentamer segment is responsible for binding the drug whereas the PEG_{5000} block provides shielding as well as water solubility.[7] Both results (drug release kinetics and solubilization) were compared with those obtained for natural peptide-PEG_{5000} conjugates.

Scheme 7.2 shows the peptide-PEG_{5000} conjugate with the highest performance for both solubilization and release of the drug, previously determined by Börner and coworkers,[7] together with the synthetically derived oligo(acrylamide) pentamer-PEG_{5000} transporter. As already stated in the introduction, the peptide-PEG_{5000} conjugate which is most promising for specific drug (*m*-THPC) solubilization and drug release is [Gln-Phe-Phe-Leu-Phe-Phe-Gln]-PEG_{5000}. In

scheme 7.2, the two amino acids phenylalanine (phe) and leucine (Leu) are replaced by the two synthetic building blocks *N*-benzyl acrylamide and *N*-isobutyl acrylamide, respectively. The synthetic sequences have the amide functionalities in their side chain and possess a strong carbon backbone. It has to be noted that the oligo(acrylamide) pentamer-PEG_{5000} conjugates, theoretically, have a purity of around 50% due to the inherent structure of the trithiocarbonate RAFT living endgroups. During aminolysis of the RAFT endgroups two thiol species are formed which can both react *in situ* with the functionalized PEG_{5000}-amine (**7**, Experimental section 7.3.4). The side products for pentamer **5** and pentamer **6** (**x_1**) are shown in Scheme 7.2. These side products could not be separated by us from the oligo(acrylamide) pentamer-PEG_{5000} conjugates. To avoid interference with the drug solubilization experiments, both side products were separately synthesized and tested. Synthesis was conducted by simple PEGylation of the preferred alkyl-thiol. At first, a trithiocarbonate RAFT agent with a C_{12} stabilizing group (RAFT Z-group) was utilized. However, solubilization experiments showed uptake of *m*-THPC by the C_{12} side product of pentamer **5**. Therefore, the synthetic strategy was changed to a C_2 RAFT Z-group, which did not show any drug uptake (side product pentamer **6 (x_1)**).

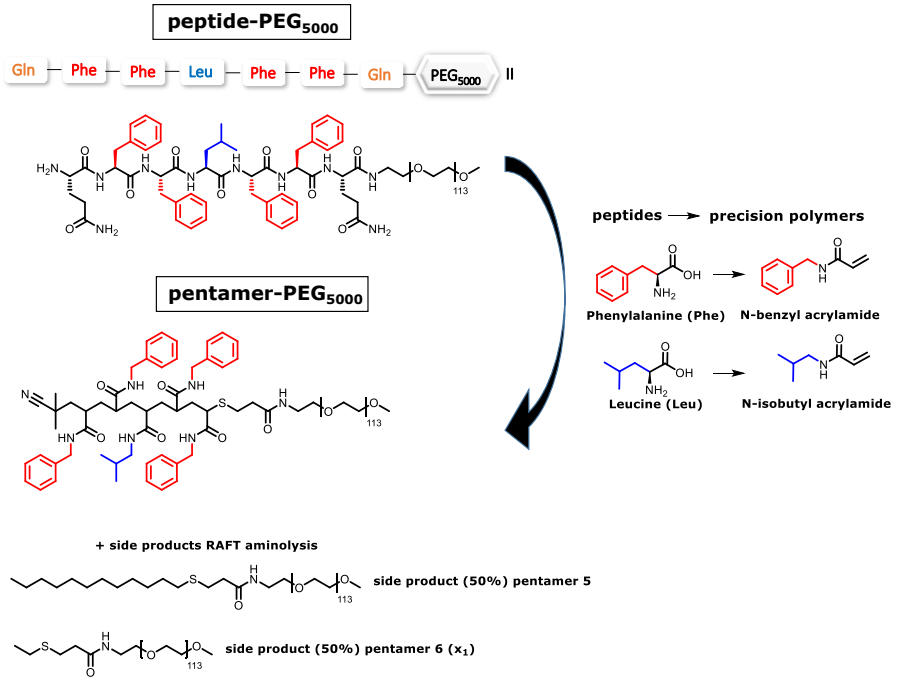

Scheme 7.2. Peptide-PEG_{5000} and oligo(acrylamide) pentamer-PEG_{5000} conjugates. The amino acids phenylalanine and leucine are replaced by *N*-benzyl acrylamide and *N*-isobutyl acrylamide. The side products shown are unavoidable after aminolysis of the trithiocarbonate RAFT endgroup.

Since first results of the oligo(acrylamide) pentamer-PEG_{5000} (pentamer **6 (x_1)**) were promising, as discussed in section 7.4.2, synthetic variations were also tested. The central functionality, which initially was a leucine, was replaced by valine and alanine. Synthetically this means replacement of the central *N*-isobutyl acrylamide by *N*-isopropyl acrylamide and *N*-methyl acrylamide, respectively. Chemical structures of the three PEGylated artificial peptides tested as a drug transporter are shown in Figure 7.3.

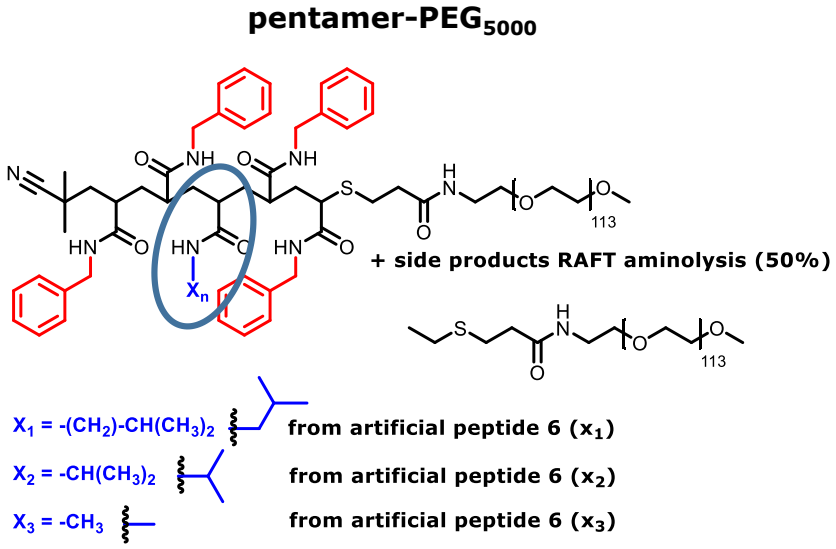

Figure 7.3. Chemical structures of the three PEGylated artificial peptides.

7.4.2 *m*-THPC Solubilization and Release Experiments

To measure *m*-THPC loading (solubilization) for these systems, aqueous solutions of the various carrier systems (conjugates) were added to ethanolic *m*-THPC solutions. The mixtures obtained were lyophilized, redissolved in pure water and non-solubilized *m*-THPC was removed by centrifugation. The amount of solubilized *m*-THPC was determined by UV-VIS absorption spectroscopy of each supernatant after loading of the conjugates with *m*-THPC to determine the payload capacity of each drug transporter. The oligo(acrylamide) pentamer sequences crucially affect the solubilization capacities (Figure 7.4B).[7] Besides the solubilization of *m*-THPC, it is important to study the release kinetics from the transporter with regards to the drug function for PDT. The activity of the solubilized drug is examined via fluorescence emission spectra since fluorescence properties correlate well with the ability to generate $^1O_2$ for cancer treatment. Photosensitizers for PDT might be intravenously administered where they get distributed throughout the

bloodstream to reach their targets (e.g. cancer cells in tissues). Hydrophobic drugs in the blood transfer rapidly to bovine serum albumin (BSA). Transfer of *m*-THPC to BSA can be detected by fluorescence, because the drug is non-fluorescent when trapped in the drug transporter but becomes fluorescent when transferred to BSA (Figure 7.4A).

Preliminary results are promising, as shown in Figure 7.4. The polymers solubilize *m*-THPC well and a clear trend can be observed that correlates well to that of the peptide conjugates. On initial inspection the synthetic conjugates show a higher payload capacity (solubilization) then the natural peptide conjugate counterparts. However, experiments are currently still being optimized. Overall, the same trend is observed in Figure 7.4B for the three derivatives. A big difference in *m*-THPC solubilization can be observed by varying the central functionality in the sequence. The initial leucine derivative indeed shows the highest performance, as initially observed by Börner and coworkers.[7] Figure 7.4C show the release kinetics of the three peptide-PEG_{5000} conjugates together with their synthetic analogues measured by fluorescence spectroscopy. The release of *m*-THPC by the oligo(acrylamide) pentamer-$peptide_{5000}$ conjugates is slower compared to their natural analogues. However, drug release could be observed for both. Although Figure 7.4C shows that the synthetic conjugates are slow releasers, first steps are taken here for real biomedical applications in the field of precision polymer design.

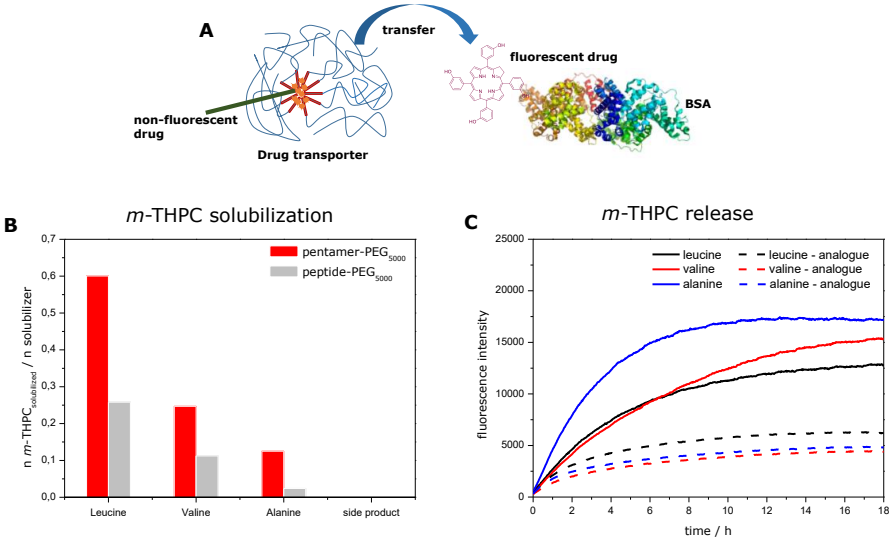

Figure 7.4. (A) The release of the drug was activated by adding BSA to the drug-polymer-solution and measured by fluorescence. (B) Solubilization experiments of *m*-THPC. (C) Release kinetics of *m*-THPC.

7.5 Conclusions & Outlook

The precision polymer and biomedical field merge to develop a new generation of drug transporters for e.g. photodynamic cancer treatment (PDT). There is a high demand for tailor-made solubilizers that improve solubility of *m*-THPC and allow for adjustement of drug-release kinetics. A set of four different synthetic peptide analogues, so-called artificial peptides, were synthesized and studied. Initial results show good solubilization of *m*-THPC. However, release kinetics are still slow compared to their natural counterparts. Today, the research field of sequence-controlled polymers mainly focuses on the fundamentals of gaining control over the primary polymer sequence. Although more optimization of the sequences and experiments is still needed, herein the first steps are taken to pave the way toward direct biomedical applications. In this ongoing research a new class of materials is developed that shows high potential for future applications in drug delivery.

7.6 References

1. Wilson, P. *Macromolecular Chemistry and Physics* **2017**, *218*, DOI: 10.1002/macp.201600595.

2. Lutz, J.-F.; Lehn, J.-M.; Meijer, E. W.; Matyjaszewski, K. *Nature Reviews Materials* **2016**, *1*, 16024.

3. Karamessini, D.; Poyer, S.; Charles, L.; Lutz, J. F. *Macromolecular rapid communications* **2017**, *341*, DOI: 10.1002/marc.201700426.

4. Singh, A.; Worku, Z. A.; Mooter, G. V. d. *Expert Opinion on Drug Delivery* **2011**, *8*, 1361.

5. Lipinski, C. A.; Lombardo, F.; Dominy, B. W.; Feeney, P. J. *Advanced Drug Delivery Reviews* **2001**, *46*, 3.

6. Duncan, R. *Nature Reviews Drug Discovery* **2003**, *2*, 347.

7. Wieczorek, S.; Krause, E.; Hackbarth, S.; Röder, B.; Hirsch, A. K. H.; Börner, H. G. *Journal of the American Chemical Society* **2013**, *135*, 1711.

8. Wieczorek, S.; Schwaar, T.; Senge, M. O.; Börner, H. G. *Biomacromolecules* **2015**, *16*, 3308.

9. Fleige, E.; Quadir, M. A.; Haag, R. *Advanced Drug Delivery Reviews* **2012**, *64*, 866.

10. Ferrari, M. *Nature Reviews Cancer* **2005**, *5*, 161.

11. Fox, M. E.; Szoka, F. C.; Frechet, J. M. *Accounts of Chemical Research* **2009**, *42*, 1141.

12. Bae, Y.; Kataoka, K. *Advanced Drug Delivery Reviews* **2009**, *61*, 768.

13. Kabanov, A. V.; Vinogradov, S. V. *Angewandte Chemie International Edition* **2009**, *48*, 5418.

14. Knop, K.; Hoogenboom, R.; Fischer, D.; Schubert, U. S. *Angewandte Chemie International Edition* **2010**, *49*, 6288.

15. Allen, T. M.; Cullis, P. R. *Science* **2004**, *303*, 1818.

16. Schneider, H. J. *Angewandte Chemie International Edition* **2009**, *48*, 3924.

17. Torchilin, V. P. *Pharmaceutical Research* **2007**, *24*, 1.

18. Lee, C. C.; MacKay, J. A.; Fréchet, J. M. J.; Szoka, F. C. *Nature Biotechnology* **2005**, *23*, 1517.

19. Menjoge, A. R.; Kannan, R. M.; Tomalia, D. A. *Drug Discovery Today* **2010**, *15*, 171.

20. Koner, A. L.; Nau, W. M. *Angewandte Chemie International Edition* **2008**, *47*, 5398.

21. Elsabahy, M.; Wooley, K. L. *Chemical Society Reviews* **2012**, *21*, 2545.

22. Schwemmer, T.; Baumgartner, J.; Faivre, D.; Bo¨rner, H. G. *Journal of the American Chemical Society* **2012**, *134*, 2385.

23. Kolodziej, C. M.; Kim, S. H.; Broyer, R. M.; Saxer, S. S.; Decker, C. G.; Maynard, H. D. *Journal of the American Chemical Society* **2012**, *134*, 247.

24. Wilke, P.; Bo¨rner, H. G. *ACS Macro Letters* **2012**, *1*, 871.

25. Börner, H. G. *Macromolecular rapid communications* **2011**, *32*, 115.

26. Senge, M. O. *Photodiagnosis and Photodynamic Therapy* **2012**, *9*, 170.

CHAPTER 8

Materials & Characterization

8.1 Materials

The monomers *n*-butyl acrylate (Acros, 99%), 2-ethylhexyl acrylate (Acros, 99%), ethylene glycol methyl ether acrylate (Acros, 98%), methyl acrylate (Acros, 99%), *tert*-butyl acrylate (Alfa-Aesar, 99%) and ethyl acrylate (Acros, 99,5%) were deinhibited over a column of activated basic alumina prior to use. 2,2'-Azobisisobutyronitrile (Sigma-Aldrich, 98%) was recrystallized twice from methanol prior to use. 1,1'-azobiscyclohexanecarbonitrile (VAZO-88, Sigma-Aldrich, 98%), ethylisocyanoacetate (Sigma-Aldrich, 98%) and hexylamine (Acros, 99%) were used as received. All solvents used are obtained from commercial sources (Acros, Sigma-Aldrich and VWR) and used without further purification. Tetrahydrofurane (THF), dimethylformamide (DMF) and dichloromethane (DCM) were dried by a solvent purification system (MBraun, MB-SPS-800), if indicated as dry solvent equipped, with alumina columns.

A video can be found in the corresponding manuscript of Chapter 2 that shows the evolution of the ESI-MS spectra during a RAFT polymerization in real time as in principle observed during measurement.[1]

8.2 Characterization Methods

Nuclear magnetic resonance (NMR) spectra were acquired in deuterated solvents ($CDCl_3$, D_2O and acetone-d_6) on 300 or 400 MHz instruments. NMR spectra were analyzed via MestReNova software. All chemical shifts are recorded in ppm (δ) and determined relative to the residual solvent absorption peaks. The multiplicities were explained using the following abbreviations: s for singlet, d for

doublet, t for triplet, m for multiplet, bs for broad signal and dd for doublet of doublets.

Size-exclusion chromatography (SEC) analysis of the MWDs of the polymer samples were performed on a Tosoh EcoSEC operated by PSS WinGPC software, equipped with a PLgel 5.0 µm guard column (50 × 8 mm), followed by three PLgel 5 µm Mixed-C columns (300 × 8 mm) and a differential refractive index detector (Tosoh EcoSEC RI) using THF as the eluent at 40 °C with a flow rate of 1 mL min^{-1}. The SEC system was calibrated using linear narrow polystyrene standards ranging from 474 to 7.5 x 10^6 g·mol^{-1} PS (K = 14.1 × 10^{-5} dL·g^{-1} and α = 0.70), and toluene as a flow marker. MHKS parameters for poly(*n*-butyl acrylate) (K = 12.2 × 10^{-5} dL·g^{-1} and α = 0.70) were applied. Polymer concentrations were in the range of 3–5 mg·mL^{-1}.

Electrospray ionization mass spectrometry (ESI-MS) was performed using an LTQ orbitrap velos pro mass spectrometer (ThermoFischer Scientific) equipped with an atmospheric pressure ionization source operating in the nebulizer assisted electrospray mode. The instrument was calibrated in the m/z range 220-2000 using a standard solution containing caffeine, MRFA and Ultramark 1621. A constant spray voltage of 5 kV was used and nitrogen at a dimensionless sheath gas flow-rate of 7 was applied. The capillary voltage, the tube lense offset voltage and the capillary temperature were set to 25 V, 120 V and 275 °C, respectively. For manual measurements a polymer solution with concentration of 10 μg mL^{-1} was injected. A mixture of THF and methanol (THF:MeOH = 3:2), all HPLC grade, was used as solvent. Spectra were analyzed in Thermo Xcalibur Qual Browser software.

Purification of products was performed on a **recycling preparative HPLC (rec-SEC)** JAI LC-9210 NEXT system operated by prepure V1.0 software in the manual injection mode (3 mL), comprising a JAIGEL-1*H* and JAIGEL-2*H* column (eluent $CHCl_3$, flow rate 3.5 mL/min) and a NEXT series UV detector using $CHCl_3$ as the eluent with a flow rate of 3.5 $mL \cdot min^{-1}$. Fractions were collected manually (in case of first run purifications) and automatically (for repeated purifications where elution times of fractions are well-known).

Purification of oligomer mixtures was performed via **flash column chromatography** performed on a Büchi sepacore system equipped with GRACE Resolve normal-phase silica cartridges (48 gram).

Kinetic modelling simulations have been carried out with Predici (CIT) version. 7.1.0 on an Intel i5 CPU.

8.3 References

1. Haven, J. J.; Vandenbergh, J.; Junkers, T. *Chemical Communications* **2015,** *51*, 4611.

CHAPTER 9

Summary & Outlook

9.1 Summary

On-line reaction monitoring represents a powerful tool which can contribute significantly to the modern world of polymer science and technology. In this thesis, the development of an on-line electrospray ionization mass spectrometer/microreactor (ESI-MS/MRT) coupling for fast and efficient screening and optimization of reactions was investigated. The setup allows the continuous "nonstop" monitoring of chemical processes, most prominently polymerizations but not limited to those. In this work, three interconnecting themes centered on the use of on-line ESI-MS/MRT have been investigated:

(1) Kinetics of *n*-butyl acrylate radical polymerization
(2) Study of the Passerini three-component reaction
(3) Efficiency assessment of single unit monomer insertion reactions (SUMIs).

In the first study, reversible addition-fragmentation chain transfer (RAFT) polymerization of *n*-butyl acrylate was monitored in real time by on-line ESI-MS/MRT. Via adjustment of flow rates in the microreactor, time-sweep experiments were carried out that allowed monitoring of the complete polymerization process. This way, the kinetics of *n*-butyl acrylate radical polymerization were revealed in a single experiment. Microreactor time-sweeps were performed between 1 and 10 minutes residence time for a wide temperature range (100, 110, 120, 130, 140, 150 and 190 °C). In all cases, full monomer conversions were reached and relatively good control over molecular weight and dispersity were obtained at the highest temperatures. However, endgroup analysis revealed that the desired RAFT product was already less abundant than

some side products at the lower temperatures. The on-line coupling method was found to deliver data with high time-resolution (second scale) and very low scatter. Further modelling of these reactions was far from trivial due to the high complexity of the reaction schemes and the very high level of detail of our data (> 55000 data points for each time-sweep). However, full time-sweep datasets for any species in the mass spectra can be provided to interested parties.

Secondly, the on-line ESI-MS/MRT setup was also used to study the Passerini three-component reaction (Passerini 3-CR) to demonstrate the high-throughput screening potential of microreactors for macromolecular design. The Passerini 3-CR was used for the synthesis of α–acyloxy carboxamides by combination of an aldehyde, isocyanide and carboxylic acid moiety. Endgroup functionalized low molecular weight polymer supports of poly(*n*-butyl acrylate) were used for screening and quantification in ESI-MS. Reaction parameters such as molarity, residence times, absolute reagent concentrations and microreactor temperatures were varied. After screening, a reaction protocol was proposed for high yields within minutes reaction time under equimolar reactant concentrations. The established reaction protocol was then transferred to a conventional batch process for the synthesis of different diblock copolymer conjugates.

Thirdly, the on-line ESI-MS/MRT setup was used to examine the reaction efficiency of single unit monomer insertions (SUMIs) via the RAFT polymerization technique. Microflow synthesis procedures were screened for optimal SUMI product yields in combination with kinetic simulations of the radical insertions process. Calibration of the ESI-MS spectra that were recorded on-line during synthesis allowed for exact information on concentrations of SUMI mixtures. Experiments revealed that

isolated yields decrease for each subsequent SUMI reaction. Kinetic simulations clearly showed that the propagation rate coefficient must display a strong chain-length dependency in order to explain the experimental observations. Optimal conditions were then copied to a mesoflow reactor for upscaling of the SUMI reactions, which nicely showed the easy upscalibility of lab-scale continuous flow reactions.

Previous SUMI assessments showed the pathway towards further developments in the synthesis of longer monodisperse sequence-defined oligomers. Purification by recycling size-exclusion chromatography (rec-SEC) limited the oligomer length to 4-5 monomer insertions. Therefore, flash column chromatography was utilized to isolate targeted monodisperse oligomers with high efficiency. This, together with the optimized SUMI strategy, allowed to construct monodisperse materials of very considerable length starting form cheap and very versatile building blocks. Linear monodisperse 18- and 20-mer oligoacrylates were obtained in batch via consecutive synthesis of two sequence-defined 9- and 10-mers followed by disulfide coupling utilizing RAFT endgroup chemistry.

Finally, to continue in the field of precision polymers, a set of artificial peptide pentamers was synthesized. A previously tested peptide sequence was mimicked by replacement of the natural amino acids by synthetic acrylamide monomers. Monodisperse pentamer sequences, so-called artificial peptides, were PEGylated to realize water soluble polymeric drug transporters for solubilization and release of tetra(hydroxyphenyl)chlorin (*m*-THPC). First results showed good solubilization of *m*-THPC. However, release kinetics were slow compared to their natural

counterparts. In any case, a new class of materials was developed that shows high potential for future application in drug delivery systems.

9.2 Nederlandse Samenvatting

In lijn opvolgen van chemische reacties is een krachtig hulpmiddel dat significant kan bijdragen aan de moderne polymere wetenschap en techniek. De ontwikkeling van een in serie gekoppelde elektrospray-ionisatie massaspectrometer (ESI-MS) aan een continu flowprocess voor de snelle en efficiënte screening van chemische reacties, is onderzocht in dit proefschrift. Een dergelijke opstelling (ESI-MS/MRT) laat toe om zonder onderbrekingen chemische processen op te volgen en meer specifiek polymerisaties. Drie domeinen werden onderzocht met behulp van de bovengenoemde opstelling:

- De kinetica van de radicalaire *n*-butyl acrylaat polymerisatie;
- Een studie van de Passerini drie-componentsreactie;
- De efficiëntie van enkelvoudige monomeer insertiereacties.

De eerste studie, de reversiebele additie-fragmentatie ketentransfer (RAFT) polmerisatie van *n*-butyl acrylaat, werd opgevolgd met behulp van ESI-MS/MRT. Het volledige polymerisatieproces kon gevolgd worden door de verblijftijden in de reactor aan te passen. Op deze manier kon de kinetica achterhaald worden in één enkel experiment. Experimenten in de microreactor werden uitgevoerd tussen 1 en 10 minuten verblijftijd bij verschillende reactortemperaturen (100, 110, 120, 130, 140, 150 en 190 °C). In ieder experiment werden volledige monomeerconversie, goede controle over het molecuulgewicht en lage dispersiteiten bereikt, ook voor de hogere reactortemperaturen. Hoe dan ook, de

analyse van de eindgroepen onthulde dat de gewenste RAFT-polymeren al in minder mate aanwezig waren dan ongewilde nevenproducten. Het verder simuleren van deze data is zeer complex, maar datasets kunnen voorzien worden voor externe geïnteresseerden.

In een tweede toepassing werd de gekoppelde ESI-MS/MRT opstelling gebruikt om de Passerini drie-componentsreactie (P-3CR) te bestuderen. De P-3CR wordt gebruik voor het synthetiseren van α-acyloxy carboxamides door combinatie van een aldehyde, isocyanide en een carbonzuur. Eindgroep gefunctionaliseerde laag-moleculaire polymeren werden gebruikt voor de screening en kwantificatie in ESI-MS van deze reactie. Verschillende parameters werden gevarieerd, zoals molaire verhoudingen, verblijftijden, reactortemperatuur en absolute concentraties in de oplossing. Na de screening werd een reactieprotocol voorgesteld voor een zeer hoog rendement in slechts enkele minuten reactietijd. Dit protocol werd daarna gebruikt voor de synthese van verschillende block copolymeren in een conventioneel batchproces.

Als laatse toepassing van de ESI-MS/MRT opstelling werd de efficiëntie van enkelvoudige monomeer insertiereacties onderzocht via de RAFT polymerisatietechniek. Verschillende microflowprocedures werden gescreend voor een optimaal rendement van deze reacties. Dit gebeurde in combinatie met kinetische simulaties van het proces. Door middel van ESI-MS calibratie kon accurate informatie verzameld over de absolute concentraties van de producten in het reactiemengsel. Volgens de experimentele data daalt het rendement na opeenvolgende enkelvoudige monomeerinserties. Simulaties toonden hierbij aan dat de propagatiesnelheid afhankelijk moet zijn van de ketenlengte om deze

experimentele data te verklaren. De gevonden optimale condities werden dan getransfereerd naar een mesoflowreactor voor opschaling. Dit toont mooi aan dat reacties in een coninue flow eenvoudig op te schalen zijn.

Via vorige bevindingen werd de weg getoond naar langere sequentiegedefinieerde ketens. Tot op dat moment gebeurde de opzuivering van deze mengsels via scheiding op basis van het hydrodynamisch volume van de oligomeermengsels. De ketelengte bleef hierdoor gelimiteerd tot 4-5 eenheden. Met behulp van chromatografische scheidingsmethoden konden op een efficiënte manier langere ketens gesynthetiseerd worden. Lineaire 18- en 20-meren, op basis van acrylaten, werden verkregen via conventionele batchreacties via syntheses van 9- en 10-meren gevolgd door een disulfidekoppeling op basis van RAFT-eindgroepchemie.

Vervolgens werd verder gewerkt in het domein van sequentiegedefinieerde polymeren. Een set van artificiële peptides (5-meren) werd gesynthetiseerd. Een voorheen geteste peptidesequentie werd nagebootst door de natuurlijke aminozuren te vervangen door synthetische acrylamide-gebaseerde monomeren. De monodisperse sequenties (5-meren), artificiële peptides genaamd, werden gekoppeld met een poly(ethyleenglycol) polymeer voor het bekomen van water oplosbare transporteerders voor het opnemen en terug vrijlaten van het medicijn tetra(hydroxyphenyl)chlorin (*m*-THPC). Uit de eerste resultaten blijkt dat de opname van *m*-THPC goed verloopt. De vrijlating van het medicijn verloopt echter nog traag. Een nieuwe klasse materialen werd hier ontwikkeld, wat veelbelovend is voor toepassingen in de biomedische sector.

9.3 Outlook

On-line monitoring of polymerizations, or chemical processes in general, still has many challenges to overcome. Especially in a continuous flow fashion, on-line monitoring of polymerizations is still in its infancy. Ideally, a flow device (e.g. microreactor) can be coupled with any analysis equipment available today. Throughout this thesis efforts has been invested in the realization of coupling a microreactor chip with ESI-MS. From a technical point of view, no complex engineering was required, however, issues in finding proper split ratios, dilution factors and tubing lengths to make it accessible for a good range of chemical reactions was time-consuming. As a first model it's highly flexible for a wide range of reaction concentrations and solvents. In principle, reactions at room temperature can proceed until injected in the ESI nozzle. However after strong dilution behind the backpressure regulator reactions will be slow. Therefore, improvements can still be made on the dead volumes present in the setup. Large datasets are obtained from screening reactions. Although we have a software script available it still takes huge human efforts to unravel and analyze datasets. Ideally, acquired data is automatically analyzed in situ and feedback for reaction optimization is integrated in the software which means reactions can be optimized fully unattended. Operation of the setup is easy for researchers with sufficient background in ESI-MS and flow chemistry.

In relation to polymers, imagine how useful it would be to perform a polymerization in a microreactor device coupled with SEC, ESI-MS, NMR spectroscopy, *etc*. Results are accessible *in situ* and reaction optimization is extremely fast. Moreover, to take it one step further, analysis could happen

automatically - software controlled – with an integrated feedback loop for adjustment of the reaction parameters. With such setup, a researcher would only have to prepare the reagent mixtures and start the flow reaction and come back later to collect the results. Such setup can also find its application in e.g. continuous quality control in commercial industries, optimization of complex chemical reactions, finding optimal conditions for upscaling purposes, *etc*.

Major contributions can still be made in the field of sequence-defined polymers (or oligomers). In the last decade, people have started a race for the synthesis of monodisperse polymers with the largest amount of building blocks inserted. Therefore, a lot of time was investigated on the fundamentals of these reactions and different methods were developed using different polymerization and simple organic synthesis techniques available today (e.g. chain-growth polymerization, step-growth polymerization, synthesis on solid supports, *etc*.). Every technique has its pros and cons dependent on its purpose. Still, further contributions can be made to optimize the production of sequence-defined materials. To continue the work performed in this thesis, new development in this field could arise from making use of endgroup chemistry in controlled radical polymerizations where endgroups are automatically present. After synthesis of a monodisperse sequence, e.g. a decamer (10-mer), orthogonal endgroup chemistry can be applied to push it further. However, in my opinion, the emphasis in this field should urgently shift towards applications. Until today, researchers gained control over the synthesis of monodisperse macromolecular materials and should use this capability now for the development of materials with a future in e.g. biomedical applications. With these ideas in mind, a collaboration was started with Humboldt-Universität zu Berlin to merge the field of precision polymers and biomedical

applications in developing a new class of materials, so-called artificial peptides, which show high potential for future application in drug delivery systems.

PUBLICATIONS

Scientific Journals

J.J. Haven, C. Guerrero-Sanchez, D.J. Keddie, G. Moad, *Rapid and systematic Access to Quasi-Diblock Copolymer Libraries with a Comprehensive Composition Range via Sequential RAFT Polymerization in an Automated Synthesizer*, Macromol. Rapid Commun. **2014**, *35*, 492-497.

J.J. Haven, C. Guerrero-Sanchez, D.J. Keddie, G. Moad, S.H. Thang, U.S. Schubert, *One Pot Synthesis of High Order Quasi-Block-Copolymer Libraries via Sequential RAFT Polymerization in an Automated Synthesizer*, Polym. Chem., **2014**, *5*, 5236-5246.

Inside front cover*

J.J. Haven, J. Vandenbergh, T. Junkers, *Watching Polymers Grow: Real Time Monitoring of Polymerizations via an On-Line ESI-MS/Microreactor Coupling*, Chem. Commun., **2015**, *51*, 4611-4614.

J.J. Haven, J. Vandenbergh, R. Kurita, J. Gruber, T. Junkers, *Efficiency Assessment on Single Unit Monomer Insertion Reactions for Monomer Sequence Control: Kinetic Simulations and Experimental Observations*, Polym. Chem., **2015**, *6*, 5752-5765.

Paper of the month in Polymer Chemistry*

J.J. Haven, E. Baeten, J. Claes, J. Vandenbergh, T. Junkers, *High-Throughput Polymer Screening in Microreactors: Boosting the Passerini Three-Component Reaction*, Polym. Chem. **2017**, *8*, 2972-2978.

J.J. Haven, N. Zaquen, M. Rubens, T. Junkers, *The Kinetics of n-Butyl Acrylate Radical Polymerization Revealed in a Single Experiment by Real Time On-Line Mass Spectrometry Monitoring*, Macromol. Reaction Eng. **2017**, *11*, DOI: 10.1002/mren.201700016.

Front cover & Featured on advanced science news*

E. Baeten, J.J. Haven, T. Junkers, *RAFT Multiblock Reactor Telescoping: From Monomers to Tetrablock Copolymers in a Continuous Multistage Reactor Cascade*, Polym. Chem. **2017**, *8*, 3815-3824.

J.J. Haven,‡ J.A. De Neve,‡ T. Junkers, *Versatile Approach for the Synthesis of Sequence-Defined Monodisperse 18- and 20-mer Oligoacrylates*, ACS Macro Lett. **2017**, *6*, 743-747.

‡These authors contributed equally

J.J. Haven, T. Junkers, *Online Monitoring of Polymerizations: Current Status*, Eur. J. Org. Chem., **2017**, DOI: 10.1002/ejoc.201700851

J.J.Haven,‡ E. Maron,‡ J. Vandenbergh, T. Junkers, H.G. Börner, *Artificial Peptides and Their Applicability as Polymeric Drug Transporters*, in preparation.

‡These authors contributed equally

Book Chapters & Proceedings

G. Moad, C. Guerrero-Sanchez, J.J. Haven, D.J. Keddie, A. Postma, E. Rizzardo, S.H. Thang, *RAFT for the Control of Monomer Sequence Distribution – Single Unit Monomer Insertion (SUMI) into Dithiobenzoate RAFT Agents*, In Sequence-Controlled Polymers: Synthesis, Self-assembly and Properties, J.F. Lutz, M. Ouchi, M. Sawamoto, T. Meyer, Eds. ACS Symposium Series. American Chemical Society: Columbus, OH, *Vol. 1170*, **2014**, chapter 9, 133-147.

J.J. Haven, T. Junkers, G. Moad, *Macro-RAFT synthesis by Single Unit Monomer Insertion (SUMI) into Dithiobenzoate RAFT Agents – Towards Biological Precision*, In Proceedings of the 1st Int. Elec. Conf. on Mat. 26-10 June 2014, Sciforum Electronic Conference Series, Vol. 1, **2014**, d004, DOI: 10.3390/ecm-1-d004.

C. Guerrero-Sanchez, R. Yañez-Macias, M. Rosales-Guzmán, J.J. Haven, C. Piñon-Balderrama, G. Moad, R. Guerrero-Santos, E. Saldivar-Guerra, T. Junkers, J. Bonilla-Cruz, J. Vitz, U.S. Schubert, *High Throughput Experimentation for Polymer Materials*, In High-Throughput Experimentation and Combinatorial Approaches in Catalysis and Materials Science, S.A. Schunk ed., Wiley-VCH Verlag, **2017**, accepted.

Conference Contributions

Oral Presentation

J.J. Haven, T. Junkers, *Precision Polymers via Controlled Radical Polymerizations: Synthesis of Monodisperse Sequence-Defined Acrylate Oligomers*, Annual Meeting of the Belgian Polymer Group (BPG) **2017**, Houffalize, Belgium.

Poster Presentations

J.J. Haven, J. Vandenbergh, T. Junkers, *Microreactor Technology for the Synthesis of Sequence Controlled Polymer Materials by RAFT – Towards Biological Precision*, Annual Meeting of the Belgian Polymer Group (BPG) **2014**, Ghent, Belgium.

J.J. Haven, J. Vandenbergh, T. Junkers, *Fast and Efficient Reaction Optimization via an On-line ESI-MS/Microreactor Coupling*, Interuniverstiy Attraction Poles (IAP) **2015**, Hasselt, Belgium.

J.J. Haven, J. Vandenbergh, T. Junkers, *Watching Polymers Grow: Real Time Monitoring of Polymerizations via an On-line ESI-MS/Microreactor Coupling*, Annual Meeting of the Belgian Polymer Group (BPG) **2015**, Houffalize, Belgium.

J.J. Haven, J. Claes, J. Vandenbergh, T. Junkers, *Microreactor/Mass Spectrometry Polymer Screening of the Passerini-3CR: Excellent Product Yields within Minutes*, Annual Meeting of the Belgian Polymer Group (BPG) **2016**, Houffalize, Belgium

J.J. Haven, J. Vandenbergh, T. Junkers, *On-Line Electrospray Ionisation MS: A Facile Tool for Fast Reaction Screening and Optimization*, Masterclass flow chemistry **2016**, Hasselt, Belgium.

J.J. Haven, J. Claes, J. Vandenbergh, T. Junkers, *Microreactor/Mass Spectrometry Polymer Screening of the Passerini 3-CR: Excellent Product Yields within Minutes*, Interuniverstiy Attraction Poles (IAP) **2016**, Luik, Belgium.

J.J Haven, J. Claes, J. Vandenbergh, T. Junkers, *Microreactor/Mass Spectrometry Polymer Screening of the Passerini 3-CR: Excellent Product Yields within Minutes*, Warwick Polymers **2016**, Warwick, United Kingdom.

DANKWOORD

"Kort maar krachtig" is hoe ik de afgelopen 4 jaar omschrijf. Een zee van tijd in het eerste jaar, maar al snel kwam ik tot het besef dat een doctoraat zo voorbij vliegt. Ik kan terugkijken op 4 mooie jaren waarin ik mij geen moment verveeld heb. Altijd tijd te kort, maar toch zeer tevreden met het eindresultaat. Dit verhaal was nooit mogelijk geweest zonder de hulp van vele collega's, familie en vrienden die allemaal een woordje van dank verdienen.

Ten eerste wil ik de UHasselt bedankten om mij 4 jaar te financieren. Uiteraard was er geen doctoraat mogelijk zonder deze steun.

Graag wil ik mijn promotor Tanja Junkers bedanken om mij 4 jaar geleden de kans te geven om bij PRD te starten. Tanja, in de afgelopen 4 jaar wist jij mij steeds te motiveren, je deur stond/staat altijd voor me open. Tijdens onze vele discussies heb ik ernorm veel bijgeleerd, mijn dank hiervoor! Ik heb veel bewondering voor de levenskeuzes die je het afgelopen jaar hebt aangekondigd: je academische carrière, maar ook je gekozen levenspad. De verhuis naar Melbourne geeft blijk van grote ambities. Ik verheug me erop om hiertoe mijn steentje te kunnen bijdragen.

Ik wil al mijn (ex-)collega's van OBPC, oud, nieuw en nieuwere, bedanken voor de fantastische jaren. Ik ben blij dat ik jullie allemaal heb leren kennen. Van de Chambers Trophee tot de gezellige after work drinks op vrijdag, het was altijd een leuke bedoening. De geweldige tijd in de G81/83 waar de "magic happened", zal

ik nooit vergeten. Heel veel gelachen en vooral veel gezeverd met een goede schijf op de achtergrond en af en toe werd er ook wel eens een wetenschappelijke discussie gevoerd. Dit verklaarde waarom ik altijd met enorm veel zin en motivatie naar het werk kwam. In het bijzonder wil ik PRD bedanken voor de vele diverse activiteiten die we samen deden. Van de wekelijkse groepsmeetings tot 3-daagse uitstapjes naar Duitsland, het was altijd even plezant! Gelukkig moet ik nog geen afscheid van jullie nemen en kunnen we de komende jaren nog verder samenwerken. Enkele mensen wil ik graag persoonlijk bedanken:

Joke, Jeroen D.N. en Lowie bedankt om deel uit te maken van de wereld van de SUMIs ☺. Ik ben er zeker van dat wij hierin de komende jaren nog veel nieuwe dingen gaan ontdekken. Joke, jij bent voor mij zeer belangrijk geweest bij de start van mijn doctoraat. Ik denk ook dat je de juiste keuze hebt gemaakt om nu de stap naar de industrie te zetten. Veel succes met je verdere carrière, met jouw ambities zal dat zeker lukken.

Neomy en Evelien, samen hebben we meerdere projecten tot een goed einde gebracht en we hebben altijd heel goed kunnen samenwerken. Ook bedankt voor de vele initiatieven en inzet binnen OBPC en vooral PRD. Evelien, we hebben samen een behoorlijk traject afgelegd, maar nu zullen onze wegen scheiden. Ik wens je veel succes met je nieuwe job! Neomy, we hebben veel frustraties gedeeld aan de GPC's, maar konden het op de een of andere manier toch wel altijd oplossen. Sterk team! Ook dank aan Gijs, Jeroen en Frederik om deze taak nu van ons over te nemen.

Ook bedankt aan de rest van mijn (ex-)PRD collega's: Maarten, Kirsten, Jogi, Stephan, Svitlana, Erika, Martijn, Luk, Nok, Dries, Axel, Ya-mi, Benjamin, Kayte en Veronique. Veel succes allemaal met het afronden van jullie doctoraat, postdoc, nieuwe job en/of alle andere uitdagingen waar jullie voor komen te staan. Dan wil ik mijn huidige bureau-collega's nog bedanken. De verhuis naar de hobunits (of is het call/infocentrum?:-)) was in het begin niet vanzelfsprekend, maar achteraf gezien viel dat allemaal wel mee toch? Pieter, jij bent een ontzettend belangrijke schakel in de organische syntheselabo's. Je was altijd wel te vinden voor een mening en van alle markten een beetje thuis: geldleningen, de aankoop van analytische toestellen, aandelen, voetbal, de koers,... zijn de revue allemaal wel eens gepasseerd. Kesters, vóór mijn doctoraat wist ik zelfs niets af van uw bestaan ☺. Kijk nu, goede vrienden voor het leven. Zowel op de werkvloer als op de squash, in een café of bij Animaux, we kunnen het altijd goed met elkaar vinden. Geert, beter een goede buur dan een verre vriend is een understatement. Op jou kan ik al vele jaren rekenen. Het begin van een nieuwe fase in jouw leven binnenkort zal ik met spijt in het hart niet kunnen meemaken waarschijnlijk. Dat maak ik achteraf wel dubbel en dik goed.

Graeme, not sure if you will ever read this but in case you do, thanks a lot for giving me the opportunity to join CSIRO twice. It was a great experience and I've learned a lot from you. I'll start a postdoc in Monash soon, right across your door, so we'll definitely meet again!

Bedankt aan alle bachelor, master en buitenlandse studenten, ook jullie hebben je steentje bijgedragen aan het eindresultaat. I want to thank all Jury members for all their efforts and willingness to evaluate my thesis. Ook een dankjewel aan

het NMR-team, jullie verrichten fantastisch werk en staan altijd open voor discussie. Wouter, bedankt om deel uit te maken van mijn doctoraatscommissie. Met onze OBPC kampioenenploeg hebben we mooie tijden beleefd. Dirk, jou herinner ik mij nog van op de opendeurdag aan de UHasselt. Ik twijfelde toen nog welke richting ik zou gaan studeren. Je bent altijd te vinden voor een leuke babbel. De OBPC zeiltrip die ons naar Engeland moest brengen zal ik nooit vergeten.

Bedankt aan al mijn goede vrienden, de boys, waar ik buiten het werk ontzettend veel tijd mee doorbreng. Samen hebben we al vele wateren doorzwommen, dit zijn vriendschappen voor het leven. Ik kan nog vele pagina's schrijven over al onze fratsen, maar ik denk niet dat een doctoraatsthesis daar de juiste plaats voor is ;-). De laatste, allerlaatste en allerallerlaatste zullen zeker nog gedronken worden voor mijn vertrek naar Australië. Ik ga jullie missen. Ook bedankt aan het bestuur van de heidefeesten, wat een topteam! Veel succes met de organisatie de komende jaren!

Save the best for last. Ma, Pa, Wouter en Anke bedankt om mij te steunen de afgelopen jaren. Bij jullie kan ik altijd terecht in de goede, maar vooral in de minder goede periodes die er ook geweest zijn. Ondanks mijn vele engagementen bij verschillende organisaties en mijn drukke leven, komen jullie nog altijd op de eerste plaats. Anke, "the day after party" zal voor altijd in mijn geheugen gegrift staan als de dag dat ik de vrouw van mijn leven leerde kennen. Het feit dat je bereid bent om mij naar de andere kant van de wereld te volgen zegt genoeg denk ik. Ik ben er zeker van dat wij daar samen een geweldige tijd gaan beleven!

DANKUWEL – THANK YOU

Joris